

University of Windsor

Scholarship at UWindor

Electronic Theses and Dissertations

Theses, Dissertations, and Major Papers

2011

NUMERICAL PREDICTION OF SHEET METAL FORMING LIMITS

Morteza Nurcheshmeh

University of Windsor

Follow this and additional works at: <https://scholar.uwindsor.ca/etd>

Recommended Citation

Nurcheshmeh, Morteza, "NUMERICAL PREDICTION OF SHEET METAL FORMING LIMITS" (2011).

Electronic Theses and Dissertations. 463.

<https://scholar.uwindsor.ca/etd/463>

This online database contains the full-text of PhD dissertations and Masters' theses of University of Windsor students from 1954 forward. These documents are made available for personal study and research purposes only, in accordance with the Canadian Copyright Act and the Creative Commons license—CC BY-NC-ND (Attribution, Non-Commercial, No Derivative Works). Under this license, works must always be attributed to the copyright holder (original author), cannot be used for any commercial purposes, and may not be altered. Any other use would require the permission of the copyright holder. Students may inquire about withdrawing their dissertation and/or thesis from this database. For additional inquiries, please contact the repository administrator via email (scholarship@uwindsor.ca) or by telephone at 519-253-3000ext. 3208.

NUMERICAL PREDICTION OF SHEET METAL FORMING LIMITS

by

Morteza Nurcheshmeh

A Dissertation
Submitted to the Faculty of Graduate Studies
through Mechanical, Automotive & Materials Engineering
in Partial Fulfillment of the Requirements for
the Degree of Doctor of Philosophy at the
University of Windsor

Windsor, Ontario, Canada
2011
© 2011 Morteza Nurcheshmeh

Numerical Prediction of Sheet Metal Forming Limits

by

Morteza Nurcheshmeh

APPROVED BY:

Dr. L. M. Smith, External Examiner
Department of Mechanical Engineering, Oakland University

Dr. D. Watt, Outside Reader
Department of Mechanical, Automotive & Materials Engineering

Dr. W. Altenhof, Department Reader
Department of Mechanical, Automotive & Materials Engineering

Dr. J. Johrendt, Department Reader
Department of Mechanical, Automotive & Materials Engineering

Dr. D. Green, Advisor
Department of Mechanical, Automotive & Materials Engineering

Dr. N. Kar, Chair of Defense
Department of Electrical and Computer Engineering

09 May, 2011

Declaration of Co-Authorship/ Previous Publications

I. Co-Authorship Declaration

I hereby declare that this dissertation does not incorporate material that is a result of joint research. In all cases, the key ideas, primary contributions, data analysis and interpretation, were performed by the author, and Dr. D. E. Green as advisor. This dissertation doesn't include any experimental work, and all utilized experimental data from already published works are fully acknowledged in accordance with the standard referencing practices.

I certify that, with the above qualification, this dissertation, and the research to which it refers, is the product of my own work.

II. Declaration of Previous Publication

This dissertation includes three original papers that have been previously published/ submitted for publication in peer reviewed journals, as follows:

Dissertation Chapter	Publication title/full citation	Publication status
Chapter 3	M. Nurcheshmeh, D.E. Green, Investigation on the Strain-Path Dependency of Stress-Based Forming Limit Curves, International Journal of Material Forming, (2011), Vol. 4, Number 1, 25-37	Published
Chapter 4	M. Nurcheshmeh, D.E. Green, Implantation of mixed nonlinear kinematic-isotropic hardening into MK analysis to calculate forming limit curves , International Journal of Mechanical Science, 53 (2010), 145-153	Published
Chapter 5	M. Nurcheshmeh, D.E. Green, Influence of out-of-plane compression stress on limit strains in sheet metals, International Journal of Material Forming, Accepted on 18 March 2011, Manuscript Number: IJFO-D-10-00144	Accepted

I certify that I have obtained a written permission from the copyright owner(s) to include the above published material(s) in my dissertation. I certify that the above material describes work completed during my registration as graduate student at the University of Windsor.

I declare that, to the best of my knowledge, my dissertation does not infringe upon anyone's copyright nor violate any proprietary rights and that any ideas, techniques, quotations, or any other material from the work of other people included in my dissertation, published or otherwise, are fully acknowledged in accordance with the standard referencing practices. Furthermore, to the extent that I have included copyrighted material that surpasses the bounds of fair dealing within the meaning of the Canada Copyright Act, I certify that I have obtained a written permission from the copyright owner(s) to include such material(s) in my dissertation.

I declare that this is a true copy of my dissertation, including any final revisions, as approved by my dissertation committee and the Graduate Studies office, and that this dissertation has not been submitted for a higher degree to any other University or Institution.

Abstract

This dissertation proposes a number of significant enhancements to the conventional Marciniak-Kuczynski (MK) approach including a more realistic definition of the imperfection band, consideration of strain rate sensitivity and the effect of material anisotropy. Each enhancement was evaluated by comparing the predictions to experimental FLCs found in the literature.

An analytical method of determining the forming limit curve (FLC) of sheet materials was developed by Marciniak & Kuczynski in 1967 and has been used extensively since then. In the current research, a numerical code was developed based on the MK analysis in order to predict the FLCs of sheet metals undergoing plane-stress loading along non-proportional strain paths. The constitutive equations that govern plastic behaviour were developed using Hill's 1948 yield function and the associated flow rule.

Stress-based FLCs were also predicted with this MK analysis code and the strain-path dependency of SFLCs was investigated for different non-proportional loading histories. It was found that the SFLC remains essentially unchanged for lower magnitudes of prestrain, but after significant levels of prestrain, it was observed to shift up somewhat toward the vicinity of plane-strain deformation.

Two different work hardening models were implemented in the MK model to predict the FLC. Both isotropic hardening and mixed isotropic – nonlinear kinematic hardening models were used in cases that involve unloading and subsequent reloading along a different strain path. The FLC predicted with the mixed hardening model was in better agreement with experimental data when the prestrain was in the domain of the positive minor strains, but the assumption of isotropic hardening led to acceptable agreement with experimental data when the prestrain was in the domain of the negative minor strains.

The consideration of a through-thickness stress applied during the forming process was also added to the model and it was shown that the normal stress has a positive effect on formability. Moreover, changes in certain mechanical properties can significantly increase the sensitivity to the normal stress.

Finally, a non-quadratic yield criterion was implemented into the predictive model and it was found that, generally, a non-quadratic yield function leads to more accurate predictions of the FLC.

Dedicated to my beloved family

Acknowledgments

This work required me to stretch beyond my previous training and preparation and would not have been possible without the help and support of the people I now wish to acknowledge.

First, I would like to warmly thank my advisor, Dr. Daniel E. Green for his guidance, support, personality, patience and for his insistence on excellence, and unwillingness to settle along the way. It was fortunate for me to be a member of his research group.

It is my pleasure to take this opportunity to acknowledge the members of my dissertation committee, Dr. D. Watt, Dr. W. Altenhof and Dr. J. Johrendt for their helpful comments and constructive suggestions.

I would also like to thank Dr. L. M. Smith from Oakland University for accepting to be the external examiner of this dissertation and for all the valuable comments on my work.

I also gratefully acknowledge the financial support of Auto21 – Network of Centres of Excellence and Ontario Centres of Excellence.

I would like to express my appreciation for my officemates for the good time we spent together as friends, sharing different experiences and intellectual discussions.

Finally, I would like to thank my parents, my sisters, and brothers, for their endless love, support, and understanding. It was my family's unwavering support that helped me through the harder times.

Table of Contents

Content	Page
Declaration of Co-Authorship/Previous Publication	iii
Abstract	v
Dedication	vii
Acknowledgments	viii
List of Tables	xiii
List of Figures	xiv
List of Appendices	xviii
List of Symbols	xix
Chapter 1. Forming limits of sheet metals	1
1.1. Introduction	1
1.2. Motivations	4
1.3. Objectives	6
1.4 Overview of the dissertation	7
1.5. References	8
Chapter 2. Literature review	10
2.1. Introduction	10
2.2. Theoretical methods in FLC calculation	11
2.2.1. Void/ Damage models	11
2.2.2. Bifurcation methods	14
2.2.2.1. Swift's diffuse neck instability criterion	14
2.2.2.2. Bifurcation method with flow theory	15
2.2.2.3. Bifurcation method with vertex theory	16
2.2.2.4. Perturbation analysis	18

2.2.3. Marciniak and Kuczynski method	19
2.3. Stress-based forming limit curve (SFLC)	25
2.4. Strain hardening law	29
2.4.1. Isotropic hardening	30
2.4.2. Kinematic hardening	31
2.4.3. Mixed hardening	34
2.5. Methodology	35
2.5.1. Definition of the imperfection factor	35
2.5.2. Orientation of the imperfection band	36
2.5.3. Extend calculations for multi-stage loading	36
2.5.4. Investigation on the path dependency of SFLC	37
2.5.5. Hardening rules	37
2.5.6. Yield function effect	39
2.5.7. Through-thickness stress component effect	40
2.6. References	40

Chapter 3. Investigation on the strain-path dependency of stress-based forming

limit curves	46
3.1. Introduction	46
3.2. Theoretical analysis	49
3.2.1. Strain-based forming limit curves	49
3.2.2. Stress-based forming limit curves	55
3.3. Results	56
3.3.1. Material characterization	56
3.3.2. Validation of the MK model	56
3.3.3. Predicted FLCs for bilinear strain paths	59
3.3.4. Stress-based forming limit curves	62
3.4. Conclusion	69
3.5. References	70

Chapter 4. Prediction of sheet forming limits with Marciniak and Kuczynski analysis using combined isotropic–non linear kinematic hardening	73
4.1. Introduction	73
4.2. Theoretical approach	76
4.3. Results and discussion	86
4.3.1. Material characterization	86
4.3.2. Validation of the MK model	89
4.3.3. FLCs in bilinear strain paths	93
4.4. Conclusion	99
4.5. References	100
Chapter 5. Influence of out-of-plane compression stress on limit strains in sheet metals	103
5.1. Introduction	103
5.2. Theoretical approach	106
5.3. Experimental validation of the modified MK model	112
5.3.1. Description of materials	112
5.3.2. Validation of the proposed MK model	113
5.4. Influence of the through-thickness stress on the FLC	118
5.5. Influence of mechanical properties on the sensitivity of FLC to out-of-plane stresses	119
5.6. Conclusion	129
5.7. References	130
Chapter 6. Prediction of FLC using Hosford's 1979 yield function	133
6.1. Introduction	133
6.2. Hill's 1948 yield criterion	135
6.2.1. Description of Hill's 1948 yield criterion	135
6.2.2. Advantages and disadvantages of Hill's 48 yield criterion	139
6.3. Non-Quadratic yield Criteria	140
6.3.1. Hosford's 1979 yield criterion	140

6.3.2. Hill's 1979 yield criterion	142
6.3.3. Hill's 1990 yield criterion	143
6.3.4. Hill's 1993 yield criterion	143
6.3.5. Barlat and Lian's 1989 yield criterion	144
6.3.6. Barlat's Yld2000-2d yield criterion	144
6.3.7. Other yield criteria	145
6.4. Results	146
6.5. Conclusion	153
6.6. References	153
Chapter 7. Summary and conclusions	157
7.1. Summary	157
7.2. Conclusions	158
7.3. Future work	160
Appendix A. Determination of $\eta=d\epsilon_e^b/d\epsilon_e^a$ ratio in MK analysis	162
Appendix B. Error between predicted and experimental FLCs	165
VITA AUCTORIS	168

List of Tables

Table	Page
3.1. Material properties of AISI-1012 low carbon steel [3.1]	56
3.2. Average mechanical properties of AA-2008-T4 [3.2]	56
4.1. Material properties of AISI-1012, low carbon steel [4.18]	86
4.2. Material properties of 2008-T4 aluminum [4.19]	86
5.1. Mechanical properties of materials	113
A.1. Final values of η at the onset of instability for AISI-1012 steel	164
B.1. Percent error of predicted FLCs	165

List of Figures

Figure	Page
Figure 1.1. Typical FLC of an aluminum alloy [1.3]	3
Figure 2.1. Damage (stages of ductile fracture) [2.1]	12
Figure 2.2. Schematic of the MK model with a thickness imperfection in the sheet	20
Figure 2.3. Code structure to predict FLC and SFLC [2.26]	25
Figure 2.4. Typical stress-based forming limit curve (SFLC)	28
Figure 2.5. (a)- Isotropic hardening (b) Schematic equivalent stress-strain curve [2.48]	30
Figure 2.6. Schematic linear kinematic hardening of materials with (a) nonlinear stress-strain curve (b) bilinear stress-strain curve [2.48]	33
Figure 2.7. Schematic plot of stress-strain behavior under (A) isotropic or kinematic hardening under proportional loading and (B) isotropic hardening following unloading and reloading under a different loading condition, and (C) kinematic hardening following unloading and reloading under a different loading condition. [2.44]	38
Figure 3.1. Thickness imperfection in the MK method	49
Figure 3.2. Comparison of theoretical and experimental FLC AISI-1012 low carbon steel in the as-received state	57
Figure 3.3. Theoretical and experimental FLCs of AA-2008-T4 with 4 and 12 percent equibiaxial prestrain after calibrating the MK model to the as-received FLC	58
Figure 3.4. Theoretical and experimental FLCs of AA-2008-T4 with 5 and 12 percent uniaxial prestrain after calibrating the MK model to the as-received FLC.	58
Figure 3.5. Effect of 0.20 uniaxial prestrain on FLC for AISI-1012 steel.....	60
Figure 3.6. Effect of 0.20 plane-strain prestrain on FLC for AISI-1012 steel.....	61
Figure 3.7. Effect of 0.20 equibiaxial prestrain on FLC for AISI-1012 steel.....	61
Figure 3.8. Predicted FLCs after 0.20 prestrain in uniaxial tension, plane-strain tension, and equibiaxial tension for AISI-1012 steel	62
Figure 3.9. Stress-based forming limit curve (SFLC) of as-received AISI-1012 steel.....	63
Figure 3.10. Comparison of the SFLC after different levels of prestrain in uniaxial tension with the as-received SFLC of AISI-1012 steel	64

Figure 3.11. Comparison of the SFLC after different levels of prestrain in equibiaxial tension with the as-received SFLC of AISI-1012 steel	64
Figure 3.12. Comparison of the SFLC after an effective prestrain $\bar{\epsilon} = 0.45$ in uniaxial and equibiaxial tension with the as-received SFLC of AISI-1012 steel.....	65
Figure 3.13. Deviation in major stress between prestrained and as-received SFLCs for an effective prestrain $\bar{\epsilon} = 0.10$ in AISI-1012 steel sheets.....	66
Figure 3.14. Deviation in major stress between prestrained and as-received SFLCs for an effective prestrain $\bar{\epsilon} = 0.20$ in AISI-1012 steel sheets.....	66
Figure 3.15. Deviation in major stress between prestrained and as-received SFLCs for an effective prestrain $\bar{\epsilon} = 0.45$ in AISI-1012 steel sheets.....	67
Figure 3.16. Maximum deviation in major stress between prestrained and as-received SFLCs for different effective prestrain values in AISI-1012 steel sheets	68
Figure 4.1. Thickness imperfection in MK method.....	76
Figure 4.2. Schematic representation of isotropic hardening [4.29].....	79
Figure 4.3. Schematic representation of combined isotropic and kinematic hardening [4.29].....	79
Figure 4.4. Experimental and predicted stress-strain curves for AISI-1012 steel alloy. ..	88
Figure 4.5. Stress-strain curves predicted with different hardening laws for 2008-T4 aluminum.	88
Figure 4.6. Comparison of predicted and experimental FLCs of as-received AISI-1012 steel sheets.	90
Figure 4.7. Comparison of predicted and experimental FLCs of AISI-1012 steel after 8% prestrain in equibiaxial tension	91
Figure 4.8. Comparison of predicted and experimental FLCs of AISI-1012 steel after 10% prestrain in uniaxial tension.....	91
Figure 4.9. Comparison of predicted and experimental FLCs of as-received 2008-T4 aluminum sheets.....	93
Figure 4.10. Comparison of predicted and experimental FLCs of 2008-T4 aluminum after different levels of prestrain in equibiaxial tension.....	94
Figure 4.11. Comparison of predicted and experimental FLCs of 2008-T4 aluminum after different levels of prestrain in uniaxial tension	95

Figure 4.12. FLCs predicted after different amounts of prestrain in uniaxial tension using the MK model with isotropic and mixed hardening.	96
Figure 4.13. FLCs predicted after different amounts of prestrain in plane-strain tension using the MK model with isotropic and mixed hardening.....	97
Figure 4.14. FLCs predicted after different amounts of prestrain in equibiaxial tension using the MK model with isotropic and mixed hardening.....	97
Figure 4.15. Percentage increase in FLC_0 from IH to mixed hardening after different amounts of prestrain in different loading paths.	98
Figure 5.1. Thickness imperfection in the MK model	106
Figure 5.2. Comparison of predicted and experimental FLCs of AISI-1012 steel sheet in-plane stress condition [5.14]	114
Figure 5.3. Comparison of predicted and experimental FLCs of AA6011 aluminum sheets under 15MPa internal pressure [5.15].....	115
Figure 5.4. Comparison of predicted and experimental FLCs of STKM-11A steel sheet under 56MPa internal pressure [5.16].....	116
Figure 5.5. FLC of AISI-1012 sheet steel predicted as a function of the applied normal stress.....	118
Figure 5.6. FLC of a sheet material that differs from AISI-1012 only by its strain hardening coefficient ($n=0.70$), predicted as a function of the applied normal stress	120
Figure 5.7. Increase in FLC_0 as a function of the applied normal stress for two sheet steels that differ only by their strain hardening coefficient ($n=0.35$ and $n=0.70$)	120
Figure 5.8. FLC of a sheet material that differs from AISI-1012 only by its strain rate sensitivity ($m=0.030$) predicted as a function of the applied normal stress.....	121
Figure 5.9. Increase in FLC_0 as a function of the applied normal stress for two sheet steels that differ only by their strain rate sensitivity ($m=0.015$ and $m=0.030$).....	122
Figure 5.10. FLC of a sheet material that differs from AISI-1012 only by its plastic anisotropy coefficients ($R_0=2.8$ and $R_{90}=2.7$), predicted as a function of the applied normal stress	123
Figure 5.11. Increase in FLC_0 as a function of the applied normal stress for two sheet steels that differ only by their plastic anisotropy coefficients ($R_0=1.4$ and $R_{90}=1.35$ versus $R_0=2.8$ and $R_{90}=2.7$).....	124

Figure 5.12. FLC of a sheet material that differs from AISI-1012 only by its grain size ($d_0=50 \mu\text{m}$), predicted as a function of the applied normal stress	125
Figure 5.13. Increase in FLC_0 as a function of the applied normal stress for two sheet steels that differ only by their initial grain size ($d_0=25 \mu\text{m}$ and $d_0=50 \mu\text{m}$)	126
Figure 5.14. FLC of a sheet material that differs from AISI-1012 only by its initial thickness ($t_0=1.25\text{mm}$), predicted as a function of the applied normal stress.....	126
Figure 5.15. Increase in FLC_0 as a function of the applied normal stress for two sheet steels that differ only by their initial thickness ($t_0=1.25\text{mm}$ and $t_0=2.5\text{mm}$).....	127
Figure 5.16. Increase in FLC_0 as a function of the applied normal stress for sheet steels that differ from AISI-1012 by only one mechanical property (see Table 5.1)	128
Figure 6.1. Von-Mises and Tresca yield surfaces [6.3]	134
Figure 6.2. Comparison of predicted and experimental FLCs of as-received AISI-1012 steel sheets	147
Figure 6.3. Comparison of predicted and experimental FLCs of AISI-1012 steel after 8% prestrain in equibiaxial tension	148
Figure 6.4. Comparison of predicted and experimental FLCs of AISI-1012 steel after 10% prestrain in uniaxial tension.....	148
Figure 6.5. Comparison of calibrated/predicted and experimental FLCs of as-received 2008-T4 aluminum sheets.....	149
Figure 6.6. Comparison of predicted and experimental FLCs of 2008-T4 aluminum after 4 % prestrain in equibiaxial tension.....	150
Figure 6.7. Comparison of predicted and experimental FLCs of 2008-T4 aluminum after 12 % prestrain in equibiaxial tension.....	151
Figure 6.8. Comparison of predicted and experimental FLCs of 2008-T4 aluminum after 5 % prestrain in uniaxial tension.....	152
Figure 6.9. Comparison of predicted and experimental FLCs of 2008-T4 aluminum after 12 % prestrain in uniaxial tension.....	152
Figure A.1. Variation of $\eta=d\epsilon_e^b/d\epsilon_e^a$ during the computation of a FLC.....	163

List of Appendices

<u>Appendix</u>	<u>Page</u>
Appendix A. Determination of $\eta = d\varepsilon_e^b / d\varepsilon_e^a$ ratio in MK analysis	162
Appendix B. Error between predicted and experimental FLCs	165

List of Symbols

ρ	strain path defined as the ratio of the two principal strains $\rho = \varepsilon_2 / \varepsilon_1$
α, β, r	principal stress ratios
θ	angle between the normal to the neck and the major strain direction
σ_e, ε_e	effective stress and strain
n	strain hardening coefficient
m	strain rate sensitivity coefficient
k	material constant in stress-strain relationship
$\varepsilon_1, \varepsilon_2, \varepsilon_3$	true principal plastic strains
$\sigma_1, \sigma_2, \sigma_3$	true principal plastic stresses
$d\varepsilon_1, d\varepsilon_2, d\varepsilon_3$	true principal plastic strain increments
t	sheet metal thickness
F_{nn}, F_{nt}	normal and shear forces
σ_{nn}, σ_{nt}	normal and shear stresses
f	initial thickness ratio
φ	groove orientation
W^p	plastic work per unit volume
S_{ij}	deviatoric stress tensor
α_{ij}	backstress tensor
Y	yield stress
c, γ	material constants in kinematic hardening law
$d\mu$	material parameter
R_z	surface roughness
C	material constant in surface roughness relation
d_0	grain size
G, F, H, P	anisotropy constants
h	plastic potential function
R_0, R_{90}	Lankford's coefficients
$d\lambda'$	plastic multiplier

N	anisotropic constants tensor
η	effective strain ratio
$\tau_x^y, \tau_y^y, \tau_z^y$	yield shear stresses
a	positive integer in non-quadratic yield function
λ	ratio between the effective strain and the major principal strain
ξ	ratio between the effective stress and the major principal stress
p, q	dimensionless anisotropic coefficients
a, c, h, p	anisotropy coefficients
L', L''	linear transformation tensors

Chapter 1

Forming limits of sheet metals

1.1. Introduction

The stamping of tin-plated steel sheets to form food containers around 1850 laid the foundation for the sheet metal working industry as it is known today. Although metal stamping was well established by 1900, the main growth of this industry came when mass production became a common feature of the automobile industry. Another surge came with the rapid expansion of the home appliance industry after World War I with such items as vacuum cleaners, washing machines, refrigerators and toasters. All these developments created a large demand for sheet metal which was met by low-carbon steel, which offered the advantages of uniform thickness, good surface finish and low cost.

The most predominant sheet-metal forming operation, stamping, consists of forming a sheet metal blank between two mating dies. It can also be noted that stamping involves essentially two different deformation modes: drawing and stretching. As a result of the two dies closing during a press stroke, metal in the central part of the blank is typically stretched over the punch face whereas drawing takes place in the peripheral region of the blank as it is drawn into the die cavity. The formability of a sheet metal is defined as its ability to undergo plastic deformations, either in stretching or drawing modes, without failure.

There are a variety of possible failures in sheet metal stamping that would require rejecting a part: scoring, wrinkling, necking, splitting or tearing, not to mention parts that fail to meet dimensional specifications or parts that exhibit unacceptable cosmetic appearance. However, the most common and most obvious failure is that of splitting or tearing of the sheet metal, which is a result of excessive and non-uniform deformation. Splitting is usually preceded by a series of increasingly more severe evidences of damage as the deformation proceeds: the first evidence of excessive deformation may appear simply as a roughening of the sheet surface. The next stage in the progression of damage is the onset of necking which appears as a narrow band in which there is a detectable reduction in thickness. As deformation progresses further, the strains localize in this band and necking becomes more severe until ultimately the reduced thickness of metal is not able to bear the load and the sheet tears. The formability of most sheet metals is limited by the occurrence of localized necking in the stamped part.

Punch-stretch tests or simply “cupping” tests have been used for a long time to qualitatively assess the formability of sheet materials. The main parameter that is determined during a cupping test is the strain to fracture. The punch-stretch test consists simply of clamping a blank firmly around its edges between two rings or dies and applying a force to the central area of the specimen, using a punch, until the cup fractures. The testing procedure is described in the ASTM Standard E643. Several punch-stretch tests have been developed throughout the years. Unfortunately, these simple “cupping” tests do not satisfactorily predict the formability of a sheet; only rough differences in formability can be determined. This has led to the development of improved simulative tests, described in the next paragraphs. Nevertheless, “cupping” tests are routinely used for inspection purposes since they provide a quick indication of ductility; they also show changes in surface appearance of the sheet during forming.

The poor correlation between the common “cupping” test and the actual performance of the sheet metal in a stamping operation led investigators to search for more fundamental formability parameters. A significant breakthrough came in 1963, when Keeler and Backofen [1.1] reported that during sheet stretching, the onset of localized necking required a critical combination of major and minor strains (along two perpendicular directions in the plane of the sheet). Subsequently, this concept was

extended by Goodwin [1.2] to drawing deformations and the resulting curve in principal strain space is known as the Keeler-Goodwin curve or the forming limit curve (FLC). A typical FLC is shown in Figure 1.1 [1.3].

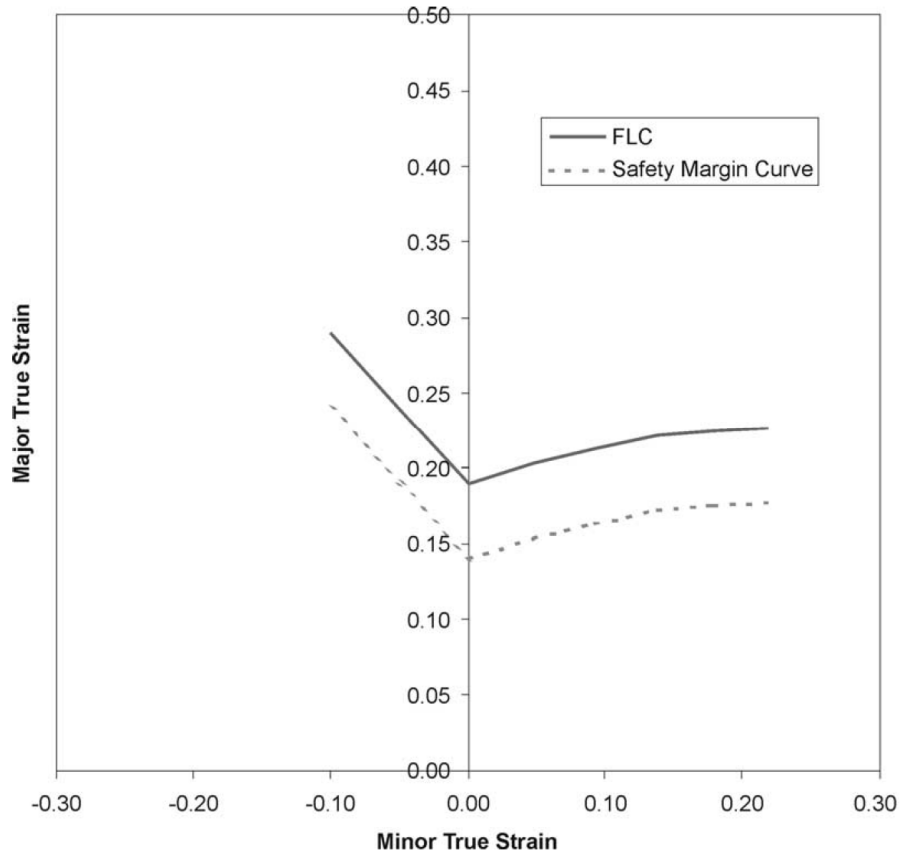


Figure 1.1: Typical FLC of an aluminum alloy [1.3]

The FLC has become an important tool for formability evaluation and it is obtained experimentally by stretching sheet metal samples over a hemispherical punch. A regular grid electro-etched or printed onto the un-deformed blank enables principal surface strains to be measured: the greater of the two principal strains is called the major strain and is always positive, whereas the minor strain can be either negative or positive depending on the mode of deformation.

The left side of the FLC (negative minor strains) is obtained by stretch forming rectangular strips or notched blanks of various widths and interrupting each test at the

onset of necking. The geometry of the blank determines the strain path (i.e. the ratio of principal strains) which varies from uniaxial tension to plane-strain tension. The right side of the FLC is obtained by using rectangular blanks of increasing width and by applying lubrication to the blank: necking can thus be obtained for strain paths that vary from plane-strain to balanced biaxial stretching. The FLC is obtained by plotting a lower-bound line beneath all data points where necking was observed. The region under the curve is therefore considered to be safe for any deformation mode, whereas combinations of principal strains that lie above the FLC lead to a part that is either failed or presents a risk of failure. The higher the FLC lies in principal strain space, the greater the formability of the sheet material. In order to account for variations in the stamping process, however, another curve is generally plotted at 10% strain below the FLC (Figure 1.1) thus creating a marginal zone between the two curves. And industrial practice requires that a stamped part be rejected if there are any locations in the part where the combination of principal strains falls in the marginal or failure zones.

The FLC has been widely used around the world as a measure of sheet metal formability in the metal forming industry for almost half a century. It is routinely used to evaluate the forming severity of virtual parts after the numerical simulation of a forming process and is the basis for modifying or validating tool design and process design. The FLC is also used to assess the forming severity of prototype parts after they are formed and provides a basis for making minor modifications to existing stamping dies. Moreover, the FLC can be used on occasion during a production run to determine how the wear in the dies might affect the quality of the parts and the robustness of the process.

1.2. Motivations

Although the FLC has been such an effective tool in the metal forming industry, the experimental determination of FLC is relatively costly as it requires specialized equipment, tooling and experienced personnel. It is also time-consuming to conduct the formability tests, measure the strains and reliably interpret where in strain space the onset of necking actually begins. The experimental determination of FLC must be done carefully, consistently and with an acceptable level of accuracy since it is used to

establish the quality of large volumes of production parts. The known variability in FLC data and the somewhat subjective nature of the experimental determination of FLC have underscored the need for a more objective determination of the FLC on the basis of theoretical models.

It is well known that sheet deformation in many industrial metal forming processes is characterized by nonlinear strain paths and it has been observed by many researchers [1.4-1.10] that the as-received FLC can translate and distort significantly in strain space due to a nonlinear loading path. This signifies that the as-received FLC cannot be used to assess the forming severity of parts that were formed, say in multi-stage forming operations. Furthermore, since each material point in such a component may follow a different (nonlinear) loading path, therefore each location in the part potentially has a different FLC. It is obviously not possible to experimentally determine the FLC for every nonlinear strain path in a given part, and even if it was, it would be practically unmanageable to accurately carry out an analysis of forming severity. So although 80% of stamped parts can be reliably evaluated with the as-received FLC, there are nevertheless a number of complex stamped parts and parts formed in multistage forming processes where the as-received FLC is not adequate to carry out formability analyses. For this reason alone, researchers have been motivated to develop reliable theoretical methods to predict sheet forming limits.

The advantages of such predictive FLC models are many. The main benefit is no doubt the fact that an FLC can be predicted almost instantaneously and at very little cost using known mechanical properties that can easily be determined by standard tests. Moreover, the underlying theoretical foundation of a predictive model enables the user to consider a wide range of forming conditions, deformation modes and strain histories which would be unduly difficult or costly to carry out experimentally. There are very definite incentives for developing an accurate model to predict the onset of plastic instability (i.e. necking) in sheet metals.

The formability of most sheet metals is limited by the occurrence of localized necking. However, the prediction of neck initiation and growth in thin metal sheets is by no means a simple task. Nevertheless much theoretical research has been conducted in an attempt to predict the FLC. A review of this research shows that the FLC is affected by

many different factors such as the strain history, crystallographic texture and anisotropy, yield behaviour, work hardening behaviour, the presence of through-thickness stresses, microstructure and material inhomogeneity as well as other parameters which all deserve due consideration. In spite of the challenge, the ability to accurately predict the onset of localized necking would indeed be of great benefit to the sheet forming industry as it would provide a reliable and unambiguous failure criterion for evaluating complex, multi-stage metal forming processes, accelerate tool design and help reduce manufacturing costs.

Among the various theoretical approaches for predicting the FLC, the MK method has probably been the most widely used. The MK approach is a mechanistic approach proposed by Marciniak & Kuzcynski [1.11], in which the inhomogeneity that exists in the sheet metal is modeled as a geometric band with a slightly reduced thickness compared to the rest of the sheet. Biaxial stresses are progressively applied to the sheet and the onset of necking is determined when the ratio of strains in the band to those outside the band reach a critical value. Since the original MK method was proposed in 1967, substantial improvements have been proposed by various researchers to make predictions more accurate. With the incorporation of more realistic constitutive models, the predicted FLC correlate reasonably well with as-received experimental FLC data for most sheet metals. As a result, the MK method is arguably the theoretical tool most commonly used to predict sheet metal forming limits, and this method will be discussed at greater length throughout this dissertation.

Other researchers have attempted to predict the FLC of sheet metals by using analytical bifurcation [1.12-1.14] or damage methods [1.15-1.16]. However, the predicted results have not always been convincing, although they do provide explicit and simplified solutions for the critical angles and the corresponding critical strains of localized neck formation in sheet metals.

1.3 Objectives

In spite of many years of research in this field, most of the predictive methods for FLC determination are still insufficiently accurate for more complex forming processes,

and there is a real need for further research to improve the current models. The main objective of this research is to develop more advanced numerical tools to predict the forming limits of sheet metals more accurately and reliably than is currently possible. The MK method was selected as the basic approach and several theoretical developments have been proposed to enhance the MK method and improve its ability to predict FLC under complex forming conditions, including nonlinear strain paths that are common in multistage forming operations. In addition, the influence of critical material parameters (e.g. work hardening behaviour) and mechanistic parameters (e.g. through-thickness stresses) on the forming limits of metal sheets will also be investigated.

1.4 Overview of the dissertation

The second chapter of this dissertation presents a comprehensive overview of the various theoretical approaches that have been proposed to predict the onset of necking in thin metal sheets, and also delves into some of the aspects of constitutive modelling that are considered essential to improve the prediction of FLC.

It has been proposed by some researchers that the onset of necking depends on reaching a critical state of stress rather than a critical state of strain. The main advantage presented in favour of a stress-based FLC is its strain path independence. The third chapter is an investigation on the uniqueness of forming limits in stress space, and is an exact reproduction of a paper jointly written by the present author and his supervisor and published in the International Journal of Material Forming [1.17].

Different sheet metals exhibit different work hardening behaviour. And the constitutive description of the material should correctly account for the evolution of the yield locus as it work hardens. However, most FLC prediction methods have employed the overly-simplistic isotropic hardening rule for forming limit determination. Different hardening models were implemented into the MK analysis for FLC prediction and this work is described in the fourth chapter of the dissertation. Again, this chapter is a reproduction of a paper co-authored by the present writer and published in the International Journal of Mechanical Sciences [1.18].

FLC determination theories have usually been developed for plane stress conditions, although there are many industrial forming processes in which material undergoes significant out-of-plane stresses. Chapter five is dedicated to studying the influence of this through-thickness stress on limit strains in sheet metals. Once again, this chapter is a reproduction of a paper published in the International Journal of Material Forming [1.19].

Non-ferrous sheet materials often exhibit a normal anisotropy coefficient that is less than 1.0, and it is well known that a quadratic yield function cannot predict their plastic behaviour correctly. Many non-quadratic yield criteria have been proposed for aluminum alloys and the sixth chapter describes the implementation of such a non-quadratic yield function into the MK analysis.

The final chapter presents the conclusions of this research and proposes other improvements that can be implemented into the MK predictive model.

1.5. References

- [1.1] Keeler S.P., Backhofen W.A., Plastic instability and fracture in sheet stretched over rigid punches, *ASM Transactions Quarterly* 56 (1964) 25–48.
- [1.2] Goodwin G.M., Application of strain analysis to sheet metal forming in the press shop, *SAE* (1968) paper 680093.
- [1.3] Stoughton T.B., Zhu X., Review of theoretical models of the strain-based FLD and their relevance to the stress-based FLD, *International Journal of Plasticity* 20 (2004) 1463-1486.
- [1.4] Graf A., Hosford W., Effect of changing Strain paths on Forming Limit Diagrams of Al 2008-T4, *Metallurgical Transactions* 24A (1993) 2503- 2512.
- [1.5] Kleemola H.J., Pelkkikangas M.T., Effect of pre-deformation and strain path on the forming limits of steel, copper and brass, *Sheet Metal Industries* 63 (1977) 559–591.
- [1.6] Arrieux R., Bedrin C., Boivin M., Determination of an intrinsic forming limit stress diagram for isotropic sheets, *Proceedings of the 12th IDDRG Congress* 2 (1982) 61–71.

- [1.7] Gronostajski I., Sheet metal forming limits for complex strain paths, *Journal of Mechanical Working Technology* 10 (1984) 349–362.
- [1.8] Stoughton T.B., A general forming limit criterion for sheet metal forming, *International Journal of Mechanical Sciences* 42 (2000) 1–27.
- [1.9] Kuwabara T., Yoshida K., Narihara K., Takahashi S., Anisotropic plastic deformation of extruded aluminum alloy tube under axial forces and internal pressure, *International Journal of Plasticity* 21 (2005) 101–117.
- [1.10] Butuc M.C., Gracio J.J., Barata da Rocha A., An experimental and theoretical analysis on the application of stress-based forming limit criterion, *International Journal of Mechanical Sciences* 48 (2006) 414–429.
- [1.11] Marciniak Z., Kuczynski K., Limit strains in the processes of stretch-forming sheet metal, *International Journal of Mechanical Sciences* 9 (1967) 609–620.
- [1.12] Swift H.W., Plastic Instability under Plane Stress, *Journal of Mechanics and Physics of Solids* 1 (1952) 1-18.
- [1.13] Hill R., On discontinuous plastic states, with special reference to localized necking in thin sheets, *Journal of Mechanics and Physics of Solids* 1 (1952) 19–30.
- [1.14] Lin T.H., Physical theory of plasticity, *Advances in Applied Mechanics*, Vol. 11, ed. Chia-Shun Yih, Academic Press, New York (1971) 256-311.
- [1.15] Chu C.C., Needleman A., Void nucleation effects in biaxially stretched sheets, *Journal of Engineering Materials and Technology* 102(1980) 249- 256.
- [1.16] Lemaitre J., A continuous damage mechanics model for ductile fracture, *Journal of Engineering Materials and Technology* 107 (1985) 83-89.
- [1.17] Nurcheshmeh M., Green D.E., Investigation on the strain-path dependency of stress-based forming limit curves, *International Journal of Material Forming* 5 (2011) 25-37.
- [1.18] Nurcheshmeh M., Green D.E., Prediction of sheet forming limits with Marciniak and Kuczynski analysis using combined isotropic–non linear kinematic hardening, *International Journal of Mechanical Sciences* 53 (2011) 145-153.
- [1.19] Nurcheshmeh M., Green D.E., Influence of out-of-plane compression stress on limit strains in sheet metals, *International Journal of Material Forming*, Accepted on 18 March 2011, Manuscript Number: IJFO-D-10-00144.

Chapter 2

Literature review

2.1. Introduction

Various theoretical and analytical methods have been developed and employed by different researchers to predict the forming limits of sheet metals. In this chapter the most common theoretical methods of FLC prediction will be reviewed, along with their historical background and development: these include void-damage models, bifurcation methods, and the Marciniak-Kuczynski (MK) approach.

Researchers have also proposed that the forming limits of sheet materials are more likely dependent on locally reaching a critical state of stress than a critical state of strain. Therefore an increasing number of researchers and engineers have adopted the stress-based forming limit (SFLC) to evaluate the forming severity of metal forming operations. The background as well as the distinct advantages of this approach will be discussed in detail in this chapter.

Each of the above-mentioned formulations for calculating forming limits is based on the classical continuum plasticity theory in which a yield function describes the onset of plastic deformation in stress space and a strain hardening law defines the evolution of the yield locus as plastic deformation progresses. Since both these elements have a profound influence on the prediction of the plastic behaviour of metallic materials, it is

essential that the prediction of forming limits be based upon the most representative yield criteria and hardening laws. Therefore, the main hardening rules considered throughout this research – isotropic hardening, kinematic hardening, and mixed isotropic-kinematic hardening laws – will be presented and briefly discussed in this chapter. A more detailed investigation on the influence of the strain hardening model will also be presented in chapter 4. The influence of the yield function will be reviewed in detail in chapter 6.

Finally, this chapter concludes with a presentation of the different aspects of the prediction of FLC that were specifically developed and that constitute original contributions to this field of research.

2.2. Theoretical methods in FLC calculation

Three different theoretical approaches have been proposed and utilized to predict the FLC as accurately as possible. They can be described as follows:

- a) Void/damage models
- b) Bifurcation methods
- c) Marciniak & Kuczynski (MK) analysis

2.2.1. Void/Damage models

At the microscopic scale, every sheet metal contains defects and inhomogeneities such as particles, inclusions, voids and micro-cracks which affect the strength and load-bearing capacity of the material. When plastic deformation occurs in ductile metal alloys, voids will nucleate at the interface between hard particles and the surrounding material, at grain boundaries or between different phases in the microstructure. As deformation progresses further, the number and the size of voids increases (see Figure 2.1). This phenomenon was the reason some researchers began to study the role of micro-defects on forming limits of the sheet metals and their investigations led to the development of damage-based FLC criteria.

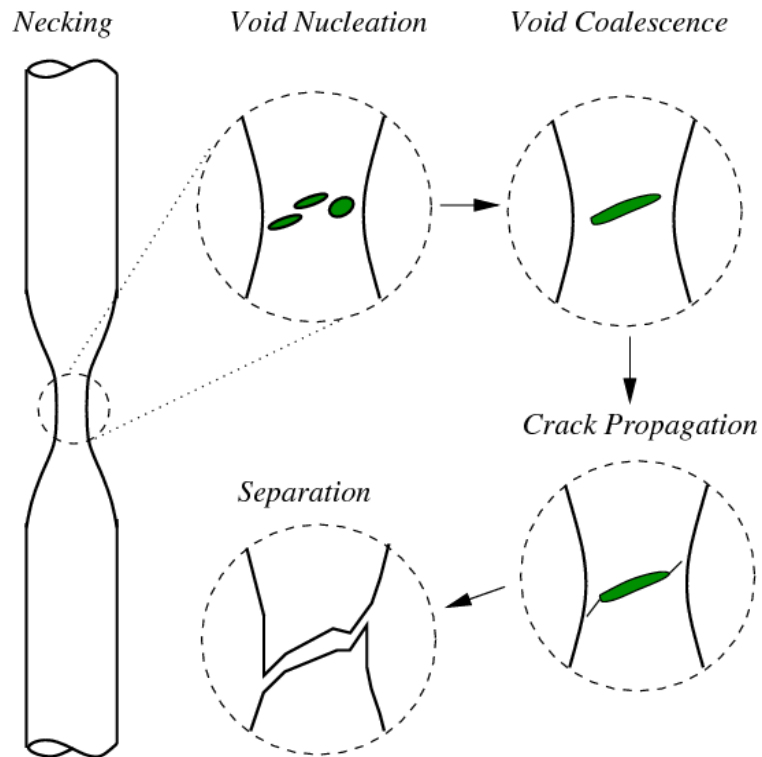


Figure 2.1. Damage (stages of ductile fracture) [2.1]

In 1978, Needleman and Triantafyllidis [2.2] investigated the role of void growth on the onset of localized necking in biaxially stretched sheet metals. This research was conducted based-on the Marciniak-Kuczynski analysis [2.3-2.4] and constitutive relations proposed by Gurson [2.5]. They concluded that void growth has a weakening effect on biaxially stretched sheets, and the appearance of a localized neck is the evidence of the forming limit for every loading path. In their analysis, the material inhomogeneity was defined in terms of micro-defects and the forming limit was predicted when the evolution of these micro-defects reached a critical limit. However, their results showed that this approach is not suitable for materials with a high rate of work hardening.

In 1980, Chu and Needleman [2.6] considered the influences of the void density variation during deformation on the forming limit curves. Their work showed that a strain-controlled void nucleation process has a significant effect on the shape of the forming limit curve; however a stress-controlled void nucleation process has little influence on the shape of the FLC.

In 1985, Lemaitre [2.7] employed the concept of effective stress and rules of thermodynamics to introduce a new damage model. The model was applicable to

isotropic, ductile materials. The work of Lemaitre showed that the distribution of voids and inclusions is the same in all directions. This work also indicated that damage varies linearly with the equivalent strain.

In 1977, Chow, Yu, and Demeri [2.8] proposed a damage model to calculate forming limit curves and predicted the FLC of a 6111-T4 aluminum alloy. They considered the effect of micro-cracks and micro-voids on sheet metal failure and divided the forming process into different stages including diffuse necking, localized necking and rupture. These researchers showed that orthotropic damage occurs rather than isotropic damage at large plastic strains. Since their model was developed to represent this type of damage, their predictions were more accurate than those of conventional models which assume isotropic damage. Later in 1998, Demeri, Chow, and Tai [2.9] modified their original formulation to include the influence of strain path changes on the FLC of the vacuum-degassed, interstitial-free (VDIF) steel sheets. The proposed model was verified against experimental FLC data that were generated for nonlinear loading paths. They demonstrated that a damage-based model can accurately predict FLC for nonlinear loading paths; their results showed that a plane-strain prestrain (in the range of $\varepsilon_1 = 0.02 - 0.08$) has no significant effect on the FLC of VDIF steel sheets.

One of the most important deficiencies of these damage models is the very approximate way in which the void volume fraction and the constants in the stress/strain evolution laws are estimated. This is difficult to overcome, however, because the experimental measurement of void volume fraction is difficult, and even current measurement methods are still insufficiently precise to make reliable predictions of FLC based on microstructural damage.

The physical damage mechanisms that take place at a microscopic scale and upon which these damage theories are developed can indeed be observed and modelled, but the direct extrapolation of microscopic behaviour to the macroscopic scale may not always be valid. Moreover, there are no straightforward experimental methods to accurately measure damage density in metals at the micro-scale which means that the options for improving damage-based models are somewhat limited and this method has not been verified experimentally in different sheet metals.

2.2.2. Bifurcation methods

The approach known as the bifurcation or instability method determines when a localized neck will develop in a uniform sheet as a result of an applied load. The bifurcation method has been used since the 1950's and is essentially an analytical approach which directly predicts the limit strains without requiring a computationally-expensive numerical simulation. Therefore, it is advantageous for use in the press shop. It is useful to distinguish between the different bifurcations-based methods and the following are some of the main models that have been used in sheet metal forming:

- Swift's diffuse necking criterion
- Bifurcation analysis with flow theory
- Bifurcation analysis with vertex theory
- Perturbation analysis

2.2.2.1. Swift's diffuse neck instability criterion

For the first time in 1952, Swift [2.10] predicted the onset of diffuse necking by developing an instability criterion based on the maximum load definition under proportional loading. He showed that the major limit strain in diffuse necking could be calculated as follow:

$$\varepsilon_1^{Limit} = \frac{2n(1 + \rho + \rho^2)}{(\rho + 1)(2\rho^2 - \rho + 2)} \quad (2.1)$$

where, ρ is the strain ratio (ratio of the minor strain to the major strain). Swift's bifurcation method can cover the entire range of deformation modes typically encountered in sheet metal forming, which is between uniaxial tension ($\rho = -0.5$) and equibiaxial tension ($\rho = 1$). Obviously, diffuse necks cannot be observed in deformed sheet metal components, therefore, the plastic limit strains predicted with Swift's method are usually considered the onset of localized necking rather than diffuse necking. But it is evident that diffuse necking appears at lower strains than localized necking, therefore

limit strain results from Swift's bifurcation approach will be conservative compared to strains measured experimentally in localized necks for negative strain ratios. It can be concluded that Swift's method for FLC prediction only provides an approximate estimation of limit strains and is therefore not a reliable method for industrial applications.

2.2.2.2. Bifurcation method with flow theory

Bifurcation analysis began from the work of Hill (1952) [2.11], who assumed that once a discontinuity appears in the Cauchy stress and the velocity, this indicates the onset of failure. Hill then formulated the restrictions on the flow stress and the rate of work hardening in the growth of the localized neck. He developed a method that shows how a local neck starts in the zero-extension direction on sheet metal surface during uniform deformation and at instability condition the magnitude of plastic work decreases below the minimum value is required for uniform deformation along zero extension direction.

According to Hill's theory, the angle between the normal to the neck and the major strain direction is defined as:

$$\theta = \tan^{-1}(\sqrt{-\rho}) \quad (2.2)$$

However, this equation only has a real solution when the minor strain is negative; that is for loading paths on the left hand side of the FLC. Therefore the drawback of this theory is that it cannot predict limiting strains on the right hand side of the FLC where minor strains are positive. But obviously, there are limits to the formability of sheets stretched in biaxial tension.

When Hollomon power law ($\sigma_e = K\varepsilon_e^n$) is used to represent the relation between the effective stress and the effective strain, Hill's theory predicts that the major in-plane limit strain will be:

$$\varepsilon_1^{Limit} = \frac{n}{1+\rho} \quad (2.3)$$

Lee and Kobayashi (1975) [2.12] and Korhonen (1978) [2.13] combined Swift's instability method and Hill's criterion. They recommended using Swift's formulation to calculate the limit strain on the right side of the FLC where instability occurs with positive strain ratios, and Hill's analysis to calculate limit strains on the left side of the FLC where the strain ratio is negative.

These researchers also investigated the influence of the strain path on the FLC and they observed that the onset of localized necking in nonlinear loading paths depends on the previous deformation history. The FLC can therefore be determined by calculating the accumulated effective plastic strain at every stage of deformation. They noticed that an equibiaxial prestrain improves sheet metal formability in the subsequent loading stage whereas a plane-strain prestrain has the opposite effect and decreases the amount of remaining formability. They also found that FLC prediction depends directly on the stress-strain relation and the anisotropy factor considered in theory.

In other work, Hillier (1966) [2.14] and Negroni et al. (1968) [2.15] independently studied the effects of changes in strain path on a sheet metal's limit strains. They assumed that once the forces applied to the sheet metal reach a critical value, localized necking will appear and their work indeed confirmed the path dependency of limit strains.

2.2.2.3. Bifurcation method with vertex theory

Line (1971) [2.16] predicted the onset of a sharp vertex at the loading point on the yield locus of a polycrystalline material. His work was based on physical theories of plasticity which employ simple crystallographic slip models. The creation of vertices or corners on a yield locus during deformation has also been validated by the continuum theory of plasticity and has been confirmed by experimental studies conducted by Hecker (1976) [2.17]. In his experimental work, Hecker showed that a vertex on the yield surface can occur at the loading point and in the direction of the stress path. However it was not

possible to experimentally determine the shape of the vertex, and it still is not clear whether the vertex is a sharp point on the yield locus or if it is a rounded corner.

Stören and Rice (1975) [2.18] developed a new bifurcation theory by using the $J2$ deformation theory of plasticity, which is a vertex-based theory, to predict the FLC for the whole range of strain paths between uniaxial tension and equibiaxial tension. They supposed that localized necking will occur for each strain path when a corner appears on the yield locus at the forming limit. They also showed that on the left hand side of the FLC (i.e. for negative minor strains), the orientation of a local neck is not parallel with the zero-strain direction, but on the right hand side of the FLC (positive minor strains), the local neck is parallel with the minor strain direction. However, Stören and Rice had to employ a numerical method to obtain limit strains for loading paths with negative minor strains, because it was not possible to predict the neck orientation using bifurcation methods.

For the sake of simplicity, if a local neck develops parallel with the minor strain direction (i.e. for a loading path with a positive minor strain), there is an analytical solution [2.18] to obtain the limit strains as a function of the strain ratio (ρ) and the strain hardening exponent (n) as follows:

$$\left\{ \begin{array}{l} \varepsilon_1^{Limit} = \frac{3\rho^2 + n(2 + \rho)^2}{2(1 + \rho + \rho^2)(2 + \rho)} \quad \rho > 0 \\ \varepsilon_1^{Limit} = \frac{n}{(1 + \rho) \left[(1 - n)/2 + \sqrt{(1 + n)^2 / 4 - \rho n / (1 + \rho)^2} \right]} \quad \rho < 0 \end{array} \right. \quad (2.4)$$

These relationships yield acceptable limit strain predictions for the right hand side of the FLC of strain-rate insensitive materials, but underestimate the forming limits on the left side of the FLC. Therefore Equations (2.4) are not recommended for the prediction of FLC if it is to be used for a critical assessment of forming severity, particularly if the sheet material exhibits strain-rate sensitivity.

Hutchinson and Neale (1978a) [2.19] employed the vertex theory with both the flow and deformation theories of plasticity to predict limit strains of sheet metals. Their

predictions were significantly better than previous predictions with the vertex method, but the predicted limit strains were still not sufficiently accurate for the left hand side of the FLC.

Until the early 1980's, vertex-based bifurcation analyses were all developed for linear loading paths; therefore they only can be employed in applications in which the loading paths are proportional. In order to investigate cases with nonlinear loading paths, Chu (1982) [2.20] extended the work of Stören and Rice (1975) [2.18]. Although his new method was limited to isotropic hardening, Chu succeeded in studying the effect of a prestrain on the FLC. In his prediction of limit strains, Chu observed that the stress state in the final forming stage is really the only factor that determines whether or not necking will take place.

According to classical plasticity theory there is a corresponding equivalent strain state for every stress state, therefore it is reasonable to suppose that every sheet material has an effective limit strain, and regardless of the number of deformation stages, plastic instability will take place once the total effective strain reaches this critical value. This can be written as:

$$\varepsilon_e^{Limit} = \varepsilon_e^1 + \varepsilon_e^2 + \dots + \varepsilon_e^{(N)} \quad (2.5)$$

where ε_e^{Limit} denotes the effective limit strain of the sheet material when it is deformed to failure in a single forming stage without prior prestrain, and superscripts 1, 2, 3 ... N indicate the order of successive forming stages.

2.2.2.4. Perturbation analysis

Perturbation analysis is another method of predicting plastic instability using the bifurcation method. In this method the sheet material is assumed to be homogeneous at the beginning of deformation. However after every increment of plastic deformation, a perturbation is considered to affect the homogeneous flow. The criterion employed in this method is based on the fact that the magnitude of the perturbation increases or decreases over time as deformation progresses. This concept was initially developed to study the

dynamics of flow in fluids, but it was adapted to the plastic flow in solids by researchers such as Zbib and Aifantis (1988) [2.21, 2.22]) in order to study shear bands and localized necking of sheet samples deformed in uniaxial tension.

The concept of effective instability as a perturbation analysis was applied by Dudzinski and Molinari (1991) [2.23] and they were able to successfully predict FLC for sheet metal forming analysis. For each loading path they defined a critical value of the instability growth rate as an indication of the onset of localized necking which in turn corresponds with a point on the FLC. The effective instability approach is somewhat similar to the MK method that was briefly introduced in the previous chapter: in the effective instability method there is an instability intensity factor, similar to the initial geometric non-uniformity factor in the MK analysis. And in each case, the factor increases with deformation until it reaches a critical value, and instability occurs. The accuracy of the perturbation method was later improved by Toth, Dudzinski and Molinari (1996) [2.24] who employed the viscoplastic crystallographic slip theory with Taylor's strain compatibility assumption. The FLC was then predicted for aluminum sheets.

In brief, if the bifurcation method is selected to predict the FLC of metal sheets, it is recommended that Hill's flow bifurcation theory be used for the right hand side of the FLC and Stören-Rice's bifurcation method for the left hand side of the FLC.

2.2.3. Marciniak and Kuczynski method

The MK method was developed by Marciniak and Kuczynski in 1967 [2.3], and is no doubt the most common theoretical approach for calculating the FLC of sheet materials. In recent years it has been used by several researchers, such as Yoshida, Kuwabara and Kuroda (2007) [2.25], Butuc (2007) [2.26], Nurcheshmeh and Green (2011) [2.27, 2.28] and others. The MK approach assumes a sheet material is initially inhomogeneous due to, for instance, a non-uniform distribution of micro-voids or the roughness at the surface of the sheet. Marciniak and Kuczynski [2.3] modelled this inhomogeneity in a sheet specimen as a geometric defect in the form of a narrow band with a reduced thickness. Figure 2.2 shows a schematic of the MK model in which the imperfection band is designated as region "b", and region "a" is the area outside the

band. This pre-existent defect could be any combination of geometric and material non-uniformities, but the most common approach is to model the initial imperfection as a variation in sheet thickness. In their original study, Marciniak & Kuczynski actually machined shallow grooves into sheet specimens that were then stretched to failure in equibiaxial tension; they observed that there is no reduction in the forming limit strain when the thickness ratio of the groove to the nominal area is $0.990 < (t_0^b / t_0^a) < 1.000$.

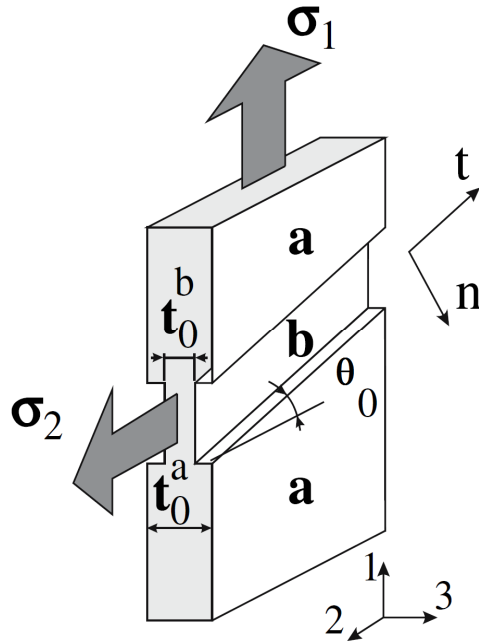


Figure 2.2. Schematic of the MK model with a thickness imperfection in the sheet

In order to predict the onset of necking, the MK model of a sheet is subjected to a uniform, proportional state of stress. As plastic deformation proceeds, the major strain in the band becomes increasingly greater than in the rest of the sheet. Consequently, the thickness ratio (t_b / t_a) decreases until, eventually, a localized neck is formed. Throughout the deformation it is assumed that the strain component in the neck direction in the imperfection band is always the same as the corresponding strain outside the groove.

$$d \varepsilon_n^a = d \varepsilon_n^b \quad (2.6)$$

Furthermore, the equilibrium of the normal and shear forces across the imperfection are also maintained throughout the deformation, i.e.:

$$F_{mn}^a = F_{mn}^b \quad (2.7a)$$

$$F_{nt}^a = F_{nt}^b \quad (2.7b)$$

where subscripts n and t denote the normal and tangential directions of the groove, respectively, and F is the force per unit width, i.e.:

$$F_{mn}^a = \sigma_{mn}^a t^a \quad (2.8a)$$

$$F_{mn}^b = \sigma_{mn}^b t^b \quad (2.8b)$$

$$F_{nt}^a = \sigma_{nt}^a t^a \quad (2.8c)$$

$$F_{nt}^b = \sigma_{nt}^b t^b \quad (2.8d)$$

Although the strain ratio ($d\rho = d\varepsilon_2/d\varepsilon_1$) outside the groove remains constant during the deformation, it actually decreases inside the groove until it eventually approaches plane-strain deformation ($d\varepsilon_2^b/d\varepsilon_1^b = 0$). At this stage, the principal strains outside the groove are identified as the limit strains for this material under the corresponding deformation mode.

As was already mentioned, the initial inhomogeneity is generally modelled as a local thickness variation, which may in fact originate from the surface roughness of the sheet as a result of the cold rolling process. When the material inhomogeneity is thus modelled as a geometrical thickness variation, the physical problem is thereby simplified to a single dimension. Because of the plane-stress assumption, the stress and strain increments inside the neck can be solved directly in terms of the strain increments prescribed outside the neck. The original analysis proposed by Marciniak and Kuczynski

only modelled biaxial stretching (i.e. positive major and minor strains), however their approach has since been used extensively to predict both the left and right sides of the FLC. This method is now commonly referred to as the MK method.

Azrin and Backofen (1970) [2.29] subjected a large number of sheet materials to in-plane stretching. They discovered that a thickness ratio $f_0 = t_b/t_a \leq 0.97$ was required to obtain agreement between the MK analysis and the experiments. However, grooves of this size cannot be detected with the naked eye. Accordingly, even though the MK analysis is a simple and elegant way to model the development of a local neck, there was an inconsistency between its predictions and the experimental data. Similar trends have also been observed by Sowerby and Duncan (1971) [2.30], as well as by Marciniak *et al.* (1973) [2.4]. In addition, Sowerby and Duncan also found that the MK predictions of limit strains are very dependent on material anisotropy.

Ghosh (1977) [2.31] found that strain-rate sensitivity becomes important after the ultimate tensile stress of the material has been reached. The additional hardening effect due to strain rate sensitivity plays a significant role in increasing the forming limits by preventing an overly rapid concentration of strains inside the neck.

Ghosh (1978) [2.32] also found that the MK method tends to predict very high limit strains for strain states near balanced biaxial tension. In other words, the MK method under-predicts the limit strains near plane-strain deformation, but over-predicts them in balanced biaxial stretching.

The effects of different types of initial non-uniformity on FLCs have been examined by several authors (Van Minh, *et al.* (1975) [2.33]; Yamaguchi and Mellor, (1976) [2.34]). Tadros and Mellor (1975) [2.35] proposed that a local neck does not start at the beginning of the deformation but at the point of instability defined by Swift. They also carried out experiments (Tadros and Mellor, 1978) [2.36] which showed that no significant necking occurs up to the Swift instability.

Even though the MK method was initially applied only to the region where both strain components are positive, (because the orientation of the initial imperfection was assumed to be in the minor strain direction, and it is thus impossible to obtain a different critical strain), their approach led to very significant developments in the prediction of FLCs. Further detailed analyses based on the MK method were numerically carried out

by Hutchinson and Neale (1978) [2.19] where the entire FLC was predicted. In their analysis, they allowed the initial imperfection to have different orientations, and obtained the minimum critical strains. Their work has made important contributions to gaining insight into the effects of constitutive equations and plasticity theories on FLCs. Following the pioneering work of the above mentioned authors, the MK method has been adopted by other researchers. The sources of disagreement between the calculated and observed FLCs have been identified and studied in detail, resulting in refined models leading to more reasonable quantitative correlations between analytical and experimental limit strains.

More recently, Friedman and Pan (2000) [2.37] introduced an angle parameter based on the point on the yield surface defined by the initial strain path and that of plane-strain. Since this parameter denotes the extent of deformation change from a particular loading path to plane-strain, it can be used to predict the effects of yield surface on limit strains.

In a typical MK analysis, the computations of stress and strain in regions “*a*” and “*b*” are carried out independently, and the connection between them is realized through the MK conditions: force equilibrium and geometrical compatibility. Small increments of equivalent strain are imposed in the homogeneous region (region “*a*”). Through the theory of plasticity, the stress and strain states in the homogeneous zone are computed. In order to define the strain and stress states in the heterogeneous band (region “*b*”), numerical methods can be used to solve the final differential equation obtained by the yield criterion and the strain compatibility requirement in tangential direction of the imperfection band.

In the MK analysis local necking is reached when the effective strain increment in the groove becomes more than ten times greater than that in the homogeneous region: i.e. $d\bar{\varepsilon}^b \geq 10d\bar{\varepsilon}^a$. When this necking criterion is reached, the computation terminates and the corresponding strains ($\varepsilon_1^a, \varepsilon_2^a$) and stresses (σ_1^a, σ_2^a) accumulated at that moment in the homogeneous zone represent the limit strains and limit stresses, respectively. The analysis can be repeated for different initial orientations (ϕ_o) of the groove in the range between 0° and 45° and the forming limit can be obtained after minimizing the ε_1^a versus

ϕ_o curve. The same calculation is then repeated for each individual strain path from uniaxial tension ($\rho = -0.5$) to balanced biaxial tension ($\rho = +1.0$), and the FLC is defined by connecting the limit strain data across the entire range of strain paths. This calculation procedure is presented in the form of a flow chart in Figure 2.3.

In predictions of the FLC for nonlinear loading paths, the loading is simulated as two successive deformation stages involving a first prestrain in the homogeneous zone followed by loading along a different strain path as follows:

$$\rho = \rho_1 \text{ for } \bar{\varepsilon} < \bar{\varepsilon}^* \text{ (stage 1)} \quad (2.9a)$$

$$\rho = \rho_2 \text{ for } \bar{\varepsilon} > \bar{\varepsilon}^* \text{ (stage 2)} \quad (2.9b)$$

where ρ_1 and ρ_2 represent the two different strain paths that are imposed and $\bar{\varepsilon}^*$ is the effective prestrain value. The simulation of nonlinear loading paths can also be extended to a series of successive linear strain paths.

It is worth underlining the fact that the MK analysis is able to calculate the stress-based forming limit curve (SFLC) at the same time as the strain FLC. Indeed, both the stress state and the strain state, inside and outside the imperfection band, are calculated after each load increment. A typical MK analysis code consists of a main program where the loading is applied, equilibrium and compatibility conditions are prescribed and stress and strain are calculated with the help of subroutines where the yield condition, the work hardening law and the constitutive equations are defined. The general structure of a MK analysis code is shown in the flow chart in Figure 2.3 [2.26].

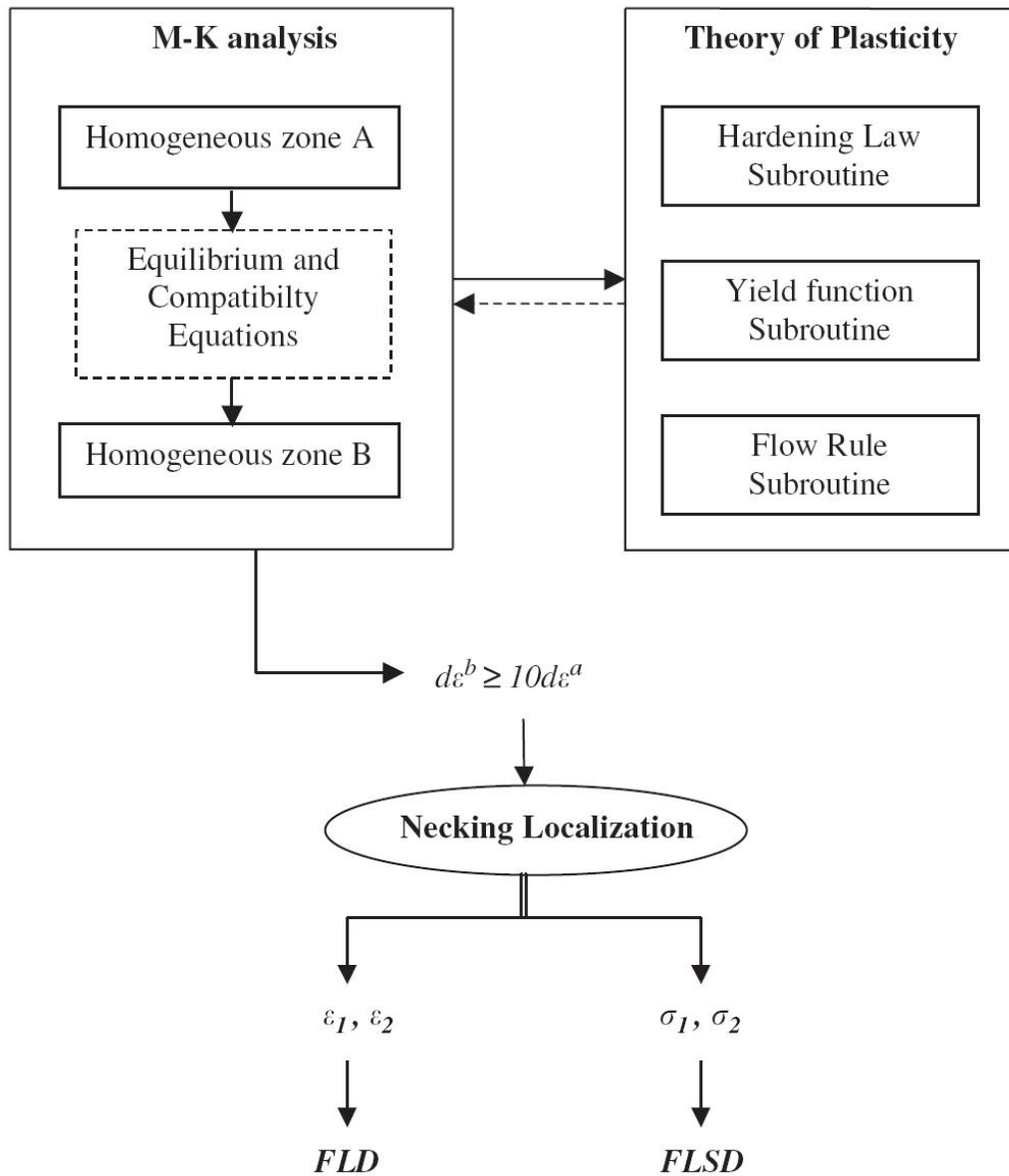


Figure 2.3. Code structure to predict FLC and SFLC [2.26]

2.3. Stress-based forming limit curve (SFLC)

The FLC remains a useful approach for evaluating the severity of sheet metal forming processes, however, the observed dependence of the FLC on strain path changes limits its applicability to linear or quasi-linear loading paths. The path-dependence of the

FLC is a real concern to designers of industrial sheet metal products, since a change in strain path during the forming process can lead to a significant translation of the FLC in strain space, which then renders the as-received FLC unreliable.

Kleemola and Pelkkikangas (1977) [2.38] discussed the limitations of the FLC in the case of copper, brass and steel sheets formed in a deep-drawing operation followed by a flanging operation. They observed significant variability of the FLC after this two-stage forming process and the resulting nonlinear strain paths, and recommended the use of a stress-based forming limit curve (SFLC) as an alternative to the FLC. They also provided experimental data that showed the path independence of the stress-based forming limit curves for these alloys.

Arrieux *et al.* (1982) [2.39] also pointed out the non-uniqueness of the FLC after nonlinear loading cases and again proposed the use of a stress-based forming limit curve in applications where there is more than one loading stage.

Graf and Hosford (1993) [2.40-2.41], showed theoretically and experimentally that strain based FLC translates in strain space significantly due to nonlinear loading path. They studied different preloading paths effects on FLC path dependency including uniaxial, plane-strain and equibiaxial prestrains in aluminum alloys.

Despite the great significance of these observations, the evaluation of formability in stress space never really gained widespread attention nor was it employed for formability evaluation till the turn of the century. Several factors contributed to the slow adoption of the SFLC. Perhaps the first reason is that the stamping process leads to essentially linear loading paths for approximately 80% of industrial sheet metal parts and therefore the strain-path dependence of the FLC was not widely recognized. A second reason is that, the results of finite element simulations of metal forming processes were not as reliable as they are today and the predicted stress states in formed parts were not considered reliable. Finally the main obstacle to the widespread implementation of the SFLC is the prohibitive cost and inaccessibility of experimental stress measurements in the metal forming industry. Therefore press shops continued to measure the strains in stamped parts and to evaluate the measured strains against the well-known FLC [2.42- 2.43].

Today, the situation is very different and the reasons for avoiding the use of the SFLC to evaluate formability are, for the most part, no longer applicable. Indeed, an

increasing number of metal forming processes are now being manufactured with multiple successive operations which can generate complex nonlinear loading paths, and in such cases it is not appropriate to use the as-received FLC for formability evaluation. For instance, there has been an increased use of tubular hydroformed components in vehicle structures since the early 1990's and these thin-walled tubes are typically bent prior to being hydroformed. The tube-bending operation leads to very severe prestrains and the subsequent hydroforming can cause strain paths that are drastically different from the prestrain path; it would be practically impossible to reliably evaluate the forming severity of such parts with the conventional FLC.

Secondly, FE analysis software is now used extensively by manufacturers to design parts, forming tools and the forming process. And since the predictions of numerical simulations have become so much more accurate (due to the increasing accuracy of constitutive models as well as the increase in expertise and experience of simulation analysts) it is now straightforward to evaluate the forming severity in a virtual part and to assess the robustness of the proposed forming process by comparing the predicted stresses to the SFLC.

Finally, since many critical mechanical responses are dependent on the stress state [2.42], such as plastic yielding, wrinkling and buckling it does seem appropriate to also evaluate the onset of plastic instability on the basis of the stress state rather than the strain state.

Similar to the FLC, the SFLC divides the principal stress space into a safe zone and failure zone (Figure 2.4). And the assessment of forming severity is carried out in the same way as it is with the FLC, by modifying the design of the part or of the forming process until all stress data in the virtual part lie safely beneath the SFLC.

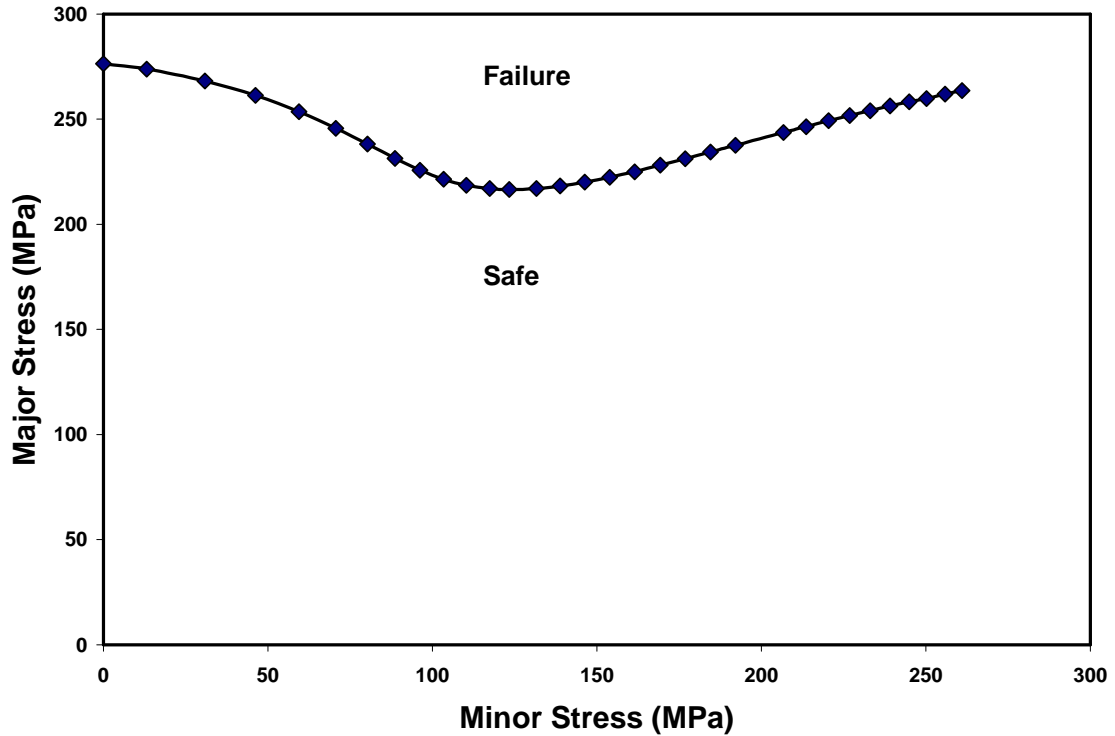


Figure 2.4. Typical stress-based forming limit curve (SFLC)

Stoughton [2.42, 2.44] showed that the SFLC is almost path-independent and his investigation indicated that formability situation can be evaluated accurately using a combination of the SFLC and finite element simulation, not only for proportional loading but also in cases where a sheet element has a complex strain history. According to the Stoughton method while it is still difficult to experimentally determine the SFLC, it can be easily determined from the as-received FLC; hence predicting the FLC is still useful.

In 2005, Yoshida *et al.* [2.45] performed biaxial tension tests on an aluminum alloy tubes utilizing a tension–internal pressure testing machine to verify the path-independence of forming limit stress. They confirmed that the forming limit stresses are path-independent. Yoshida *et al.* [2.25] subsequently calculated the forming limit stresses for a variety of two-stage combined stress paths using the Marciniak and Kuczynski (MK) model [2.3] based on a phenomenological plasticity theory to clarify the mechanism behind the path-independent SFLC. In this work they confirmed the experimental observations of Yoshida *et al.* [2.45]. Again, Yoshida *et al.* [2.46] investigated the path dependency of the SFLC using different work hardening models.

They concluded that the path dependency of SFLC depends on the stress-strain behaviour during subsequent loading stages. Their work shows that SFLC is only path independent when the work hardening behaviour remains unchanged with a change of strain path.

In order to take advantage of the path-independence of the SFLC in a prototype shop or a manufacturing plant, it is possible to predict the FLC from the SFLC once the strain path in a given location of a part is known [2.47].

2.4. Strain-hardening law

In general, materials can be categorized in three different classes, depending upon the way their strength evolves with deformation [2.48]:

- a- Strain-hardening materials
- b- Perfectly-plastic materials
- c- Strain-softening materials

The majority of metals and their alloys usually exhibit strain-hardening (or work-hardening) which signifies that increasing levels of stress are required to achieve further deformation. In contrast, geotechnical materials typically show evidence of strain-softening. Strain hardening materials are stable. In 1951, Drucker [2.49] introduced a new classification of materials which is known as Drucker's postulate. The mathematical framework for describing the plastic behaviour of metals depends on Drucker's postulate.

Drucker defined the condition for a stable plastic material. According to his postulate, a deformable solid object subjected to the boundary tractions t_i causes some displacements u_i . Traction changing into $t_i + \Delta t_i$ will induce increased displacements Δu_i . To satisfy the stability condition of material according to Drucker's rule, the work done by the tractions Δt_i through the displacements Δu_i should be zero or positive for all Δt_i . As a result of this theory, every stable plastic material should possess a convex yield surface, the plastic strain rate should be normal to the yield surface which indicates associated flow rule, and the strain hardening rate should be positive or zero. As an extra requirement for materials to obey Drucker's postulate, the principle of maximum plastic resistance should be satisfied in order to be considered a stable material.

The strain-hardening phenomena that are observed in most metals can be formulated as hardening rules that describe how the stress state evolves with plastic

deformation. As a result of experimental studies conducted by many researchers for well over a century, it is now well known that the yield locus may undergo a combination of expansion, translation, distortion, and rotation as a result of plastic deformation. In this section, the most common hardening rules used in the numerical simulation of metal forming processes will be reviewed: isotropic hardening (when the yield surface simply expands uniformly), kinematic hardening (when the yield surface merely translates in stress space) and mixed isotropic-kinematic hardening (when the yield surface expands and translates).

2.4.1. Isotropic hardening

Strain-hardening is called isotropic hardening when the initial yield surface expands uniformly in all directions in stress space during plastic deformation. Isotropic hardening is illustrated in Figure 2.5(a).

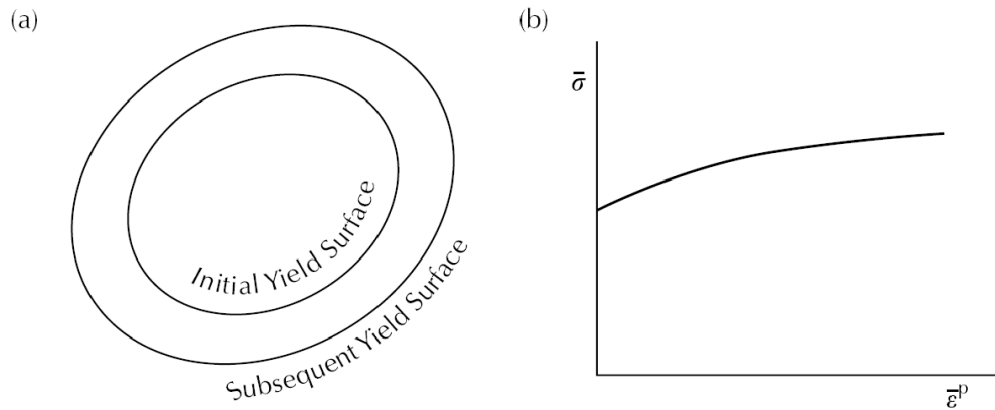


Figure 2.5. (a)- Isotropic hardening (b) Schematic equivalent stress-strain curve [2.48]

In isotropic hardening, the yield function can be defined as:

$$f(\sigma_{ij}) = Y^2 \tag{2.10}$$

where Y denotes the yield stress of the material. Y also represents the radius of the yield locus. As the magnitude of Y increases, the yield locus expands in all directions. Y can be expressed as a function of strain hardening quantities such as the plastic work per unit volume or the equivalent incremental plastic strain [2.48]. The plastic work per unit volume is defined as:

$$W^p = \int \sigma_{ij} d\varepsilon_{ij}^p = \int \bar{\sigma} d\bar{\varepsilon}^p \quad (2.11)$$

and the equivalent plastic strain increment is determined as:

$$d\bar{\varepsilon}^p = \sqrt{2/3} (d\varepsilon_{ij}^p d\varepsilon_{ij}^p)^{0.5} \quad (2.12)$$

and the equivalent stress for an isotropic (von Mises) material is defined as:

$$\bar{\sigma} = \sqrt{3/2} (S_{ij} S_{ij})^{0.5} \quad (2.13)$$

where, S_{ij} represents the deviatoric stress tensor.

The isotropic hardening rule is very simple to implement in a numerical simulation code and has been used extensively to describe the work hardening behaviour of sheet metal components. However, it does not accurately represent the behaviour that is observed in many metals, because it over-predicts the yield stress in reverse loading.

2.4.2. Kinematic hardening

According to the rule of isotropic hardening, the elastic region becomes increasingly larger as plastic deformation progresses and the yield stress in reverse loading is the same as the flow stress after the first loading. However, this is often not the behaviour that is observed experimentally. In fact in many metals, the yield stress in reverse loading is actually much smaller than what would be expected: this is called the Bauschinger effect. In order to more accurately model the Bauschinger effect, Prager

[2.50] introduced the kinematic strain hardening rule for the first time in 1956. Kinematic hardening signifies that the yield surface can translate in stress space without any rotation or expansion, and therefore the shape and size of the yield surface remains unchanged with plastic deformation. Later, Hodge [2.51] showed how this rule should be applied in nine-dimensional stress space.

The initial yield surface in nine-dimensional stress space can be defined as:

$$f(\sigma_{ij}) = 0 \quad (2.14)$$

and with the kinematic hardening rule subsequent yield surfaces can be described by:

$$f(\sigma_{ij} - \alpha_{ij}) = 0 \quad (2.15)$$

where α_{ij} is a kinematic hardening indicator that represents the translation of the centre of the initial yield locus; α_{ij} is called the back stress tensor.

If the von Mises yield function for isotropic materials is used, the yield function can be written as:

$$(s_{ij} - \alpha_{ij})(s_{ij} - \alpha_{ij}) = 2K^2 \quad (2.16)$$

where $K^2 = 1/3Y^2$. In order to define the evolution of the back stress tensor α_{ij} in stress space, Prager [2.50] proposed a linear relationship with the plastic strain increment such that:

$$d\alpha_{ij} = cd\varepsilon_{ij}^p \quad (2.17)$$

where c is a material constant that can be determined by fitting the theoretical stress-strain curve to the experimental one. In 1959, Ziegler [2.52] modified Prager's definition of the back stress tensor in the following way:

$$d\alpha_{ij} = d\mu(\sigma_{ij} - \alpha_{ij}) \quad , \quad d\mu > 0 \quad (2.18)$$

where $d\mu$ is a material parameter.

The limitation of the linear kinematic hardening rule is that it is only valid for materials with a bilinear stress-strain curve in loading and reverse loading; however, most metallic materials exhibit nonlinear stress-strain behaviour. The combination of nonlinear stress-strain relation and linear kinematic hardening leads to behaviour in reverse loading that has never been observed (Figure 2.6(a)). Therefore the linear kinematic hardening rule gives an incorrect prediction of work hardening for materials with nonlinear stress-strain curve.

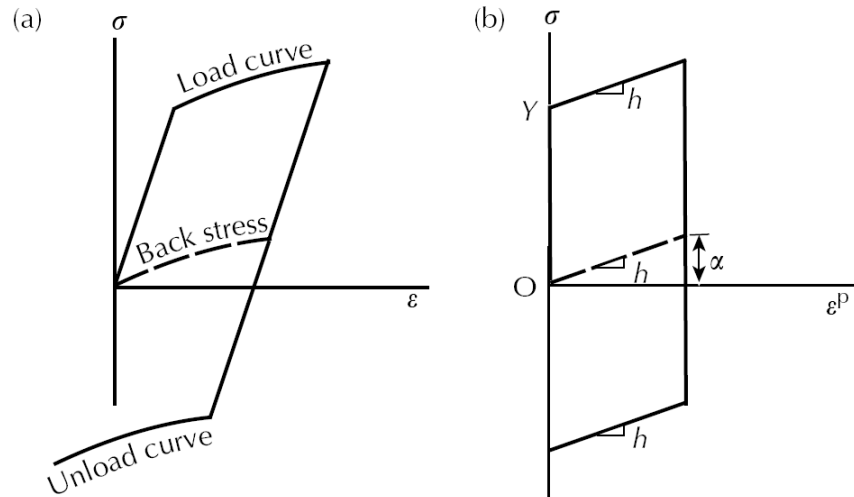


Figure 2.6. Schematic linear kinematic hardening of materials with (a) nonlinear stress-strain curve (b) bilinear stress-strain curve [2.48]

In Figure 2.6(b), the effect of the linear kinematic hardening rule is shown in terms of the loading and reverse loading behaviour of a material with a bilinear stress-strain curve. Y is the initial yield stress and h is a material parameter that represents the slope of the stress-strain curve and at the same time it shows linear kinematic hardening effect. In this case, linear kinematic hardening can be simply defined as:

$$d\alpha = h d\epsilon^p \quad (2.19)$$

If we consider the case of uniaxial loading, the back stress increment will be as:

$$d\alpha_{ij} = \begin{bmatrix} d\alpha & 0 & 0 \\ 0 & 0 & 0 \\ 0 & 0 & 0 \end{bmatrix} \quad \text{and} \quad d\alpha_{ij}^{deviatoric} = d\alpha_{ij} - \frac{1}{3}d\alpha_{kk}\delta_{ij} = \begin{bmatrix} 2/3d\alpha & 0 & 0 \\ 0 & -d\alpha/3 & 0 \\ 0 & 0 & -d\alpha/3 \end{bmatrix} \quad (2.20)$$

Considering Equation 2.17, we have:

$$2/3d\alpha = cd\varepsilon^p \quad (2.21)$$

And using Equations 2.19 and 2.21 the expression for h becomes:

$$h=3/2c \quad (2.22)$$

Therefore, the stress-strain curve formula in loading is:

$$\sigma = Y + h\varepsilon^p \quad (2.23)$$

Finally the definition of the yield function for materials with nonlinear loading curves is:

$$f(\sigma_{ij} - \alpha_{ij}) = Y^2 \quad (2.24)$$

2.4.3. Mixed Hardening

In order to overcome the limitations of the isotropic and kinematic hardening rules, Hodge [2.51] proposed a combination of both hardening laws in 1957. This mixed hardening rule allows the yield locus to expand uniformly and to translate in stress space at the same time. Yield surface translation was defined by the back stress tensor α_{ij} , and

the variation of K describes its expansion. Therefore, factors Y and α_{ij} are not constant in the case of combined isotropic–kinematic hardening in Equation 2.24.

For the same reason that the linear kinematic hardening rule is not suitable to predict the behaviour of metals subjected to reverse loading, the combined isotropic-linear kinematic-hardening rule is also not able to predict this type of behaviour. Therefore the kinematic portion of the mixed hardening rule requires some modification. In 1966, Armstrong and Frederick [2.53] proposed a nonlinear kinematic hardening rule in which the back stress tensor is defined as follows:

$$d\alpha_{ij} = 2/3cd\varepsilon_{ij}^p - \gamma\alpha_{ij}d\bar{\varepsilon}^p \quad (2.25)$$

where c and γ are material constants that can be obtained by fitting the predicted stress-strain curve to the experimental data. This nonlinear relation has gained much popularity and is now widely used in numerical simulations of metal forming processes, particularly when seeking to predict the springback after a forming operation.

2.5. Methodology

In this research the MK method was selected as the basic approach for predicting the FLC and SFLC of sheet metals. However, in order to improve the accuracy and robustness of the MK method, several additions and enhancements are proposed. These various improvements will now be presented one by one.

2.5.1. Definition of the imperfection factor

One of the main drawbacks of the conventional MK approach is the somewhat arbitrary determination of the initial imperfection factor ($f_0 = t_0^b/t_0^a$). Indeed, the predicted forming limits are very sensitive to the value selected for this factor and, in many cases, it has simply become an adjustment factor to fit theoretical results to known experimental data. In order to overcome this deficiency, it is proposed that the thickness

imperfection be correlated to an actual, measurable source of heterogeneity such as the surface roughness of the as-received sheet. By adopting a definition of the initial imperfection that is based on a physical parameter, the MK method will no longer be dependent on the subjective and arbitrary selection of “the best fitting factor”, and it will be easier to determine which constitutive parameters are most significant for predicting the onset of plastic instability.

2.5.2. Orientation of the imperfection band

Another assumption made in the original MK analysis was to consider the imperfection band to be perpendicular to the maximum principal stress direction, but in general, this band could be oriented in any direction with respect to the principal loading axes (Figure 2.2). In the current work, just as other researchers have done, the imperfection band will be made to rotate in small increments relative to the principal loading axes so that the most critical orientation can be determined at every stage of deformation and for each strain path. This feature is considered essential for the accurate prediction of the FLC.

2.5.3. Extend calculations for multi-stage loading

As mentioned already, many industrial sheet forming processes inherently cause the sheet metal or the thin-walled tube to deform along nonlinear strain paths. During multi-stage forming processes the loading path can even change abruptly from one direction to another in strain space. Since the FLC is strongly path dependent, the as-received FLC (generated by experiments in which the strain paths are quasi-linear) is not valid in most cases for formability evaluation. It is therefore necessary that a numerical code for predicting FLC be able to determine the onset of plastic instability for any random, nonlinear loading path that might be encountered in an actual forming process. This ability to model nonlinear load paths will initially be implemented as a bilinear

strain path, knowing that this can easily be extended to multi-linear strain paths which are in fact a reasonable approximation of nonlinear strain paths.

2.5.4. Investigation on the path dependency of SFLC

Due to the considerable strain-path dependency of FLC, it may be questionable whether the FLC should even be utilized as a formability evaluation tool in the case of forming processes involving complex loading paths. Even in a virtual forming process, where each integration point in the FE model can follow a different loading path, the FLC at each point may be sufficiently different one from the other that it becomes practically unmanageable to carry out an evaluation of forming severity. One of the best ways to overcome this challenge is to consider forming limits in stress space rather than strain space. Experimental investigations on the SFLC have shown that it is almost path-independent in many cases of nonlinear loading, however further research is needed to determine the extent and limitations of this quasi path-independence. The current work will therefore ensure that the MK analysis is able to calculate both stress-based and strain-based FLC simultaneously, so that the purported strain-path independence of SFLC can be investigated.

2.5.5. Hardening rules

The prediction of FLC using the MK analysis is based on the classical continuum theory of plasticity. As such, a yield criterion, a hardening law and a flow rule must be used to establish the constitutive equations required in the analysis. However, the influence of the hardening model on the prediction of FLC has never been investigated broadly. Isotropic hardening is the simplest and most widely used strain hardening rule and it is well suited to predict the outcome of metal forming processes involving monotonic loading. Therefore it has been always been used in the MK analysis.

As discussed in section 2.4, both linear and nonlinear kinematic hardening models have also been proposed in order to model the Bauschinger effect when the forming

process involves unloading, reverse loading or cyclic loading. However, under complex loading histories, some discrepancies still exist between actual material behaviour and that predicted by these purely kinematic models. So it is now common to combine both isotropic and nonlinear kinematic hardening models in plasticity calculations to obtain results that are closer to the actual hardening behaviour of metals.

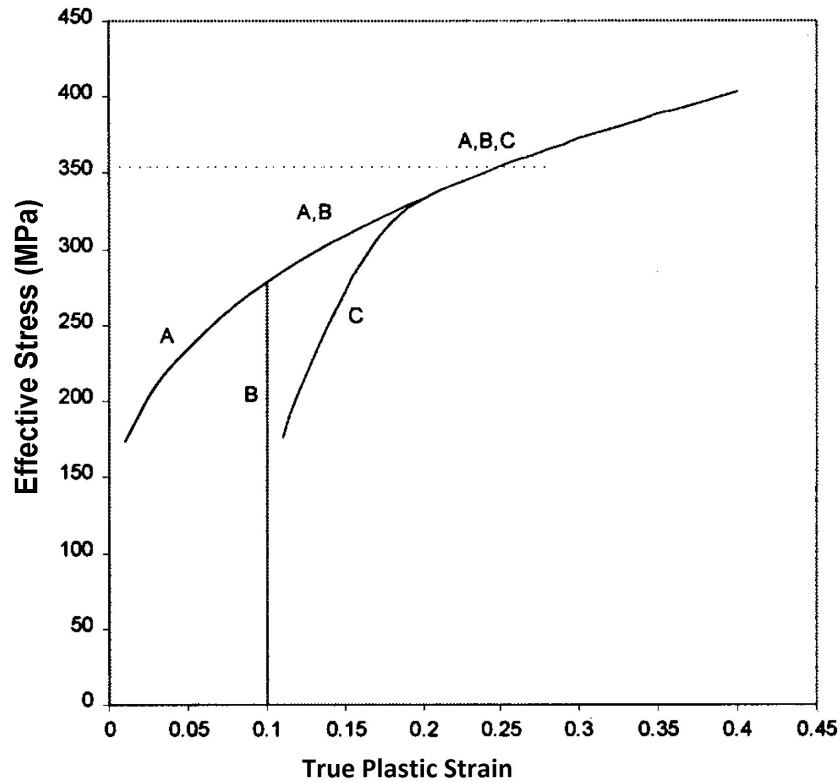


Figure 2.7. Schematic plot of stress-strain behaviour under (A) isotropic or kinematic hardening under proportional loading and (B) isotropic hardening following unloading and reloading under a different loading condition, and (C) kinematic hardening following unloading and reloading under a different loading condition. [2.44]

Until now, the effects of the hardening rules on FLC have not been systematically investigated. Moreover, many common grades of steel deformed in a process that involves loading, unloading and reloading will exhibit a transient yielding behaviour upon reloading (path C in Figure 2.7) [2.44]. This transient behaviour can only be accurately predicted with a nonlinear kinematic hardening law. Therefore, it seems essential to implement different work hardening models into the MK analysis to investigate the effect of the hardening law on the FLC, when the metal is subject to such

nonlinear loading paths. First, isotropic hardening will be considered to determine the FLC in cases involving loading, unloading and reloading along a different strain path. Secondly, FLCs will be predicted with the mixed isotropic - nonlinear kinematic hardening model proposed by Armstrong-Frederick [2.53] and later by Chaboche [2.54].

2.5.6. Yield function effect

In classical plasticity theory, the yield function, which is generally assumed to take the same form as the plastic potential function (associated flow rule), plays a very important role. It defines not only the direction of the plastic strain increments via the flow rule, but also the material anisotropy and rigidity by its variation during plastic deformation.

Because of its simplicity and good accuracy, Hill's 1948 yield criterion [2.55] has been widely used to predict the behaviour of orthotropic steel sheets. This quadratic yield function only requires a limited number of mechanical properties to determine the shape of the yield locus: under plane-stress conditions, only three parameters are sufficient, namely the plastic anisotropy coefficients in the rolling (R_0) and transverse (R_{90}) directions and the yield stress in uniaxial tension in either the rolling direction (σ_0) or in the transverse direction (σ_{90}).

Throughout the present research Hill's 1948 yield criterion [2.55] was used to describe material anisotropy and to predict forming limits. However, in spite of its widespread usage, Hill's 1948 yield criterion also has some drawbacks which will be discussed in more detail in chapter 6, but not the least of which is its inability to describe the behaviour of aluminum alloys. In such cases, a non-quadratic yield criterion is more suitable than Hill's first yield criterion. Therefore Hosford's 1979 non-quadratic yield function [2.56] will also be implemented in the MK analysis to investigate the effect of the yield function on the FLC.

2.5.7. Through-thickness stress component effect

Forming limit diagrams were initially developed to determine the conditions under which plastic instability would occur in thin metal sheets. Therefore, predictions of the FLC have generally assumed plane-stress conditions and the through-thickness stress component has been neglected in the calculations. Plane stress conditions certainly pertain in traditional stamping operations, but in many metal forming processes today, very significant through-thickness stresses can be generated. For instance, when sheet steels with increasingly high tensile strengths are formed over a die radius, the contact forces at the interface between the sheet and the die radius can lead to through-thickness stresses that are no longer negligible. Similarly, when hydroforming thin-walled tubes the internal fluid pressure can generate very significant through-thickness stresses in the tube wall in the areas of contact with the die. Some studies have been done to consider the effect of the third principal stress on the formability of sheet metals (Gotoh *et al.* [2.57], Smith *et al.* [2.58]) and these works show that the through-thickness compressive stress component has the potential to delay the onset of necking and thereby raise the level of the FLC.

In this research, the influence of the out-of-plane stress component on the FLC will be investigated. Additionally, the effect of sheet material properties on the sensitivity of the FLC to the applied out-of-plane stress component will also be studied: for instance, this study will consider how the sensitivity of the FLC to the through-thickness stress may vary for sheet materials with different strain hardening coefficients (n), a different strain rate sensitivity (m) or a different initial sheet thickness (t_0).

Following the implementation of these various features into a numerical MK analysis code, it is expected that it will be possible to predict FLCs and SFLCs more accurately and reliably than it was possible until now.

2.6. References

- [2.1] http://en.wikipedia.org/wiki/Brittle_failure, accessed on March 15, 2011.
- [2.2] Needleman A., Triantafyllidis N., Void growth and local necking in biaxially

- stretched sheets, *Journal of Engineering Materials and Technology Transactions of the ASME* 100 (1978) 164- 169.
- [2.3] Marciniak Z., Kuczynski K., Limit strains in the processes of stretch-forming sheet metal, *International Journal of Mechanical Sciences* 9 (1967) 609–620.
- [2.4] Marciniak Z., Kuczynski K., and Pokra T., Influence of The plastic properties of a material on the forming limit diagram for sheet metal in tension, *International Journal of Mechanical Sciences* 15 (1973) 789-805.
- [2.5] Gurson A.L., Continuum theory of ductile rupture by void nucleation and growth: Part I - yield criteria and flow rules for porous ductile materials, *Journal of Engineering Materials and Technology Transactions of the ASME* 99 (1977) 2-15.
- [2.6] Chu C.C., Needleman A., Void nucleation effects in biaxially stretched sheets, *Journal of Engineering Materials and Technology* 102(1980) 249- 256.
- [2.7] Lemaitre J., A continuous damage mechanics model for ductile fracture, *Journal of Engineering Materials and Technology* 107 (1985) 83-89.
- [2.8] Chow C.L., Yu L.G., Demeri M.Y., A unified damage approach for predicting forming limit diagram, *Journal of Engineering Materials and Technology* 119 (1977) 346-353.
- [2.9] Demeri M.Y., Chow C.L., Tai W.H., Prediction and experimental validation of path-dependent forming limit diagrams of VDIF steel, SAE paper NO. 980079 (1998) 53-58.
- [2.10] Swift H.W., Plastic Instability under Plane Stress, *Journal of Mechanics and Physics of Solids* 1 (1952) 1-18.
- [2.11] Hill R., On discontinuous plastic states, with special reference to localized necking in thin sheets, *Journal of Mechanics and Physics of Solids* 1 (1952) 19–30.
- [2.12] Lee S.H., Kobayashi S., The effects of strain paths on the stretching limit strains of sheet metal with planar anisotropy, *Proceedings of the Third North American Metal Working Research Conference, Carnegie Press* (1975) 277- 290.
- [2.13] Korhonen A.S., On the theories of sheet metal necking and forming limits, *Journal of Engineering Materials and Technology* 100 (1978) 303-309.
- [2.14] Hillier M.J., Instability strains in plane sheet under biaxial stress, *Journal of Applied Mechanics* 5 (1966) 282-288.

- [2.15] Negroni F., Kobayashi S., Thomsen E.G., Plastic instability in simple stretching of sheet metals, *Journal of Engineering for Industry- Transactions of ASME* 90 (1968) 387-392.
- [2.16] Lin T.H., Physical theory of plasticity, *Advances in Applied Mechanics*, Vol. 11, ed. Chia-Shun Yih, Academic Press, New York (1971) 256-311.
- [2.17] Hecker S.S., Experimental studies of yield phenomena in biaxially loaded metals in constitutive equations in viscoplasticity: Computational and Engineering Aspects, ASME, New York (1976) 1-33.
- [2.18] Stören S., Rice J.R., Localized necking in thin sheets, *Journal of the Mechanics and Physics of Solids* 23 (1975) 421-41.
- [2.19] Hutchinson J.W., Neale K.W., Sheet necking—II: time-independent behavior. In: Koistinen D.P., Wang N.M. (Eds.), *Mechanism of Sheet Metal Forming*, Plenum, New York (1978a) 127.
- [2.20] Chu C.C., An Investigation of the strain path dependence of the forming limit curve, *International Journal of Solids and Structures* 18 (1982) 205-215.
- [2.21] Zbib H.M., Aifantis, E.C., On the localization and post localization behavior of plastic deformation II: On the evolution and thickness of shear bands, *Res. Mechanica* 23(1988a) 279-292.
- [2.22] Zbib H.M., Aifantis E.C., On the concept of relative and plastic spins and its implications to large deformation theory, I, II, *Acta Mechanica* 75 (1998b) 15-33; 55-56.
- [2.23] Dudzinski D., Molinari A., Perturbation analysis of thermal-visco-plastic instabilities in biaxial loading, *International Journal of Solids and Structures* 27 (1991) 601-613.
- [2.24] Toth L.S., Dudzinski D., Molinari A., Forming limit predictions with the perturbation method using stress potential functions of polycrystal viscoplasticity, *International Journal of Mechanical Sciences* 38 (1996) 805-811.
- [2.25] Yoshida K., Kuwabara T., Kuroda M., Path-dependence of the forming limit stresses in a sheet metal, *International Journal of Plasticity* 23 (2007) 361–384.
- [2.26] Butuc M.C., Gracio J.J., Barata da Rocha A., An experimental and theoretical analysis on the application of stress-based forming limit criterion, *International Journal of Mechanical Sciences* 48 (2006) 414–429.

- [2.27] Nurcheshmeh M., Green D.E., Investigation on the strain-path dependency of stress-based forming limit curves, *International Journal of Material Forming* 5 (2011) 25-37.
- [2.28] Nurcheshmeh M., Green D.E., Prediction of sheet forming limits with Marciniak and Kuczynski analysis using combined isotropic–non linear kinematic hardening, *International Journal of Mechanical Sciences* 53 (2011) 145-153.
- [2.29] Azrin M., Backofen W.A., The deformation and failure of a biaxially stretched sheet, *Metallurgical Transactions (Physical Metallurgy and Materials Science)* 10 (1970) 2857-65.
- [2.30] Sowerby R., Duncan D.L., Failure in sheet metal in biaxial tension, *International Journal of Mechanical Sciences* 13 (1971) 217-229.
- [2.31] Ghosh A.K., A Numerical analysis of the tensile test for sheet metals, *Metallurgical Transactions* 8A (1977) 1221-1232.
- [2.32] Ghosh A.K., Plastic flow properties in relation to localized necking in sheets, in *mechanics of sheet metal forming*, eds. Koistinen D.P. and Wang, N.M. Plenum. New York (1978) 287-311.
- [2.33] Van Minh H., Sowerby R., Duncan J.L., Probabilistic model of limit strains in sheet metal, *International Journal of Mechanical Sciences* 17 (1975) 339-349.
- [2.34] Yamaguchi K., Mellor P.B., Thickness and grain size dependence of limit strains in sheet metal stretching, *International Journal of Mechanical Sciences* 18 (1976) 85-93.
- [2.35] Tadros A.K., Mellor P.B., Some comments on the limit strains in sheet metal stretching, *International Journal of Mechanical Sciences* 17 (1975) 203-208.
- [2.36] Tadros A.K., Mellor P.B., An Experimental study of the in-plane stretching of sheet metal, *International Journal of Mechanical Sciences* 20 (1978) 121-134.
- [2.37] Friedman P.A., Pan J., Effects of plastic anisotropy and yield criteria on prediction of forming limit curves, *International Journal of Mechanical Sciences* 42 (2000) 29-48.
- [2.38] Kleemola H.J., Pelkkikangas M.T., Effect of pre-deformation and strain path on the forming limits of steel, copper and brass, *Sheet Metal Industries* 63 (1977) 559–591.
- [2.39] Arrieux R., Bedrin C., Bovin M., Determination of an intrinsic forming limit

- stress diagram for isotropic sheets, In: Proceedings of the 12th IDDRG Congress 2 (1982) 61–71.
- [2.40] Graf A.F., Hosford W.F., Calculations of forming limit diagrams for changing strain paths, *Metallurgical Transactions A*, 24a (1993) 2497-2501.
- [2.41] Graf A.F., Hosford W.F., Effect of changing strain paths on forming limit diagram of Al 2008-T4, *Metallurgical Transactions A*, 24a (1993) 2503- 2512.
- [2.42] Stoughton T.B., A general forming limit criterion for sheet metal forming, *International Journal of Mechanical Sciences* 42 (2000) 1-27.
- [2.43] Stoughton T.B., Zhu X., Review of theoretical models of the strain-based FLD and their relevance to the stress-based FLD, *International Journal of Plasticity* 20 (2004) 1463–1486.
- [2.44] Stoughton T.B., Stress-based forming limits in sheet-metal forming, *Journal of Engineering Materials and Technology* 123(2001) 417-422.
- [2.45] Yoshida K., Kuwabara T., Narihara K., Takahashi S., Experimental verification of the path dependence of forming limit stresses, *International Journal of Forming Processes* 8 (2005) 283–298.
- [2.46] Yoshida K., Suzuki N., Forming limit stresses predicted by phenomenological plasticity theories with anisotropic work-hardening behavior, *International Journal of Plasticity* 24 (2008) 118–139.
- [2.47] Green D.E., Formability Analysis for Tubular Hydroformed Parts, in *Hydroforming for Advanced Manufacturing*, Woodhead Publishing Limited, ed. M. Koc (2008) 93-120.
- [2.48] Wu H.C., *Continuum mechanics and plasticity*, Chapman & Hall/CRC Press (2005).
- [2.49] Drucker D.C., A more fundamental approach to plastic stress–strain relations, in *Proceedings of the first U.S. National Congress in Applied Mechanics*, ASME 487 (1951).
- [2.50] Prager W., The theory of plasticity: a survey of recent achievements (James Clayton Lecture), *Proceedings of the Institution of Mechanical Engineers* 169 (1995) 41.
- [2.51] Hodge P., Piecewise linear plasticity, *Proceedings of the 9th International*

Congress in Applied Mechanics 8 (1957) 65.

- [2.52] Ziegler H., A modification of Prager's hardening rule, Quarterly of Applied Mathematics 17 (1959) 55.
- [2.53] Armstrong P.J., Frederick C.O., A mathematical representation of the multiaxial Bauschinger effect, G.E.G.B. Report RD/B/N 731, Berkeley Nuclear Laboratories, (1966).
- [2.54] Chaboche J.L., Constitutive equations for cyclic plasticity and cyclic viscoplasticity, International Journal of Plasticity 5 (1989) 247-302.
- [2.55] Hill R., The mathematical theory of plasticity, University Press, Oxford (1950).
- [2.56] Hosford W.F., On yield loci of anisotropic cubic metals, 7th North American Metalworking Conference, SME, Dearborn, MI (1979) 191-197.
- [2.57] Gotoh M., Chung C., Iwata N., Effect of Out-of-Plane Stress on the Forming Limit Strain of Sheet Metals, JSME International Journal 38 (1995) 123-132.
- [2.58] Smith L.M., Averill R.C., Lucas J.P., Stoughton T.B., Matin P.H., Influence of Transverse Normal Stress on Sheet Metal Formability, International Journal of Plasticity 19(2003) 1567-1583.

Chapter 3

Investigation on the strain-path dependency of stress-based forming limit curves

3.1. Introduction

The formability of sheet metals is commonly evaluated using a forming limit curve (FLC), a curve in principal strain space that defines a boundary between combinations of strain that lead to a part that is free of necks and those that present a risk of necking and splitting. The concept of the FLC was initially developed by Keeler and Backhofen [3.3] and Goodwin [3.4] and provides a useful empirical gauge of forming severity in the absence of a visible neck or split. The shape and location of the forming limit curve (FLC) in principal strain space are a characteristic of the metal that is independent of the forming process or work piece geometry. Forming limit curves are determined experimentally by conducting hemispherical punch stretching tests up to the onset of necking on gridded blanks. The experimental testing and grid strain measurement procedure is costly, time-consuming and requires both experience and care in order to determine accurate forming limits. Therefore many researchers have sought to better predict the forming limits of sheet materials.

The most common analytical approach for the prediction of FLCs have generally relied on the continuum theory of plasticity, which includes a yield criterion, a flow or hardening rule and an instability criterion [3.5]. In recent years, however, various aspects of the microstructure have been incorporated into the theoretical methods to improve their predictive capability [3.6-3.8]. In a metal sheet, failure by splitting usually occurs when the local thickness strain reaches a critical value, such that the sheet has thinned significantly and can no longer sustain the imposed in-plane tensile stresses. The theoretical estimation of the limit strain, which is the largest strain produced in the neighborhood of a neck before failure, is evidently an extremely difficult proposition when all of the relevant parameters in the forming operation are duly taken into consideration.

The influence of strain path changes on the FLC limits its applicability to processes in which the loading path is quasi linear; in other words, one in which the ratios of the plastic strains are approximately constant throughout the forming process. However, many industrial stampings of complex shapes involve multistage forming, and in such cases, the FLC is unreliable. Both the shape and the position of the FLC in strain space are dependent on the strain history, and this has been shown for all sheet materials including steel, copper and brass, as reported, for example, by Kleemola and Pelkkikangas [3.9].

Some researchers [3.10- 3.14] have proposed that the formability of sheet metals should be based on stress state rather than strain state. They constructed the stress forming limit curve (SFLC) by plotting the combinations of stress at the onset of localized necking. They found that the SFLC is almost path-independent. Moreover, if the path-dependence of the SFLC can be quantified, either experimentally or analytically, then the limits of formability will be predicted accurately using a combination of the SFLC and finite element simulation, not only for proportional loading but also in cases where a sheet element has a complex strain history [3.15- 3.17].

In 2005, Yoshida *et al.* [3.18] carried out biaxial tension tests on an aluminum alloy tube using a tension–internal pressure testing machine in order to verify the path-independence of forming limit stress. They measured forming limit stresses, which are determined from the load, internal pressure and geometry measurements of the tube, for

many linear and combined stress paths and concluded that the forming limit stresses are path-independent. Yoshida *et al.* [3.19] subsequently calculated the forming limit stresses for a variety of two-stage combined stress paths using the Marciniak and Kuczynski (MK) model [3.20] based on a phenomenological plasticity theory with isotropic hardening in order to clarify the mechanism behind the path-independent SFLC. In this work they confirmed the experimental observations of Yoshida *et al.* [3.18] and Kuwabara *et al.* [3.21] that the work hardening behaviour of an aluminum alloy tube is well described by the isotropic hardening rule in conjunction with an appropriate anisotropic yield function and that the forming limit stresses of the aluminum alloy tube are almost path independent.

Butuc *et al.* [3.22] performed a detailed experimental and theoretical study to validate the use of a stress-based forming limit curve. They considered different constitutive equations in conjunction with the MK theory, and investigated the influence of the hardening law and yield criterion on stress-based forming limit curves. These researchers concluded that the SFLC is independent of strain path and proposed a path-induced anisotropic hardening model to better explain stress-based forming limit curves obtained under combined loading histories.

Finally, Yoshida *et al.* [3.23] investigated the path dependency of the SFLC using different work hardening models. They concluded that the path dependency of SFLC is related to the stress-strain relation during the second loading stage. Their work shows that SFLC is only path independent when the work hardening behaviour remains unchanged with a change of strain path.

In the present work, history-dependent forming limit curves were computed for sheet metals undergoing various combinations of plane-stress loading conditions. This paper presents a modified MK model for predicting SFLCs. Forming limit curves were calculated for AISI-1012 steel and AA-2008-T4 sheets and were compared with the corresponding experimental data [3.1- 3.2]. Finally, the path dependency of SFLCs based on different non-proportional loading histories was evaluated quantitatively.

3.2. Theoretical analysis

3.2.1. Strain-based forming limit curves

The stress-based forming limit curve represents the forming limit of a sheet material in terms of the in-plane principal stress components. The stress state cannot be measured directly on industrial parts but it can be calculated using appropriate constitutive equations. Knowing the experimental or predicted forming limits in strain space, the forming limit stresses can be computed using classical plasticity theory. In this work a modified MK model was used to predict the FLC.

The MK analysis used in this work assumes a pre-existing thickness imperfection in the form of a groove inclined relative to the principal strain directions, as shown in Figure 3.1. In this model, the area of nominal thickness is designated by (a) and the weaker area is denoted by (b).

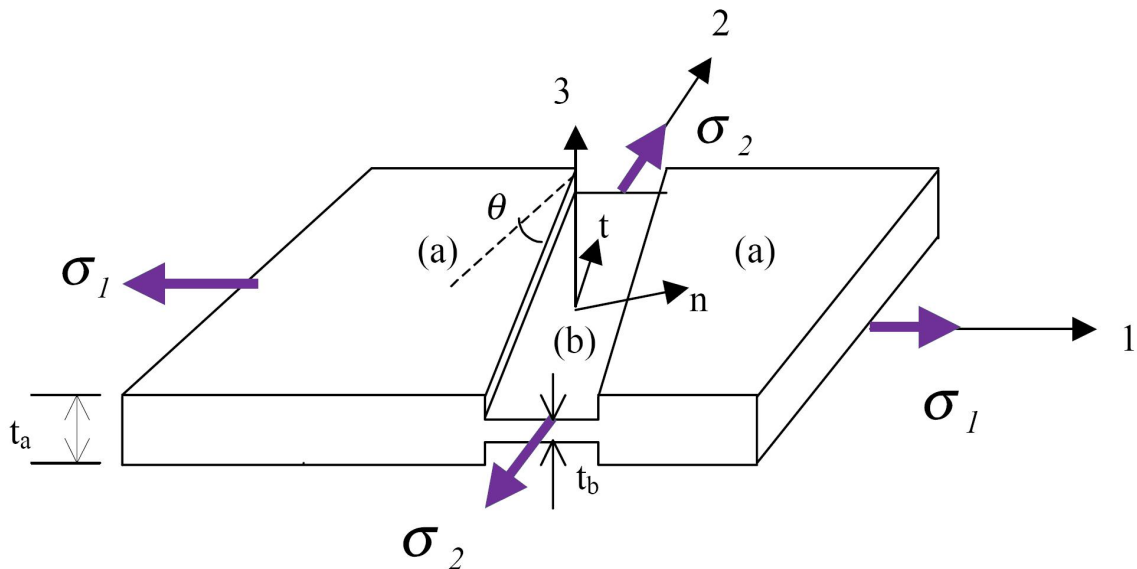


Figure 3.1. Thickness imperfection in the MK method

The physical basis for the MK analysis was well presented by McCarron *et al.* [3.24]. In their study, imperfections in the form of grooves were machined into samples made from two different steels and tested under equibiaxial stretching. It was found that

no reduction in the forming limit strain was observed for shallow grooves: i.e. when the imperfection factor f_0 - the ratio of the thickness in the groove to the nominal thickness - was greater than 0.992. The imperfection factor represents the micro-structural defects that exist in the sheet material prior to deformation.

In the current work, the initial imperfection factor of the groove, f_0 , is defined as the thickness ratio as follow:

$$f_0 = \frac{t_0^b}{t_0^a} \quad (3.1)$$

where t denotes the sheet thickness, and subscript '0' denotes the initial state. From consideration of Equation (3.1), it is possible to calculate an updated thickness imperfection as deformation progresses as below:

$$\frac{df}{f} = d\varepsilon_3^b - d\varepsilon_3^a \quad (3.2a)$$

$$f = f_0 \exp(\varepsilon_3^b - \varepsilon_3^a) \quad (3.2b)$$

where ' ε_3 ' denotes the true thickness strain. Considering Equation (3.2), it was considered that the imperfection factor changes with the deformation of the sheet. In order to estimate the initial value of the imperfection factor, it is reasonable to relate it to the surface roughness of the sheet. By supposing that the maximum thickness difference between regions (b) and (a) is equal to the surface roughness of the sheet, the initial imperfection factor can be written as follows:

$$f_0 = \frac{t_0^a - 2R_z}{t_0^a} \quad (3.3)$$

where R_z is the maximum surface roughness of the sheet.

Research carried out by Stachowicz [3.25] shows that surface roughness also changes with deformation and these changes depend upon initial surface roughness, grain size, and strain, according to the following empirical relation:

$$R_z = R_{z_0} + Cd_0^{0.5} \bar{\varepsilon} \quad (3.4)$$

where ' R_{z_0} ' is the surface roughness before deformation, C is a material constant, $\bar{\varepsilon}$ is the effective strain, and d_0 is the initial grain size. Combining Equations (3.2), (3.3) and (3.4) yields:

$$f_0 = \frac{t_0^a - 2[R_{z_0} + Cd_0^{0.5} \bar{\varepsilon}^b]}{t_0^a} \quad (3.5a)$$

$$f = \frac{t_0^a - 2[R_{z_0} + Cd_0^{0.5} \bar{\varepsilon}^b]}{t_0^a} \exp(\varepsilon_3^b - \varepsilon_3^a) \quad (3.5b)$$

As shown in Figure 3.1, the orientation θ of the thickness imperfection with respect to the minor principal stress direction is considered in the analysis. Furthermore, the initial value of this angle at the start of the deformation can be arbitrarily selected, since it changes throughout the deformation; in other words, the angle θ between the imperfection and the principal direction is updated from an initial value θ_0 at each increment of plastic deformation. Sing and Rao [3.26] showed that by considering uniform deformation, the rotation of the initial thickness imperfection can be expressed as a function of the strain increments in the nominal area (a) of the sheet as follows:

$$\tan(\theta + d\theta) = \tan(\theta) \frac{1 + d\varepsilon_1^a}{1 + d\varepsilon_2^a} \quad (3.6)$$

Where $d\varepsilon_1^a$ and $d\varepsilon_2^a$ are the major and minor principal strains in the nominal area of the sheet, respectively.

Sheet material is generally anisotropic, and it was assumed that the principal axes of anisotropy are coincident with the principal stress directions in the sheet. Hill's quadratic yield function [3.27] was adopted to describe the sheet anisotropy, and for plane-stress conditions, this function can be written as:

$$2h = \sigma_e^2 = (G + H)\sigma_{xx}^2 + (F + H)\sigma_{yy}^2 - 2H\sigma_{xx}\sigma_{yy} + 2P\sigma_{xy}^2 \quad (3.7)$$

where F, G, H and P are anisotropic constants that can be calculated by the following expressions [3.27]:

$$F = \frac{R_0}{R_{90}(1 + R_0)} \quad (3.8a)$$

$$G = \frac{1}{R_0 + 1} \quad (3.8b)$$

$$H = \frac{R_0}{R_0 + 1} \quad (3.8c)$$

$$G + H = 1 \quad (3.8d)$$

where R_0 and R_{90} are the anisotropic coefficients in the rolling and transverse directions, respectively.

The associated flow rule in the principal axes of orthotropic anisotropy is expressed in the form [3.28]:

$$d\varepsilon_{ij} = d\lambda' \frac{\partial h}{\partial \sigma_{ij}} \quad (3.9)$$

where, $d\lambda' = \frac{d\varepsilon_e}{\sigma_e}$ is the plastic multiplier.

Material work hardening is expressed in an equivalent form using Swift's power law:

$$\sigma_e = k \dot{\varepsilon}_e^m (\varepsilon_e + \varepsilon_0)^n \quad (3.10)$$

where σ_e and ε_e are the effective stress and strain values, respectively. Moreover, it is assumed that the yield surface expands isotropically in stress space.

The hardening law can also be expressed in differential form:

$$d(\ln \sigma_e) = m d(\ln \dot{\varepsilon}_e) + n d(\ln(\varepsilon_e + \varepsilon_0))$$

where ε_0 is a uniform prestrain applied to the sheet prior to the current forming process; m is the strain-rate sensitivity coefficient; and n is the strain-hardening coefficient.

Considering the yield criterion and its associated flow rule, the strain path ρ can be written as:

$$\rho = \frac{d\varepsilon_2}{d\varepsilon_1} = \frac{(F + H)\alpha - H}{1 - H\alpha} \quad (3.11)$$

where α is the ratio of principal stresses:

$$\alpha = \frac{\sigma_2}{\sigma_1} = \frac{\sigma_{yy}}{\sigma_{xx}} \quad (3.12)$$

$d\varepsilon_1$, $d\varepsilon_2$, σ_1 and σ_2 are the principal strain increments and the principal stresses in the area of nominal thickness (i.e. in region (a) of the sheet).

The basic compatibility equations for the MK analysis are:

$$d\varepsilon_{tt}^a = d\varepsilon_{tt}^b \quad (3.13)$$

where $d\varepsilon_t^a$ and $d\varepsilon_t^b$ denote the tangential strain increment to the groove in regions (a) and (b), respectively. The requirement of force equilibrium across the imperfection groove is written as:

$$F_m^a = F_m^b \quad (3.14)$$

$$F_{nt}^a = F_{nt}^b \quad (3.15)$$

where F_m^a and F_m^b denote the force per unit width in the direction normal to the groove in regions (a), and (b), respectively, and F_{nt}^a and F_{nt}^b are the shear forces per unit width in regions (a) and (b), respectively, i.e.:

$$\begin{cases} F_m^a = \sigma_m^a t^a \\ F_m^b = \sigma_m^b t^b \end{cases} \quad (3.16)$$

$$\begin{cases} F_{nt}^a = \sigma_{nt}^a t^a \\ F_{nt}^b = \sigma_{nt}^b t^b \end{cases} \quad (3.17)$$

Considering these MK equations, the governing equation of strain for each region can be determined. A biaxial stress state is imposed in the nominal area and causes development of strain increments in both the nominal area (a) and in the weaker area (b). Strain development in thinner region (b) is greater than in thicker region (a) and the difference in strain rate between both regions increases with deformation. The limiting strains due to necking are calculated numerically by a combination of the Newton-Raphson and the (4th order) Runge-Kutta methods, with the assumption that necking occurs once the effective strain rate in the groove area reaches 10 times that in the nominal area; that is when $d\varepsilon_e^b/d\varepsilon_e^a > 10$. The limiting values of ε_1 and ε_2 in area (a) were

determined for various linear strain paths ranging from $\rho = \varepsilon_2/\varepsilon_1 = -0.5$ to 1.0 and were plotted on the FLC.

3.2.2. Stress-based forming limit curves

In order to determine stress-based FLCs, the general method proposed by Stoughton [3.11] was employed to translate limit strains into limit stresses. If a prestrain leads to an initial strain state $(\varepsilon_{1i}, \varepsilon_{2i})$, and a secondary forming operation results in a final strain state $(\varepsilon_{1f}, \varepsilon_{2f})$, then the principal stresses at the end of the secondary stage are given by [3.13]:

$$\sigma_1 = \frac{\bar{\sigma}(\bar{\varepsilon}(\varepsilon_{1i}, \varepsilon_{2i}) + \bar{\varepsilon}(\varepsilon_{1f} - \varepsilon_{1i}, \varepsilon_{2f} - \varepsilon_{2i}))}{\xi(\alpha(\varepsilon_{2f} - \varepsilon_{2i})/(\varepsilon_{1f} - \varepsilon_{1i}))} \quad (3.18)$$

and

$$\sigma_2 = \alpha \left(\frac{\varepsilon_{2f} - \varepsilon_{2i}}{\varepsilon_{1f} - \varepsilon_{1i}} \right) \sigma_1 \quad (3.19)$$

$$\bar{\varepsilon}_f = \bar{\varepsilon}_i + \lambda \varepsilon_{1f} \quad (3.20)$$

The plasticity assumptions used in the MK analysis were also used to calculate parameters $\alpha(\rho)$ and $\lambda(\rho)$ and transform the forming limit curve into stress space; i.e. Hill's quadratic yield function, the associated flow rule and Swift's work hardening law. The related formulation is presented in appendix d of reference [3.13].

Equations (3.18) and (3.19) can be used to calculate the limit stresses for bilinear strain paths. These equations can also be employed to calculate the SFLC for the as-received state, and in this case there is no prestrain ($\varepsilon_{1i} = \varepsilon_{2i} = 0$).

3.3. Results

3.3.1. Material characterization

The materials considered throughout this investigation for model verification are a low carbon steel AISI-1012 [3.1] and AA-2008-T4 reported by Graf and Hosford [3.2]. Tables 3.1 and 3.2 present the anisotropy coefficients, the corresponding yield stresses and other related material properties for AISI-1012 and AA-2008-T4 alloys [3.1- 3.2], respectively.

Table 3.1: Material properties of AISI-1012 low carbon steel [3.1]

R₀	R₄₅	R₉₀	F	G	H	K (MPa)
1.4	1.05	1.35	0.432	0.417	0.583	238
n	m	d₀ (μ)	R_{Z0} (μm)	C	t₀ (mm)	
0.30	0.01	25	6.5	0.104	2.5	

Table 3.2: Average mechanical properties of AA-2008-T4 [3.2]

R₀	R₄₅	R₉₀	F	G	H	K (MPa)
0.58	0.48	0.78	0.246	0.633	0.367	535
n	m	d₀ (μ)	R_{Z0} (μm)	C	t₀ (mm)	
0.27	-0.003	8*	2.5*	0.70*	1.7	

* Data determined by calibration

As a result of Equations (3.3) and (3.4), the value of the initial imperfection factor in the MK analysis is $f_0 = 0.995$ for AISI-1012 steel and $f_0 = 0.997$ for AA-2008-T4 alloy.

3.3.2. Validation of the MK model

The proposed MK model was used to calculate the FLC of as-received AISI-1012 low carbon steel sheets, and Figure 3.2 shows the comparison between the theoretical results and the experimental FLC [3.1]. It can be seen that the predicted FLC is in good agreement with the experimental data for as-received AISI-1012. In order to validate the proposed MK model for bilinear strain paths, the predicted FLC for the AA-2008-T4 alloy was calibrated to the experimental FLC in the as-received state by adjusting the values of C , d_0 , R_{Z0} (these material constants were not provided in [3.2]). The values of the material parameters determined by the calibration were $C = 0.70$, $d_0 = 8.00\mu\text{m}$ and $R_{Z0} = 2.5\mu\text{m}$. Then forming limit curves were calculated for two sets of bilinear strain paths for which experimental data were provided in [3.2]. First, FLCs were determined after 4 and 12 percent equibiaxial prestrains and secondly, FLCs were calculated after 5 and 12 percent uniaxial prestrains. The predicted FLCs and the corresponding experimental FLCs for the AA-2008-T4 alloy [3.2] are shown in Figures 3.3 and 3.4.

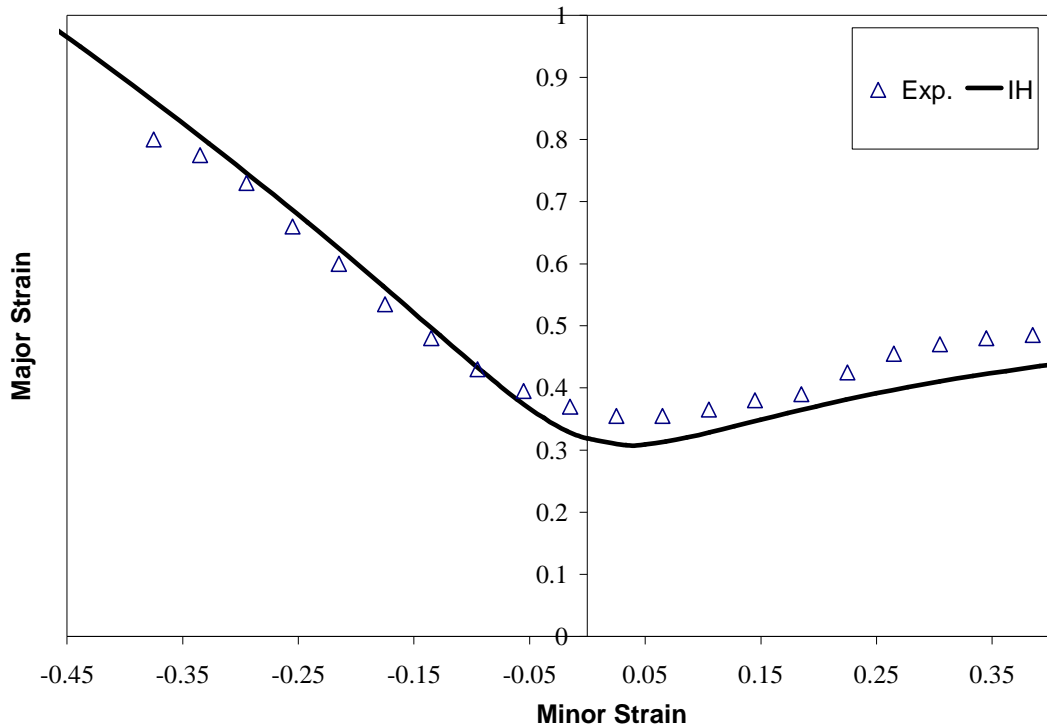


Figure 3.2. Comparison of theoretical and experimental FLC AISI-1012 low carbon steel in the as-received state

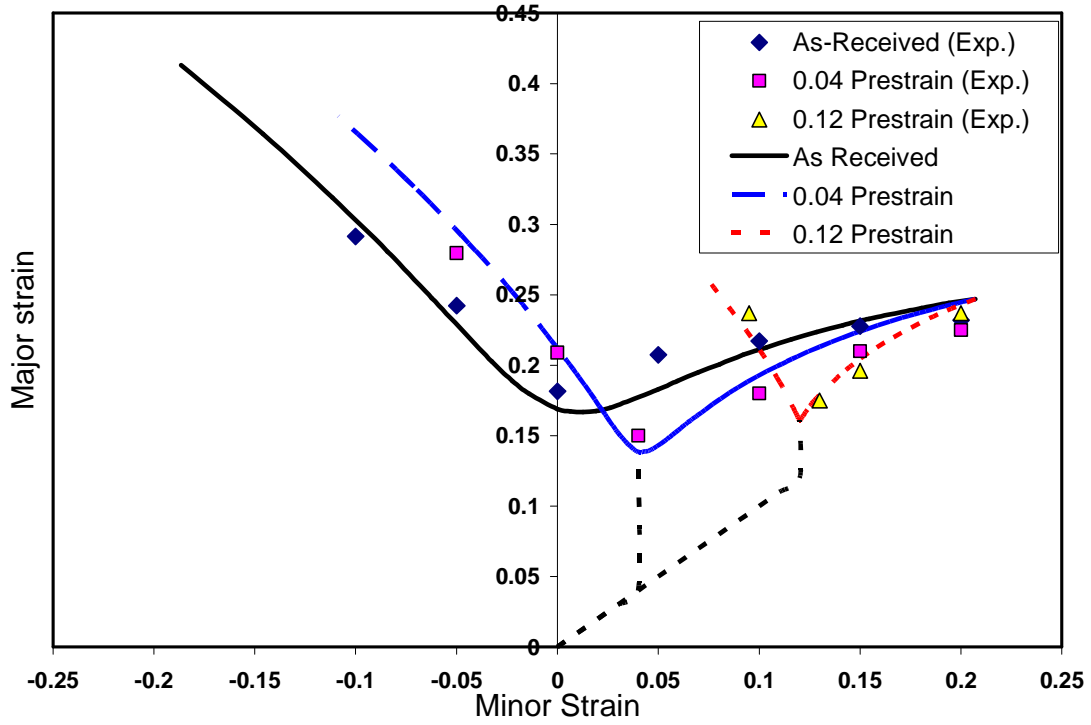


Figure 3.3. Theoretical and experimental FLCs of AA-2008-T4 with 4 and 12 percent equibiaxial prestrain after calibrating the MK model to the as-received FLC.

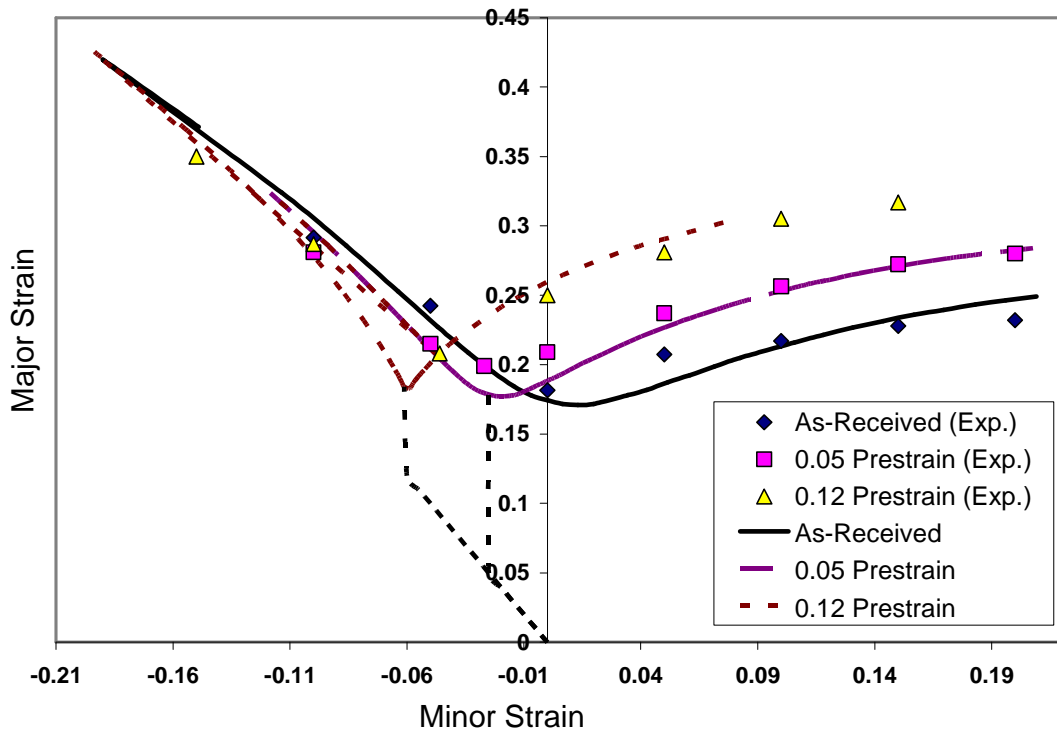


Figure 3.4. Theoretical and experimental FLCs of AA-2008-T4 with 5 and 12 percent uniaxial prestrain after calibrating the MK model to the as-received FLC.

As can be seen, the correlation between predicted and experimental FLC after bilinear strain paths is quite good for both sheet materials.

3.3.3. Predicted FLCs for bilinear strain paths

The theoretical MK model described in section 2 was used to compute FLC of AISI-1012 sheet material for a variety of non-linear strain histories that consisted of two successive loading stages. The first stage was 20 percent strain in each of the following modes: uniaxial tension, plane-strain tension, and equibiaxial tension. The second loading stage consisted of a set of strain paths ranging from uniaxial tension ($\rho = -0.5$) to equibiaxial tension ($\rho = 1.00$) at increments $\Delta\rho = 0.05$ in order to determine the complete FLC. Every bilinear strain-path was simulated with the MK model without unloading between the first and second loading stages, and three cases of prestrain will be discussed.

Case 1: the FLC was determined after the sheet metal was virtually prestrained 0.20 in uniaxial tension along the rolling direction. The FLC predicted for this case is plotted in Figure 3.5 with the corresponding as-received FLC (also predicted with this MK model). Theoretical results in this FLC show that after uniaxial prestraining, the forming limit decreases somewhat for subsequent drawing operations (i.e. negative minor strains), but improves for stretch-forming operations (i.e. positive minor strains). Also, the plain-strain intercept of the FLC shifts slightly towards the negative minor strains.

Case 2: In order to observe the effects of a prestrain in plane-strain, the FLC was calculated after the material was prestrained 0.20 in plane-strain along the sheet rolling direction. The influence of this prestrain is shown in Figure 3.6, where the as-received and prestrained FLCs are compared. It appears that after a prestrain in plane-strain, the forming limit increases for all deformation modes except plane-strain where the forming limit remains almost unchanged. It should be noted, however, that isotropic hardening was assumed in this MK model and an assumption of kinematic or mixed isotropic-kinematic hardening may well lead to different conclusions.

Case 3: The FLC was computed after a 0.20 prestrain in equibiaxial tension. The effect of a prestrain in equibiaxial tension is shown in Figure 3.7, and it can be observed that the left hand side of the FLC shifts up significantly, but the plain-strain intercept of the FLC decreases and shifts towards the positive minor strains resulting in a decrease in formability for strain paths on the right side of the FLC.

The strain-path dependency of the FLC can be evaluated by considering the various FLCs in Figure 3.8 for these three cases of prestrain. It is evident from this figure that the FLC is strongly path dependent as evidenced by the shape changes and significant translations of the FLCs in strain space for all prestrain modes.

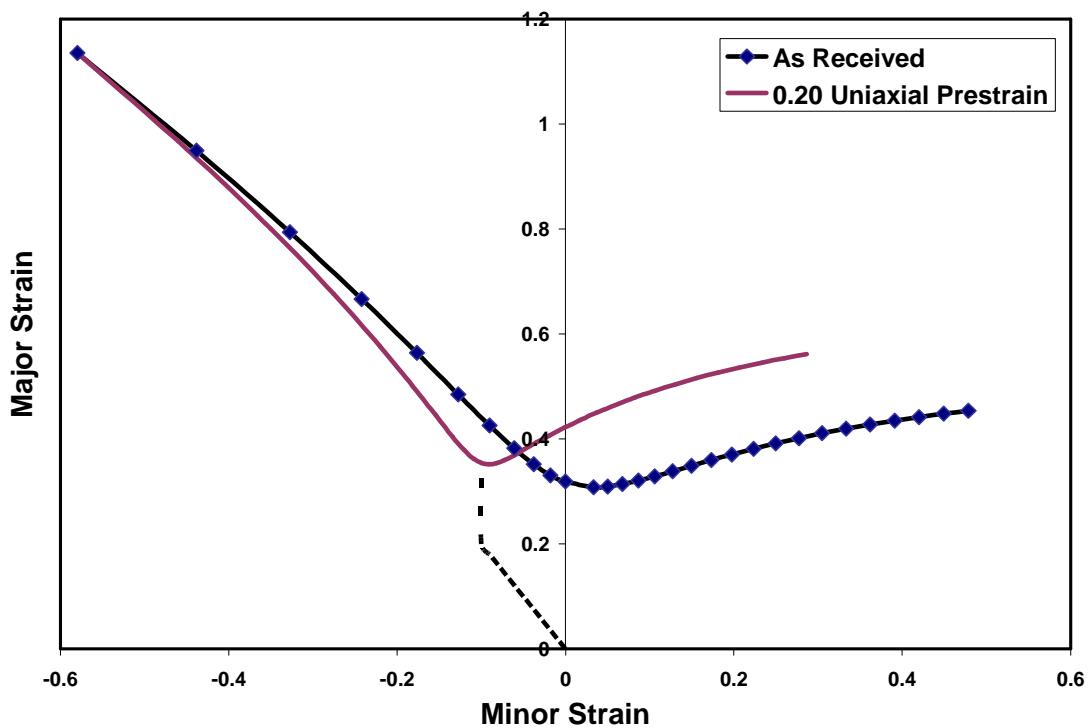


Figure 3.5. Effect of 0.20 uniaxial prestrain on FLC for AISI-1012 steel

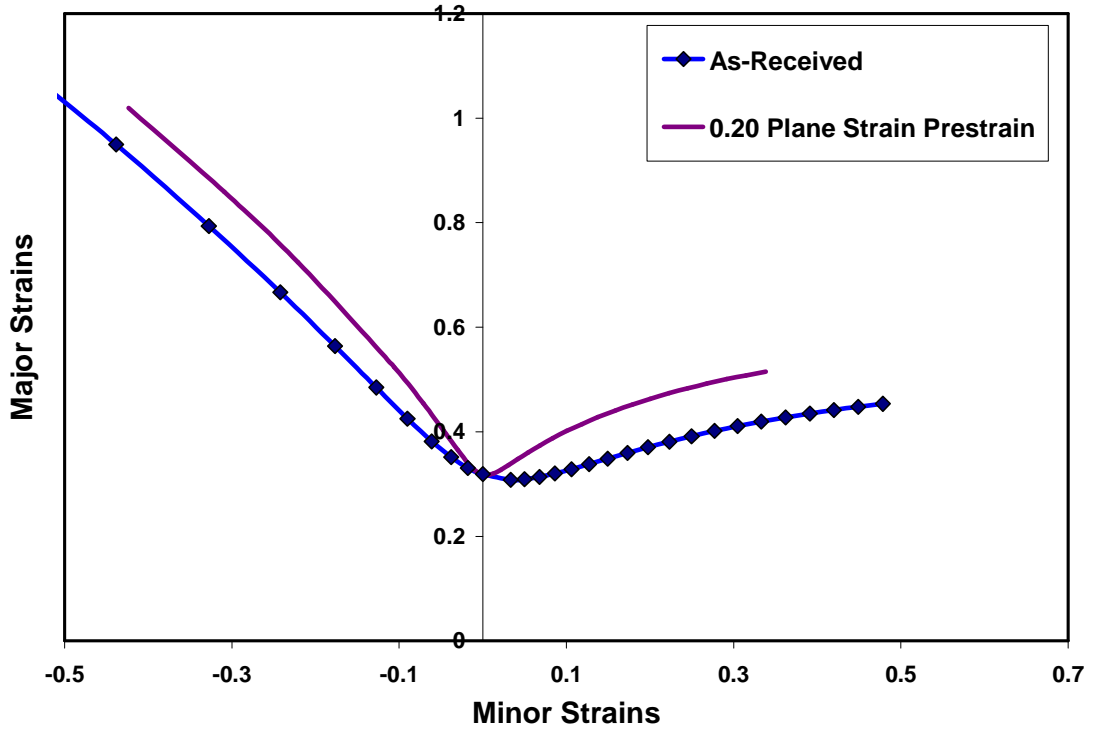


Figure 3.6. Effect of 0.20 plane-strain prestrain on FLC for AISI-1012 steel

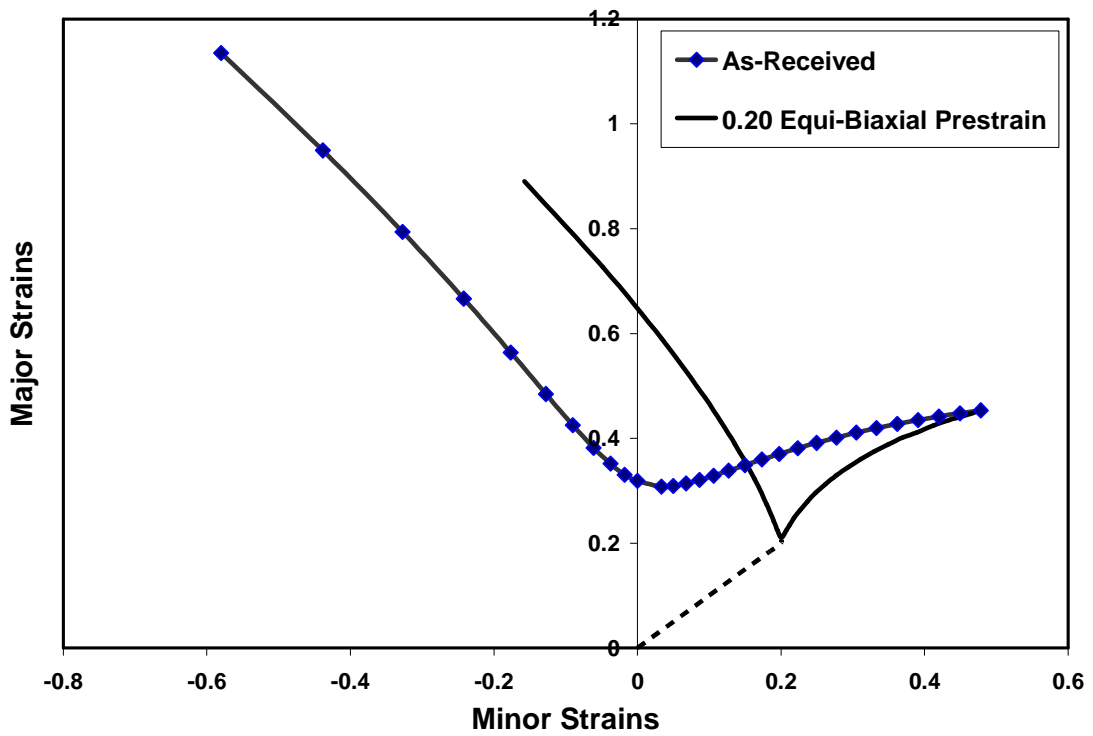


Figure 3.7. Effect of 0.20 equibiaxial prestrain on FLC for AISI-1012 steel

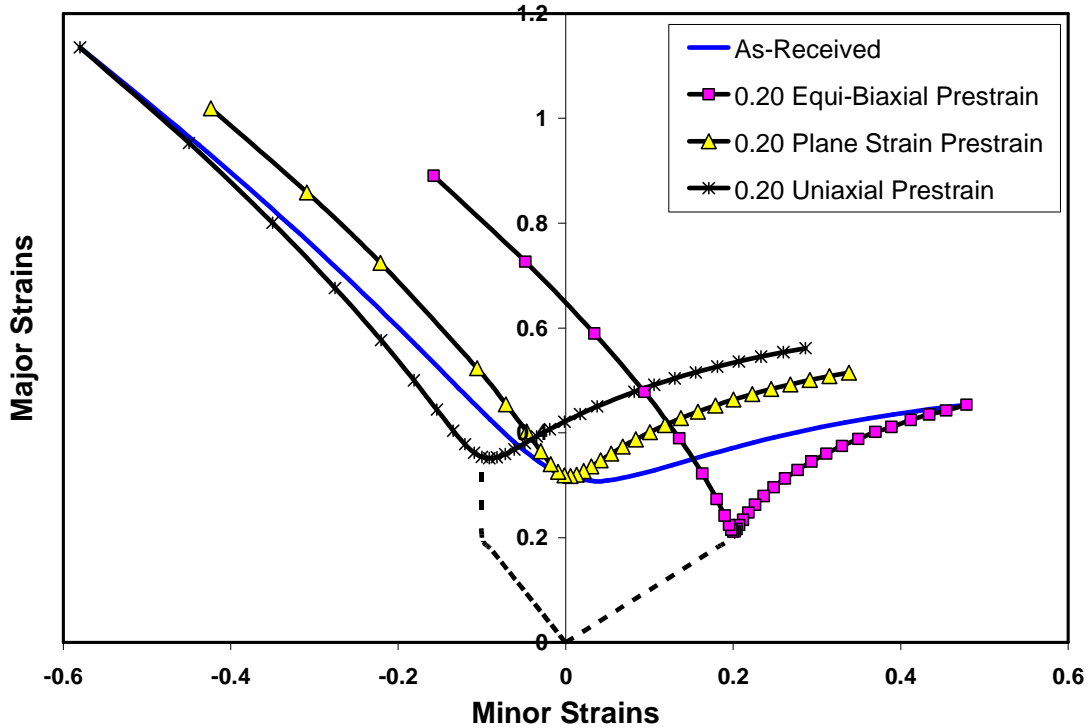


Figure 3.8. Predicted FLCs after 0.20 prestrain in uniaxial tension, plane-strain tension, and equibiaxial tension for AISI-1012 steel

3.3.4. Stress-based forming limit curves

According to the investigations of Arrieux [3.10], Stoughton [3.13- 3.14] and other researchers [3.9, 3.11, 3.16], the most significant characteristic of stress-based forming limit curves (SFLC) is their strain-path independence. However, more recent experimental investigations by Yoshida *et al.* [3.18- 3.19] have pointed out that abrupt changes in strain path can lead to some path-dependency of the SFLC.

In order to further investigate this path-dependence of SFLCs, the current MK model was used to predict the FLC of AISI-1012 steel sheets after a prestrain in either uniaxial tension or in equibiaxial tension. In addition, the FLC was computed in each case for values of effective prestrain $\bar{\epsilon} = 0.10, 0.20$ and 0.45 . As mentioned in Section 2.2, the theoretical SFLCs were obtained by using Stoughton's method [3.13] to translate the limiting strains into stress space, using the same constitutive assumptions as in the MK model. In other words, for every FLC predicted using the current modified MK

analysis, a corresponding SFLC was also predicted. The stress-based forming limit curve of as-received AISI-1012 steel is shown in Figure 3.9.

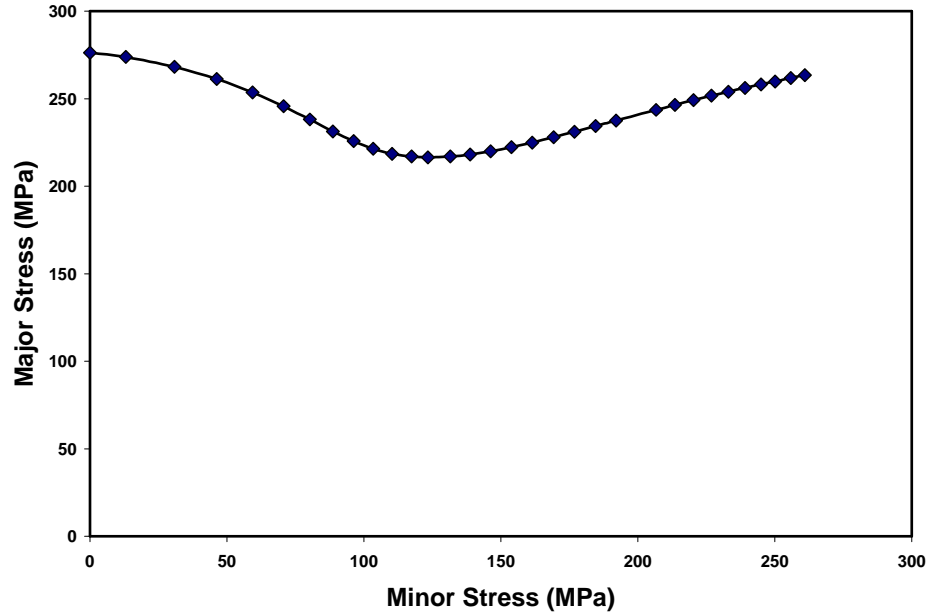


Figure 3.9. Stress-based forming limit curve (SFLC) of as-received AISI-1012 steel

Figure 3.10 demonstrates the effect of various levels of prestrain in uniaxial tension on the SFLC of AISI-1012 steel. It can be seen that the SFLCs obtained after an effective prestrain in uniaxial tension $\bar{\epsilon} = 0.10$ and $\bar{\epsilon} = 0.20$ are practically identical. However, the SFLC obtained after an effective prestrain $\bar{\epsilon} = 0.45$ in uniaxial tension is significantly different than those obtained at lower levels of prestrain, with the greatest difference being in the mode of plane-strain.

The final evaluation was carried out to determine the influence of the magnitude of prestrain in equibiaxial tension on the SFLC. Similar to the previous case, the FLC was predicted with the MK model after the material was prestrained to an effective strain in equibiaxial tension $\bar{\epsilon} = 0.10$, 0.20 , and 0.45 , and the SFLC was calculated from the FLC. Once again, no strain-path dependency was observed for lower levels of prestrain ($\bar{\epsilon} = 0.10$ and $\bar{\epsilon} = 0.20$), however, some path dependency was observed for the highest value of prestrain ($\bar{\epsilon} = 0.45$) as seen in Figure 3.11.

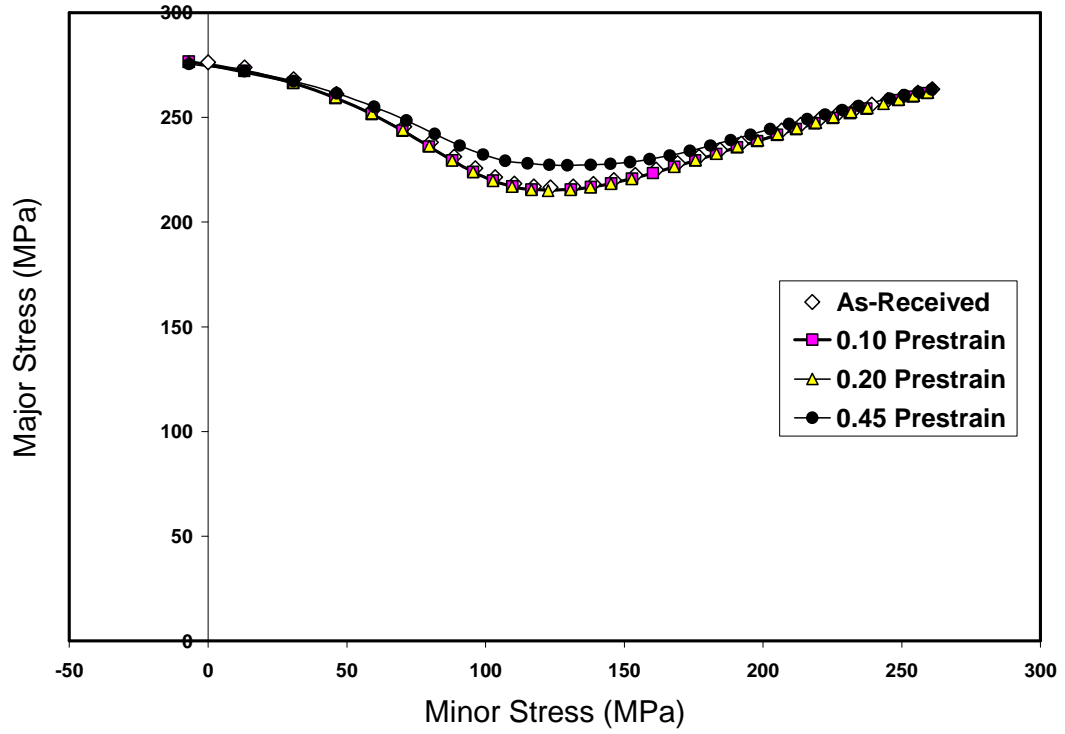


Figure 3.10. Comparison of the SFLC after different levels of prestrain in uniaxial tension with the as-received SFLC of AISI-1012 steel

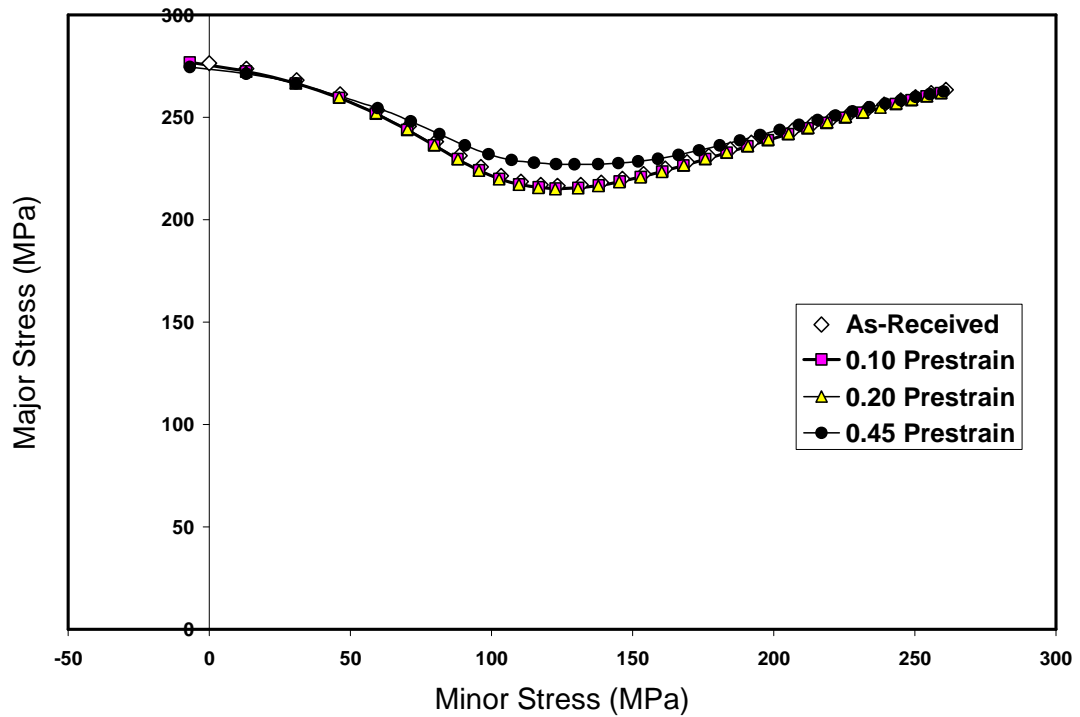


Figure 3.11. Comparison of the SFLC after different levels of prestrain in equibiaxial tension with the as-received SFLC of AISI-1012 steel

In order to visually compare the path dependency of the SFLC after both types of prestrain, the SFLCs obtained after an effective prestrain $\bar{\epsilon} = 0.45$ in uniaxial and in equibiaxial tension are shown together in Figure 3.12. It is clear from this figure that the path dependency of SFLC is similar for both types of prestrain, and the greatest discrepancy with the as-received SFLC occurs around the mode of plane-strain.

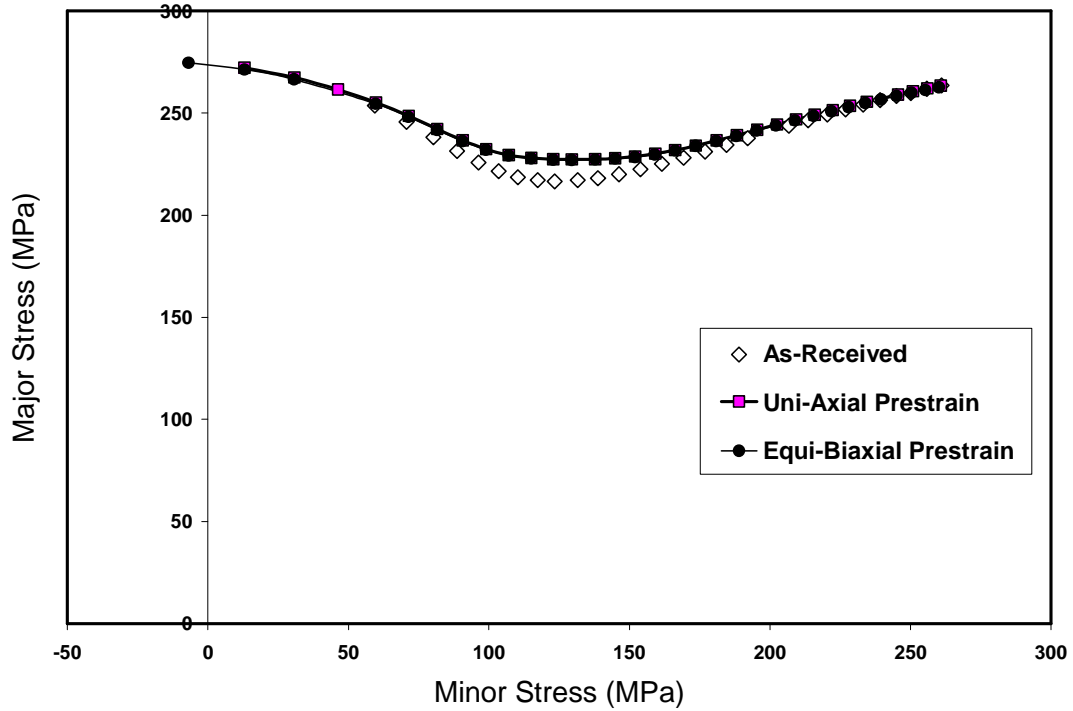


Figure 3.12. Comparison of the SFLC after an effective prestrain $\bar{\epsilon} = 0.45$ in uniaxial and equibiaxial tension with the as-received SFLC of AISI-1012 steel

In order to quantify the strain path dependency of SFLCs as a function of the magnitude of prestrain and the type of strain path, the absolute difference in major stress (for a given strain ratio) was determined between the SFLC predicted after bilinear strain paths and the as-received SFLC. These absolute differences are presented in Figures 3.13-3.15 in terms of a percent deviation as a function of the principal strain ratio for effective prestrains $\bar{\epsilon} = 0.10$, 0.20 and 0.45, respectively. According to these charts, the difference in major stress between the as-received and prestrained SFLCs is less than 1.0% when the effective prestrain is $\bar{\epsilon} = 0.10$ and $\bar{\epsilon} = 0.20$ (Figures 3.13 & 3.14). However, the maximum deviation from the as-received SFLC reaches about 5.0% for an effective

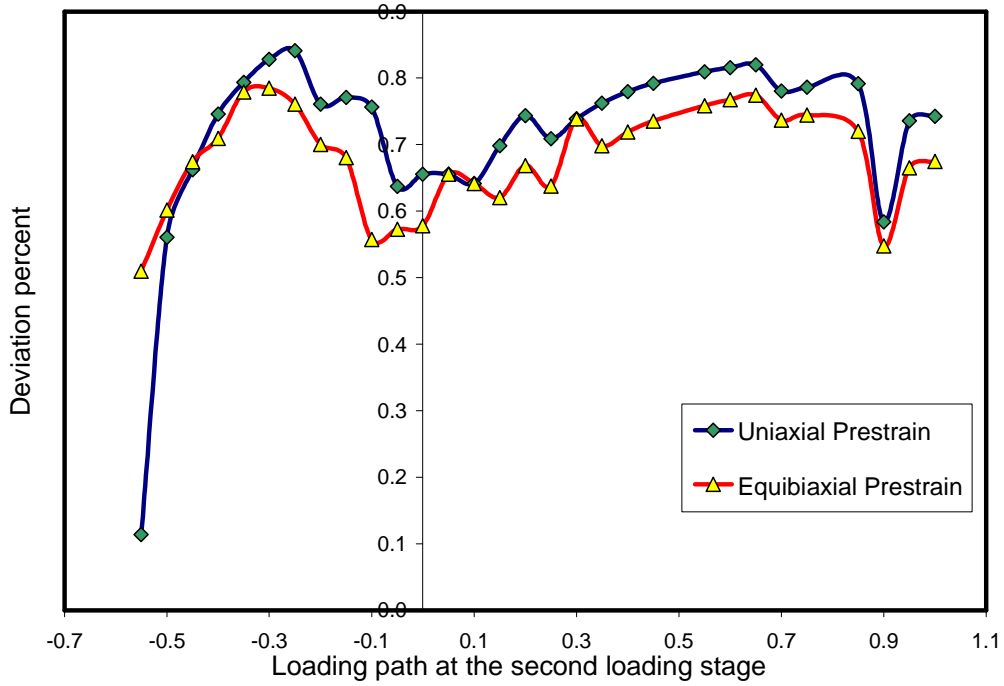


Figure 3.13. Deviation in major stress between prestrained and as-received SFCLs for an effective prestrain $\bar{\epsilon} = 0.10$ in AISI-1012 steel sheets

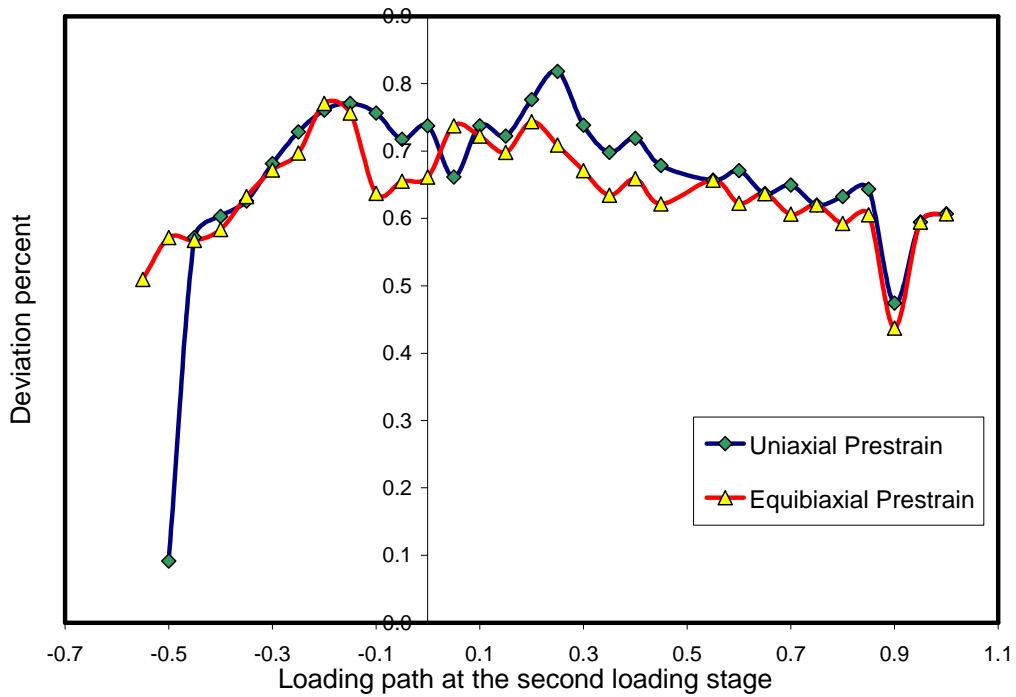


Figure 3.14. Deviation in major stress between prestrained and as-received SFCLs for an effective prestrain $\bar{\epsilon} = 0.20$ in AISI-1012 steel sheets

prestrain $\bar{\epsilon} = 0.45$ (Figure 3.15). In Figure 3.15 the deviation from the as-received SFLC is greatest in the vicinity of plane-strain deformation and less severe for other modes of deformation, however it reveals the non-uniqueness of the SFLC when loading follows a bilinear strain path and when the prestrain exceeds a certain value.

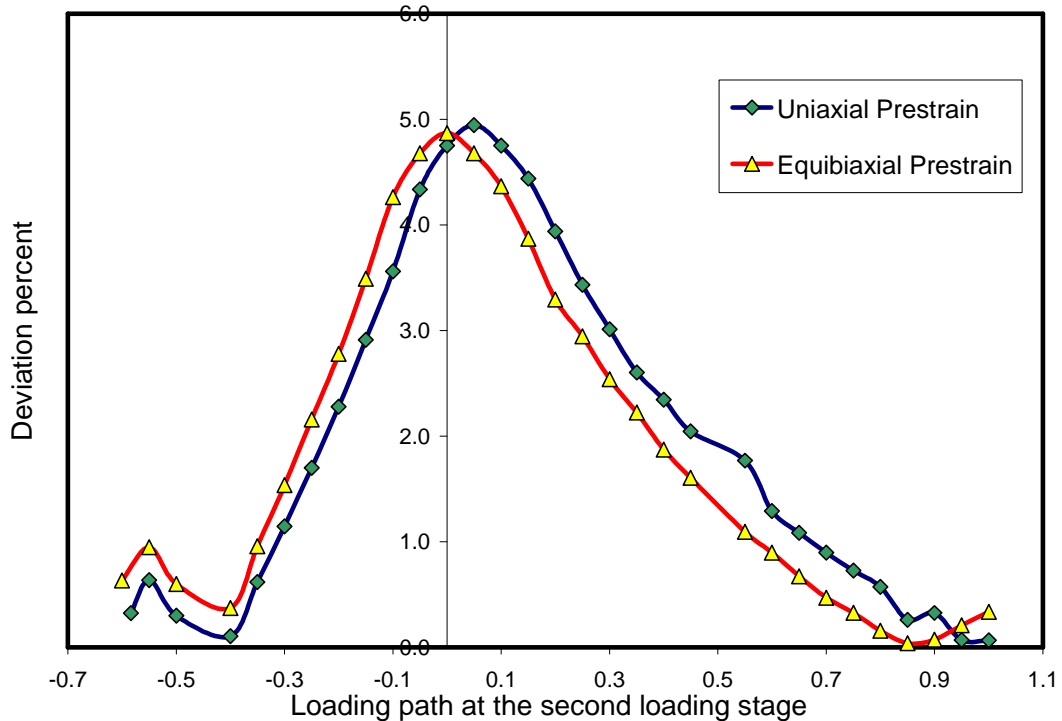


Figure 3.15. Deviation in major stress between prestrained and as-received SFLCs for an effective prestrain $\bar{\epsilon} = 0.45$ in AISI-1012 steel sheets

In order to understand how the maximum deviation in major stress between the prestrained and as-received SFLCs evolves with effective prestrain, additional levels of prestrain were considered up to an effective prestrain $\bar{\epsilon} = 0.5$. The maximum deviation between the prestrained and as-received SFLCs was calculated and plotted as a function of effective prestrain (Figure 3.16). This figure shows that the deviation between the two SFLCs increases above 1% for effective prestrains greater than $\bar{\epsilon} = 0.35$. Although prestrains greater than $\bar{\epsilon} = 0.35$ are not common in stamping operations, they can be seen in tube bending prior to a hydroforming application. In such cases the as-received SFLC would not be a reliable measure of formability. Therefore the non-uniqueness of the

SFLC appears to be dependent on the magnitude of the prestrain in a bilinear strain path, as was reported by Yoshida *et al.* [3.18].

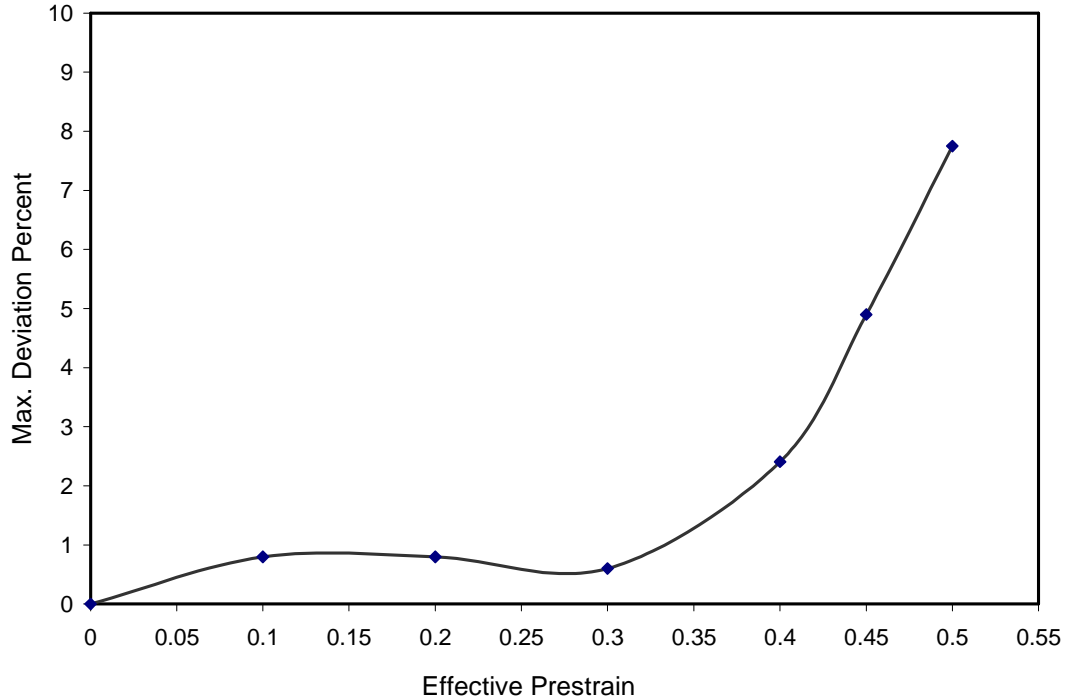


Figure 3.16. Maximum deviation in major stress between prestrained and as-received SFLCs for different effective prestrain values in AISI-1012 steel sheets

Further work is still required to understand the influence of the magnitude of the prestrain in the first stage of the bilinear strain path and the influence of the severity of the strain path non-linearity on the SFLC. A possible cause of this dependency is the manner in which the yield locus changes with work hardening during the first stage of the strain path. Indeed, isotropic hardening assumes that the yield locus expands uniformly in both stages of the bilinear strain path, but kinematic or mixed isotropic-kinematic hardening assumes there is some translation of the yield locus. Furthermore, Yoshida *et al.* [3.23] demonstrated that the change in work-hardening behaviour during the second loading stage is the main reason for path dependency of the SFLC. Also, the transient effects that might exist during the reloading between the first and second stages of the strain history may also have an effect on the evolution of the SFLC. Finally, as the

prestrain increases, the yield locus may expand into the plane-strain region above the SFLC, which may have an effect on the shape change of the SFLC that was observed in the vicinity of plane-strain deformation.

3.4. Conclusion

In this paper, the MK analysis was employed to investigate the strain path dependency of stress-based forming limit curves. The current model was developed in such a way as to incorporate effects of material properties such as grain size, surface roughness, and rotation of the initial thickness imperfection (Equation 3.6). The thickness imperfection was considered to be a function of the surface roughness, and both the surface roughness and the thickness ratio, f , were incrementally updated throughout the loading process (Equations 3.4 and 3.5) as the effective strain evolved. The FLC of AISI-1012 steel and AA-2008-T4 aluminum sheets were determined with this MK model for bilinear strain paths where various magnitudes of prestrain were applied in either uniaxial or equibiaxial tension. Finally, Stoughton's method [3.13] was subsequently employed to translate limit strains into limit stresses, using the same constitutive assumptions as in the MK analysis.

Results indicate that the SFLC remains essentially unchanged for lower levels of prestraining and therefore the path dependency of SFLCs is neither evident nor significant for effective prestrains less than $\bar{\epsilon} = 0.35$. However, a large prestrain ($\bar{\epsilon} \geq 0.35$) in either uniaxial or equibiaxial tension causes an upward shift in the SFLC in the vicinity of plane-strain deformation. Furthermore the SFLCs obtained after a prestrain in uniaxial and equibiaxial tension with the same level of effective strain are practically identical, therefore the SFLC appears to be more dependent on the magnitude of the prestrain than on the strain path itself.

Further work is still required to fully understand the sources of path dependency in SFLCs. Nevertheless, in comparison with strain-based FLCs that show a very significant strain-path dependency, stress-based FLCs remain much less sensitive to

strain path. And the current observations certainly support the use of SFLCs for formability evaluation in finite element analyses of metal forming processes in which the material undergoes nonlinear strain paths with a moderate level of prestrain.

3.5. References

- [3.1] Molaei B., Strain path effects on sheet metal formability, Amirkabir University of Technology, Iran (1999) PhD thesis.
- [3.2] Graf A., Hosford W., Effect of changing strain paths on forming limit diagrams of Al 2008-T4, Metallurgical Transactions 24A (1993) 2503- 2512.
- [3.3] Keeler S.P., Backhofen W.A., Plastic instability and fracture in sheet stretched over rigid punches, ASM Transactions Quarterly 56 (1993) 25-48.
- [3.4] Goodwin G.M., Application of strain analysis to sheet metal forming in the press shop, SAE (1968) paper 680093.
- [3.5] Hillier M.J., Tensile plastic instability under complex stress, International Journal of Mechanical Sciences 5 (1963) 57-67.
- [3.6] Kim K.K., Kim D.W., Effect of void growth on the limit strains of steel sheets, International Journal of Mechanical Sciences 25 (1983) 293-300.
- [3.7] Tai W.H., Predictions of limit strains in sheet metal using a plastic damage model, International Journal of Mechanical Sciences 30 (1988) 119-126.
- [3.8] Bressan J.D., Williams J.A., The use of a shear instability criterion to predict local necking in sheet metal deformation, International Journal of Mechanical Sciences 25 (1983) 155-168.
- [3.9] Kleemola H.J., Pelkkikangas M.T., Effect of pre-deformation and strain path on the forming limits of steel, copper and brass, Sheet Metal Industries 63 (1977) 559-59.
- [3.10] Arrieux R., Bedrin C., Boivin M., Determination of an intrinsic forming limit stress diagram for isotropic sheets, Proceedings of the 12th IDDRG Congress 2 (1982) 61-71.
- [3.11] Gronostajski I., Sheet metal forming limits for complex strain paths, Journal of

- Mechanical Working Technology 10 (1984) 349-362.
- [3.12] Zhao L.R., Sowerby R., Sklad M.P., A theoretical and experimental investigation of limit strains in sheet metal forming, *International Journal of Mechanical Sciences* 38 (1996) 1307-1317.
- [3.13] Stoughton T.B., A general forming limit criterion for sheet metal forming, *International Journal of Mechanical Sciences* 42 (2000) 1-27.
- [3.14] Stoughton T.B., Stress-based forming limits in sheet metal forming, *Journal of Engineering Materials and Technology*, ASME 123 (2001) 417-422.
- [3.15] Zimniak Z., Application of a system for sheet metal forming design, *Journal of Materials Processing Technology* 106 (2000a) 159-162.
- [3.16] Zimniak Z., Implementation of the forming limit stress diagram in FEM simulations, *Journal of Materials Processing Technology* 106 (2000b) 261-266.
- [3.17] Stoughton T.B., Yoon J.W., Sheet metal formability analysis for anisotropic materials under non-proportional loading, *International Journal of Mechanical Sciences* 47 (2005) 1972-2002.
- [3.18] Yoshida K., Kuwabara T., Narihara K., Takahashi S., Experimental verification of the path dependence of forming limit stresses, *International Journal of Forming Processes* 8 (2005) 283-298.
- [3.19] Yoshida K., Kuwabara T., Kuroda M., Path-dependence of the forming limit stresses in a sheet metal, *International Journal of Plasticity* 23 (2007) 361-384.
- [3.20] Marciniak Z., Kuczynski K., Limit strains in the processes of stretch-forming sheet metal, *International Journal of Mechanical Sciences* 9 (1967) 609-620.
- [3.21] Kuwabara T., Yoshida K., Narihara K., Takahashi S., Anisotropic plastic deformation of extruded aluminum alloy tube under axial forces and internal pressure, *International Journal of Plasticity* 21 (2005) 101-117.
- [3.22] Butuc M.C., Gracio J.J., Barata da Rocha A., An experimental and theoretical analysis on the application of stress-based forming limit criterion, *International Journal of Mechanical Sciences* 48 (2006) 414-429.
- [3.23] Yoshida K., Suzuki N., Forming limit stresses predicted by phenomenological plasticity theories with anisotropic work-hardening behavior, *International Journal of Plasticity* 24 (2008) 118-139.

- [3.24] McCarron T.J., Kain K.E., Hahn G.T., Flanagan W.E., Effect of geometrical defects in forming sheet steel by biaxial stretching, *Metallurgical Transactions* 19A (1988) 2067-2074.
- [3.25] Stachowicz F., Effect of annealing temperature on plastic flow properties and forming limits diagrams of Titanium and Titanium alloy sheets, *Transactions of the Japan Institute of Metals* 29 (1988) 484-493.
- [3.26] Sing W.M., Rao K.P., Influence of material properties on sheet metal formability limits, *Journal of Materials Processing Technology* 48 (1995) 35-41.
- [3.27] Hill R., *The mathematical theory of plasticity*, Oxford University press (1950).
- [3.28] Ravishankar C., Venkadesan S., Ductility of sheet metal in the negative minor strain region of forming limit diagrams, *Scripta Materialia* 35 (1996) 323-326.

Chapter 4

Prediction of sheet forming limits with Marciniak and Kuczynski analysis using combined isotropic–non linear kinematic hardening

4.1. Introduction

The formability of sheet metal, or the amount of uniform deformation the sheet can sustain in a forming process, is limited by the occurrence of localized necking, i.e. non-uniform strains within a small region in the plane of the sheet. The forming limit of a metal sheet is generally given in terms of the limiting principal strains under different loading conditions and represented by the so-called forming limit curve (FLC). The shape and location of the FLC in principal strain space defines the boundary between strain states that are always free of necks from those that are prone to necking and splitting. Therefore, the distance between the FLC and all of the measured or predicted strains throughout a formed part characterizes the degree of safety. However, the deformation behavior of metals is strongly dependent on the loading history, in particular, on the specific strain paths imposed by the forming process.

The forming limit curve, initially developed by Keeler and Backhofen in 1964 [4.1] and Goodwin in 1968 [4.2], has provided a useful empirical gauge of forming

severity for stamping processes for almost half a century. However the FLC of as-received sheets is valid only in processes in which the loading path is quasi linear; in other words, one in which the ratio of the plastic strains is constant throughout the forming process. The changes in shape and position of the FLC in strain space due to non-linear strain paths is typical of all sheet materials including steel, copper and brass, as reported, for example, by Kleemola and Pelkkikangas [4.3]. Therefore the strong influence of strain path changes on the FLC is a definite disadvantage when evaluating the forming severity of industrial stampings that involve multistage forming operations.

In view of the difficulty to experimentally determine the forming limits of sheet materials that have been subjected to a non-linear strain history, many researchers have sought to predict the FLC. Three different approaches have been introduced to calculate FLC: the bifurcation method, damage analysis and the Marciniak and Kuczynski (MK) approach. Bifurcation analysis was first proposed by Hill in 1952 [4.4], then further developed by Stören and Rice [4.5] and by Hutchinson and Neale [4.6- 4.7]. The damage method considers micro-defects in the material structure and FLC is predicted when the density of micro-defects reaches a specified critical value. This method was applied by Tjotta [4.8] to predict void growth during plastic deformation and using a finite element model to study uniaxial tension and plane-strain tension. Similarly, Huang *et al.* [4.9] used a microscopic yield function for anisotropic sheet metal to predict rupture progress that can be used to investigate the failure of sheet metals under forming operations.

In 1967, Marciniak and Kuczynski [4.10- 4.11] developed another method to predict failure in thin sheets based on classical plasticity theory by assuming a higher void volume fraction inside a randomly oriented imperfection band, and by modeling this imperfection as a geometric groove in the sheet. This approach is commonly called the MK method and the physical basis for the MK analysis was presented by McCarron *et al.* [4.12]. Chow *et al.* [4.13] developed a viscoplastic constitutive law using an anisotropic damage model. In their study, imperfections in the form of grooves were applied to samples loaded in equal biaxial stretching and, using their proposed damage criterion for localized necking, the FLCs of AA6111-T4 under nonlinear strain paths were predicted in good agreement with the experimental results. It was found that no reductions in the forming limit strain were obtained with shallow grooves for which the imperfection

index, which was defined as the thickness ratio of the groove to the nominal area, was greater than 0.990 and 0.992 for two different steels. These imperfection indices represented the pre-existing micro-structural defects in the two steels.

In classical plasticity theory, a yield function determines the stress states beyond which plastic deformation occurs, and is generally assumed to take the same form as the plastic potential function. This function determines not only the direction of the plastic strain increments via the associated flow rule, but also the material stiffness by its variation during plastic deformation.

In order to predict the work hardening behavior of sheet materials the most widely used assumption is that of isotropic hardening, which assumes the yield locus expands uniformly with plastic deformation. This hardening model is well suited to predicting the outcome of metal forming processes involving monotonic loading.

Another well-known type of hardening model is the kinematic hardening model, initially proposed by Prager [4.14] and Ziegler [4.15] to model the Bauschinger effect. However, under complex loading histories, such as those involving unloading and reloading, substantial deviation of actual material behavior from that predicted by these two models is often observed.

It is also common to implement a combination of isotropic and kinematic hardening models in plasticity calculations, in order to more accurately represent actual hardening behavior. The combined strain hardening model seems particularly well suited to applications that include nonlinear loading paths.

In the present study, two different work hardening models were implemented in a modified version of the imperfection approach proposed by Marciniak and Kuczynski [4.10] to predict the forming limit curve (FLC) after different nonlinear loading paths. First, isotropic hardening was considered to determine the FLC in cases that involve unloading and subsequent reloading along a different strain path. Secondly, FLCs were predicted with the mixed isotropic and nonlinear kinematic hardening model proposed by Armstrong-Frederick [4.16] or Chaboche [4.17]. Results obtained from both hardening methods were validated with available experimental data for AISI-1012 [4.18] and 2008-T4 [4.19] alloys in the as-received state and also when subjected to an initial prestrain. For the AISI-1012 steel sheet, a 10 percent prestrain in uniaxial tension and an 8 percent

prestrain in equibiaxial tension were applied prior to determining the FLC [4.18]. For the 2008-T4 aluminum alloy, sheets were prestrained to 5 and 12 percent in uniaxial tension and to 4 and 12 percent in equibiaxial tension [4.19]. The proposed MK model was used to predict the FLC for each of these materials and for each nonlinear loading path.

4.2. Theoretical approach

As mentioned already, one of the best known theoretical methods to predict the onset of localized deformation was introduced by Marciniak and Kuczynski [4.10- 4.11]. The MK approach is based on the assumption that a thin sheet has an initial geometric imperfection (Figure 4.1) and a localized neck would develop from this region. This explanation of localized necking is based on the fact that inhomogeneities are unavoidable in actual sheet materials. In reality it is more likely that the initial imperfection is a material inhomogeneity. The MK method has been used with different plasticity theories and hardening models to predict history-dependent forming limits [4.12-4.13, 4.20-4.21].

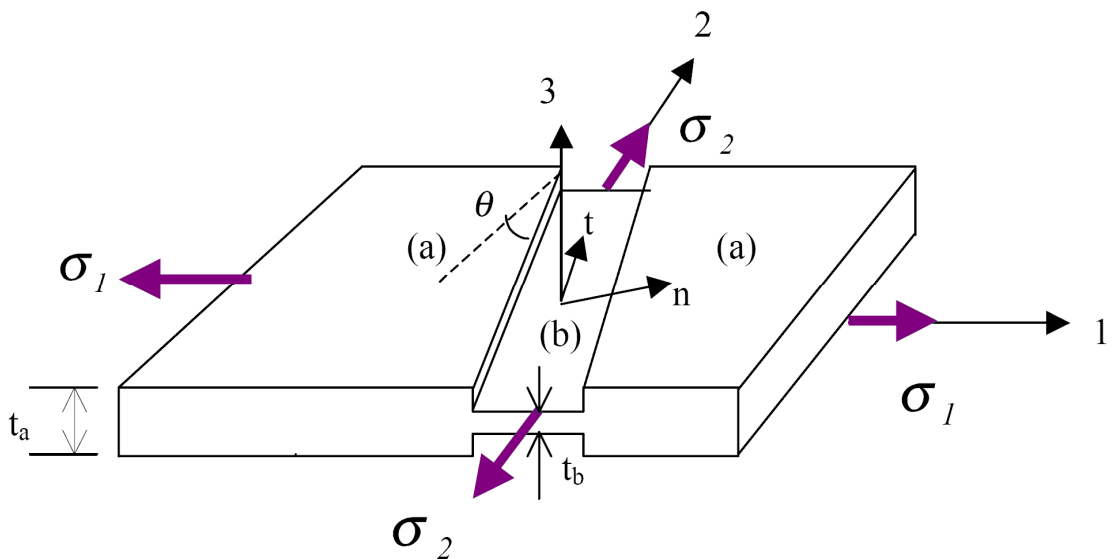


Figure 4.1. Thickness imperfection in MK method

As it is shown in Figure 4.1, it was assumed that the principal axes of anisotropy are collinear with the principal axes of applied stresses. In other words, the principal in-plane directions (i.e. direction of major and minor stress components) are parallel with the rolling and transverse directions of the sheet, respectively. The effects of having principal stress axes that are rotated compared to the orthotropic axes were discussed by other researchers [4.22- 4.25].

In the MK model, a sheet with a nominal thickness is assumed to have an area (in the shape of a groove) that is slightly thinner; these two areas are denoted by (a) and (b), respectively. The initial imperfection factor of the groove, f_0 , is defined as the thickness ratio:

$$f_0 = \frac{t_0^b}{t_0^a} \quad (4.1)$$

where t denotes the sheet thickness, and subscript '0' denotes the initial state. In most cases, researchers consider the imperfection factor to be an arbitrary constant that can be adjusted within a reasonable range to better correlate predictions with experimental data. In order to estimate the initial imperfection factor, it seems reasonable to relate it to the surface roughness of the sheet. Research carried out by Stachowicz [4.26] shows that surface roughness changes with deformation and these changes depend upon initial surface roughness, grain size, and strain. By relating the thickness difference between regions (a) and (b) to the surface roughness of the sheet metal, the imperfection factor not only takes on a value that has physical meaning but also the option of adjusting this value so that the predicted FLC better fit experimental data is eliminated. Stachowicz's assumption was adopted in this work and the imperfection factor was assumed to change with the deformation of the sheet according to the following relationship:

$$f_0 = \frac{t_0^a - 2[R_{z0} + Cd_0^{0.5}\epsilon_e^b]}{t_0^a} \quad (4.2a)$$

$$f = \frac{t_0^a - 2[R_{Z0} + Cd_0^{0.5}\varepsilon_e^b]}{t_0^a} \exp(\varepsilon_3^b - \varepsilon_3^a) \quad (4.2b)$$

where R_{Z0} is the surface roughness before deformation, ε_e^b is the effective strain in region (b), d_0 is the material's initial grain size, and C is a material constant that shows how the surface roughness varies with plastic deformation. This constant can be determined experimentally by measuring the surface roughness at different levels of effective plastic strains, and based on the empirical equation ($R_Z - R_{Z0} = Cd_0^{0.5}\varepsilon_e^b$), C represents the slope of a line fitted to the data points on the “ $R_Z - R_{Z0}$ ” vs. “ $d_0^{0.5}\varepsilon_e^b$ ” graph [4.26]. Additional details regarding the calculation of the imperfection factor are also provided in the authors' previous work [4.27].

As shown in Figure 4.1, the thickness imperfection is considered with an orientation θ inclined to the principal stress directions. Although the value of this angle at the start of the deformation can be arbitrarily selected, it changes with deformation. In other words, the angle θ between the imperfection and the principal direction is updated from an initial value θ_0 at each increment of the plastic deformation. Sing and Rao [4.28] showed that with consideration of uniform deformation, the rotation of the initial thickness imperfection can be expressed as a function of the true plastic strain increments in the nominal area (a) of the sheet as follows:

$$\tan(\theta + d\theta) = \tan(\theta) \frac{1 + d\varepsilon_1^a}{1 + d\varepsilon_2^a} \quad (4.3)$$

where $d\varepsilon_1^a$ and $d\varepsilon_2^a$ are the major and minor principal strains in the nominal area of the sheet, respectively.

In this investigation, both isotropic hardening and combined isotropic – nonlinear kinematic hardening were considered. With isotropic hardening, the yield surface expands uniformly in all directions in stress space and the center of the yield locus remains fixed (Figure 4.2). However, with mixed hardening the yield surface not only expands, but the centre of the yield surface also translates simultaneously (Figure 4.3) as a result of work hardening. The translation of the centre of the yield surface was defined

by a nonlinear function of the plastic strain components and will be further described in the following paragraphs.

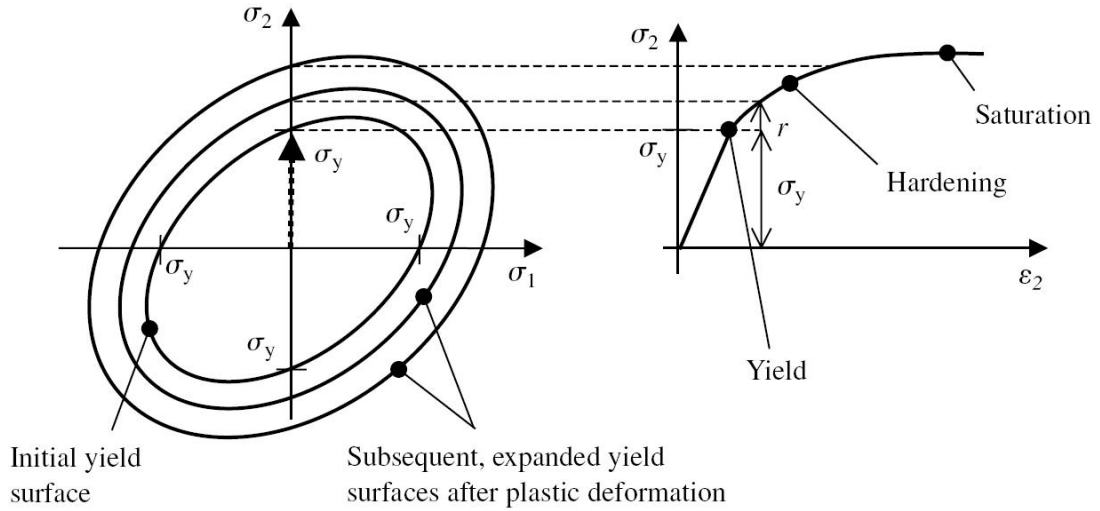


Figure 4.2. Schematic representation of isotropic hardening [4.29]

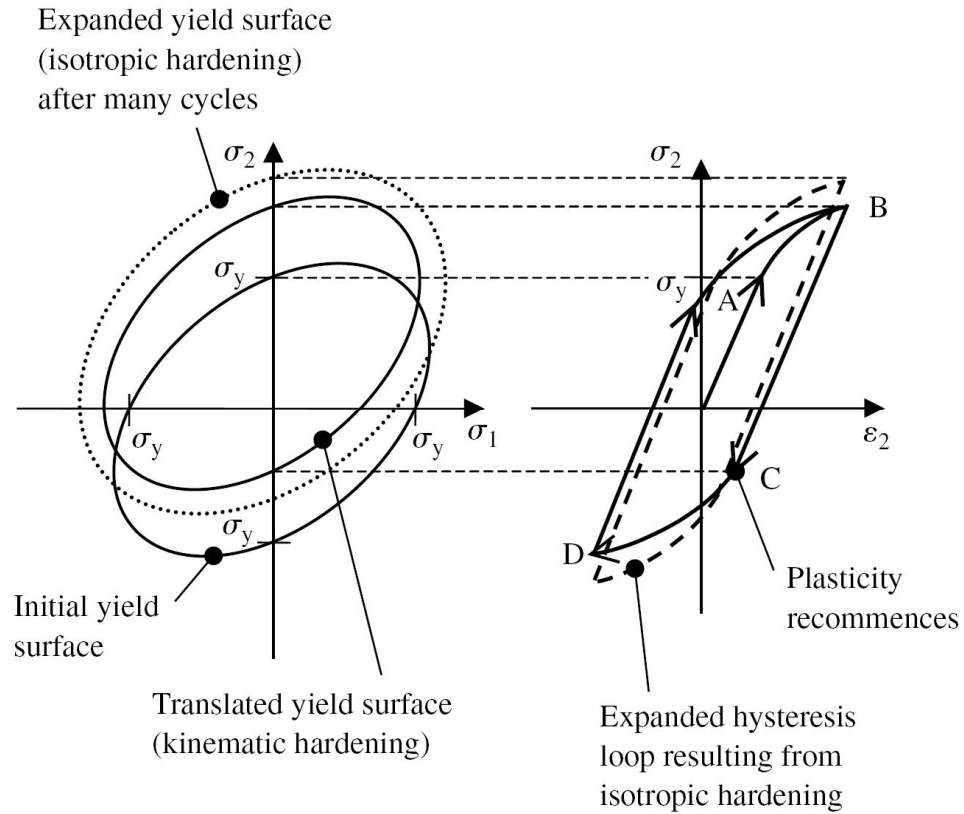


Figure 4.3. Schematic representation of combined isotropic and kinematic hardening [4.29]

A constitutive equation was derived in which the yield function can be expressed in the following general form for isotropic hardening and mixed hardening in Equations (4.4a) and (4.4b), respectively:

$$f = \left(\frac{3}{2} S_{ij} : N : S_{ij} \right)^{1/2} - \sigma_e^{Isotropic} \quad (4.4a)$$

$$f = \left(\frac{3}{2} (S_{ij} - \alpha_{ij}) : N : (S_{ij} - \alpha_{ij}) \right)^{1/2} - \sigma_e^{Mixed IH \& NLKH} \quad (4.4b)$$

where, S is the deviatoric stress tensor, N is a tensor that includes the anisotropic constants of Hill's 1948 yield function [4.30], and α is the back-stress tensor that describes the translation of the centre of the yield surface.

In this work, non-linear kinematic hardening was defined by the Armstrong-Frederick [4.16] or Chaboche relation [4.17] in which the evolution of the back stress is defined as follows:

$$d\alpha_{ij} = c d\varepsilon_{ij}^p - \gamma \alpha_{ij} d\varepsilon_{ij}^p \quad (4.5a)$$

where c and γ are material constants. By integrating Equation (4.5a) and taking α_{ij} to be zero when $\varepsilon_{ij}^p = 0$, we obtain:

$$\alpha_{ij} = \frac{c}{\gamma} (1 - e^{-\gamma \varepsilon_{ij}^p}) \quad (4.5b)$$

As the plastic strain increases, the back stress α_{ij} in Equation (4.5b) saturates to the value c/γ , where the constant γ determines the rate of stress saturation and c/γ determines the magnitude of the saturation stress.

For plane-stress conditions, the plastic potential function is written as Equations (4.6a) and (4.6b) for the isotropic and mixed hardening cases, respectively:

$$2h = (G + H)\sigma_x^2 + (F + H)\sigma_y^2 - 2H\sigma_x\sigma_y + 2N\sigma_{xy} = f^2 \quad (4.6a)$$

$$2h = (G + H)(\sigma_x - \alpha_x)^2 + (F + H)(\sigma_y - \alpha_y)^2 - 2H(\sigma_x - \alpha_x)(\sigma_y - \alpha_y) + 2N(\sigma_{xy} - \alpha_{xy})^2 = f^2 \quad (4.6b)$$

where F, G, H and N can be calculated using the anisotropic coefficients.

Strain hardening is described by the power law:

$$\sigma_e = k \left(\dot{\varepsilon}_e \right)^m (\varepsilon_e + \varepsilon_0)^n \quad (4.7)$$

where ε_0 is a prior uniform pre-strain applied to the sheet, m is the strain-rate sensitivity coefficient, n is the strain-hardening coefficient, σ_e and ε_e are the effective stress and strain, respectively.

The power law used for the second stage loading is then modified according to the prestrain level. The power laws used in the nominal and weak areas of the sheet at the second loading stage are represented by the following equations, respectively:

$$\sigma_e^a = k \left(\dot{\varepsilon}_e^a \right)^m (\varepsilon_e^{(1)a} + \varepsilon_e^{(2)a} + \varepsilon_0)^n \quad (4.8a)$$

$$\sigma_e^b = k \left(\dot{\varepsilon}_e^b \right)^m (\varepsilon_e^{(1)b} + \varepsilon_e^{(2)b} + \varepsilon_0)^n \quad (4.8b)$$

Where $\varepsilon_e^{(1)a}$ and $\varepsilon_e^{(1)b}$ are the effective plastic strains reached in the prestraining stage.

The associated flow rule was used to calculate the plastic strain components:

$$d\varepsilon_{ij} = d\lambda \text{grad}(h) = d\lambda \frac{\partial h}{\partial \sigma_{ij}} \quad (4.9)$$

Where $d\lambda$ is a plastic multiplier, and h is the plastic potential function.

Equation (4.9) was used to determine the plastic strain increments for mixed hardening:

$$d\varepsilon_x = d\lambda[(G + H)(\sigma_x - \alpha_x) - H(\sigma_y - \alpha_y)] \quad (4.10a)$$

$$d\varepsilon_y = d\lambda[-H(\sigma_x - \alpha_x) + (H + F)(\sigma_y - \alpha_y)] \quad (4.10b)$$

$$d\varepsilon_z = -(d\varepsilon_x + d\varepsilon_y) \quad (4.10c)$$

The coefficients of Equation (4.6b) can be determined at the condition of initial yielding ($\alpha_x = \alpha_y = 0$ and $f=1$) [4.31]:

$$2G = \frac{1}{(\sigma_x^Y)^2} - \frac{1}{(\sigma_y^Y)^2} + \frac{1}{(\sigma_B^Y)^2} \quad (4.11a)$$

$$2F = \frac{1}{(\sigma_y^Y)^2} - \frac{1}{(\sigma_x^Y)^2} + \frac{1}{(\sigma_B^Y)^2} \quad (4.11b)$$

$$2H = \frac{1}{(\sigma_x^Y)^2} + \frac{1}{(\sigma_y^Y)^2} - \frac{1}{(\sigma_B^Y)^2} \quad (4.11c)$$

where σ_x^Y , σ_y^Y , and σ_B^Y are the yield stresses in the x, y, and equibiaxial directions, respectively. Anisotropy data provided in Tables 4.1 and 4.2 are valid for isotropic hardening, but for the mixed hardening case, when a tensile stress (σ) is applied on the specimen at an angle (β) to the rolling direction [4.31], Lankford's coefficients can be calculated by the following equation:

$$\begin{aligned}
R_\alpha = & -\left\{ \left[(G+H)(\sigma \cos^2 \beta - \alpha_x) - H(\sigma \sin^2 \beta - \alpha_y) \right] \sin^2 \beta \right. \\
& + \left[(H+F)(\sigma \sin^2 \beta - \alpha_y) - H(\sigma \cos^2 \beta - \alpha_x) \right] \cos^2 \beta \\
& \left. - 2N(\sigma \sin \beta \cos \beta - \alpha_{xy}) \sin \beta \cos \beta \right\} / \{ G(\sigma \cos^2 \beta - \alpha_x) + F(\sigma \sin^2 \beta - \alpha_y) \}
\end{aligned} \tag{4.12a}$$

Finally, the following relations can be written:

$$R_0 = \frac{\sigma H - H\alpha_x + (H+F)\alpha_y}{\sigma G - G\alpha_x - F\alpha_y} \tag{4.12b}$$

$$R_{90} = \frac{\sigma H + (G+H)\alpha_x - H\alpha_y}{\sigma F - G\alpha_x - F\alpha_y} \tag{4.12c}$$

Assuming that the necking strain in the nominal area is $\varepsilon_{ij}^{(2)a}$ during the second loading stage, the final forming limit as a result of a bilinear strain path can be calculated by:

$$\varepsilon_{ij} = \varepsilon_{ij}^{(1)a} + \varepsilon_{ij}^{(2)a} \tag{4.13}$$

Where ε_{ij} is the forming limit and $\varepsilon_{ij}^{(1)a}$ is the plastic prestrain in the nominal area.

The basic equations for the MK analysis are the geometric compatibility equations expressed as:

$$d \varepsilon_n^a = d \varepsilon_n^b \tag{4.14}$$

and the force equilibrium equations across the imperfection groove:

$$F_{mn}^a = F_{mn}^b \tag{4.15a}$$

$$F_m^a = F_m^b \tag{4.15b}$$

where subscripts n and t denote the normal and tangential directions of the groove, respectively, and F is the force per unit width, i.e.:

$$F_{nn}^a = \sigma_{nn}^a t^a \quad (4.16a)$$

$$F_{nn}^b = \sigma_{nn}^b t^b \quad (4.16b)$$

$$F_{nt}^a = \sigma_{nt}^a t^a \quad (4.16c)$$

$$F_{nt}^b = \sigma_{nt}^b t^b \quad (4.16d)$$

By combining Equations (4.1), (4.7) and (4.16a,b), we obtain:

$$\left[\frac{\sigma_{nn}^a}{\sigma_e^a} \right] / \left[\frac{\sigma_{nn}^b}{\sigma_e^b} \right] = f \left(\left[\varepsilon_0 + \varepsilon_e^b \right]^n \dot{\varepsilon}_e^{b \cdot m} \right) / \left(\left[\varepsilon_0 + \varepsilon_e^a \right]^n \dot{\varepsilon}_e^{a \cdot m} \right) \quad (4.17)$$

From the Equations (16) and the stress transformation rule:

$$\frac{\sigma_{nt}^b}{\sigma_{nn}^b} = \frac{\sigma_{nt}^a}{\sigma_{nn}^a} = \left[(r^a - 1) \sin \theta \cos \theta \right] / \left[1 + (F + H) \left(\frac{\sigma_2^a - \alpha_2^a}{\sigma_2^a - \alpha_2^a} \right)^2 - 2H \left(\frac{\sigma_2^a - \alpha_2^a}{\sigma_2^a - \alpha_2^a} \right) \right]^{0.5} \quad (4.18)$$

where r^a is a stress path factor and is equal to the ratio of the minor stress component (σ_2) to the major stress component (σ_1) in the nominal area:

$$r^a = \sigma_2^a / \sigma_1^a \quad (4.19)$$

With consideration of Equations (4.6), (4.9), (4.14), and the strain transformation rule:

$$\frac{d\varepsilon_e^a(\sigma_1^a - \alpha_1^a)}{\sigma_e^a} \left\{ \left[(F + H) \left(\frac{\sigma_2^a - \alpha_2^a}{\sigma_2^a - \alpha_2^a} \right) - H \right] \cos^2 \theta + \left(1 - H \left(\frac{\sigma_2^a - \alpha_2^a}{\sigma_2^a - \alpha_2^a} \right) \right) \sin^2 \theta \right\} =$$

$$\frac{d\varepsilon_e^b(\sigma_1^b - \alpha_1^b)}{\sigma_e^b} \left\{ \left[(F + H) \left(\frac{\sigma_2^b - \alpha_2^b}{\sigma_2^b - \alpha_2^b} \right) - H \right] \cos^2 \theta + \left(1 - H \left(\frac{\sigma_2^b - \alpha_2^b}{\sigma_2^b - \alpha_2^b} \right) \right) \sin^2 \theta \right\} \quad (4.20)$$

Equations (4.17), (4.18), and (4.20) were used to develop a final differential equation which can be used to determine the onset of necking. This final governing equation is expressed as a function of the ratio of effective strains $\eta = \varepsilon_e^b / \varepsilon_e^a$ and indicates the evolution of η as deformation progresses; the rate at which η increases determines the onset of strain localization in the sheet.

Using the formulation and assumptions of the MK approach and the plasticity equations previously described, a biaxial stress state can be incrementally imposed in the nominal area. The imposed stresses cause a development of strain both in the nominal area (a) and in the weaker area (b). The strain and stress states in region (b) are calculated numerically from the stress and strain states in region (a) by the governing equation using a combination of Newton-Raphson and Runge-Kutta methods. Because of the thickness difference between the two areas, the strain rate increases faster in the thinner region (b) than in the thicker region (a) and it is assumed that localized necking takes place once the effective strain rate in the groove exceeds 10 times that in the nominal area. In other words, the limit strains were obtained when $\eta = \varepsilon_e^b / \varepsilon_e^a > 10$. When this condition is reached, the values of ε_1 and ε_2 in area (a) represent the limiting strains for a given linear strain path ($\rho = \varepsilon_2 / \varepsilon_1$ constant). This procedure is then repeated for different linear strain paths in the range of $-0.5 \leq \rho \leq 1.0$ and the limiting strains in each case are used to plot the FLC. The same method was followed to obtain the FLC for non-linear loading paths, by subjecting the sheet material to two different linear loading paths and by considering the values of the principal strain components at the end of the first loading stage as the initial strain values for the second loading stage. This procedure can also be expanded to compute the limit strains after multiple loading stages.

As mentioned earlier in this section, there is a particular orientation of the imperfection band that minimizes the computed limit strains for each strain path (Equation 4.3). In order to determine the lowest limit strains for each linear loading path,

the initial orientation of the imperfection band was incrementally rotated between 0 and 45 degrees until the minimum limit strains were found. The same approach was also followed in the case of bilinear strain paths, and the value of the critical band orientation in the first deformation stage was used as the initial orientation for the second loading stage. This method can also be followed for multi-linear strain paths.

4.3. Results and discussion

4.3.1. Material characterization

The materials considered in this investigation for model verification are a low carbon steel (AISI-1012) [4.18] and 2008-T4 aluminum [4.19]. Table 4.1 presents the plastic anisotropy coefficients for the rolling, diagonal and transverse directions and other mechanical properties for the steel and Table 4.2 shows the same data for the 2008-T4 aluminum alloy.

Table 4.1. Material properties of AISI-1012, low carbon steel [4.18]

R_0	R_{45}	R_{90}	F	G	H	$K(IH)$ (MPa)	$K(MH)$ (MPa)	$n(IH)$
1.4	1.05	1.35	0.432	0.417	0.583	238	230	0.35
$n(MH)$	m	d_0 (μm)	R_{Z0} (μm)	C	t_0 (mm)	c	γ	
0.33	0.01	25	6.5	0.104	2.5	500	60	

Table 4.2. Material properties of 2008-T4 aluminum [4.19]

R_0	R_{45}	R_{90}	F	G	H	$K(IH)$ (MPa)	$K(MH)$ (MPa)	$n(IH)$
0.58	0.48	0.78	0.246	0.633	0.367	535	500	0.27
$n(MH)$	m	d_0 (μm)	R_{Z0} (μm)	C	t_0 (mm)	c	γ	
0.29	-0.003	8*	2.5*	0.70*	1.7	1350	40	

* Data determined by calibration of the predicted FLC with the experimental as-received FLC

Some material constants (C , d_0 , R_{Z0}) were not provided in [4.19], therefore these values were calibrated by adjusting the FLC of the 2008-T4 alloy predicted using isotropic

hardening until it correlated with the experimental as-received FLC. The material parameters determined by the calibration were $C = 0.70$, $d_0 = 8.00 \mu\text{m}$ and $R_{z0} = 2.5 \mu\text{m}$.

Equation (4.2a) was used to calculate the value of the initial imperfection factor in the MK analysis. It was found that $f_0 = 0.995$ for AISI-1012 steel and $f_0 = 0.997$ for 2008-T4 aluminum.

The determination of strain hardening coefficients is straightforward for isotropic hardening: K and n are the only two unknowns and they are determined by fitting the theoretical stress-strain curve $\sigma = K\varepsilon^n$ to the experimental stress-strain curve. However, there are four parameters (K , n , c and γ) which need to be identified for mixed isotropic – nonlinear kinematic hardening behavior, and in this case, K and n are likely to differ from the values for isotropic hardening. The best way to obtain these four coefficients is to use experimental stress-strain data obtained after reverse or cyclic loading of the specimen. When cyclic data is not available it is nevertheless possible to estimate these parameters with an acceptable level of accuracy by using an experimental monotonic stress-strain curve. The theoretical stress-strain curve for the mixed hardening law should coincide with the experimental monotonic stress-strain curve both before any unloading takes place and also after the transient Bauschinger effect appears [4.32]. It should be pointed out that this fitting technique does lead to a single value of the c/γ ratio.

The fit of the theoretical stress-strain curve calculated with the mixed hardening rule and with the monotonic experimental stress-strain curve is shown in Figure 4.4 for AISI-1012 steel. The strain hardening coefficients (K , n , c and γ) that were obtained are also given in Table 4.1. The experimental stress-strain curve for the 2008-T4 aluminum alloy was not provided in [4.19] but the strain hardening coefficients (K and n) were given. By fitting the theoretical stress-strain curve obtained using the mixed hardening rule with the stress-strain curve calculated with parameters K and n before unloading takes place and after the transient Bauschinger effect disappears, the kinematic hardening coefficients (K , n , c , and γ) were obtained for this alloy (Figure 4.5) and the related strain hardening data are listed in Table 4.2.

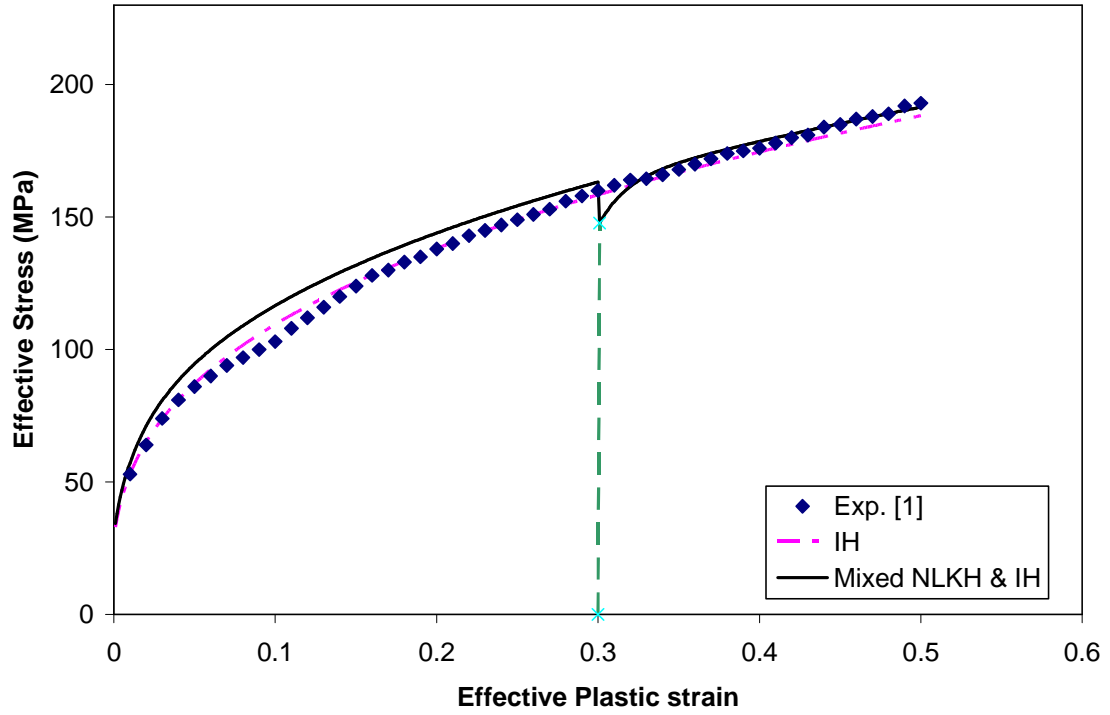


Figure 4.4. Experimental and predicted stress-strain curves for AISI-1012 steel alloy

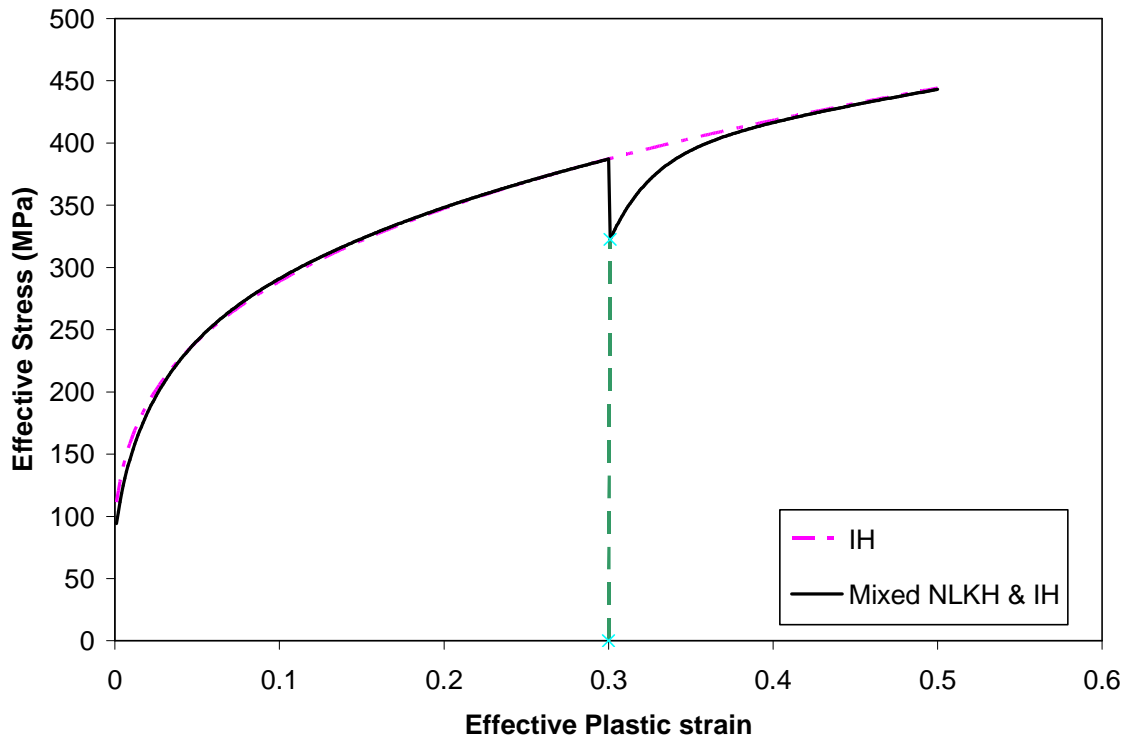


Figure 4.5. Stress-strain curves predicted with different hardening laws for 2008-T4 aluminum

4.3.2. Validation of the MK model

In order to validate this MK model, the FLCs of AISI-1012 steel and 2008-T4 aluminum sheets were calculated with both isotropic and mixed isotropic – nonlinear kinematic hardening rules, and the predicted FLCs were compared with experimental data [4.18- 4.19] determined for both the as-received sheets and also after the application of nonlinear loading paths.

Molaei [4.18] determined the experimental FLC of as-received AISI-1012 sheets by carrying out stretch forming tests using rectangular and notched blanks of various widths with different conditions of lubrication to achieve a range of strain states $-0.5 \leq \rho = \varepsilon_2/\varepsilon_1 \leq 1.0$. Each blank was electro-etched with a 3.0-mm diameter circle grid and formed over a hemispherical punch until the onset of local necking became apparent. The major and minor strains were measured directly from the deformed grids using a profile projector. FLCs were also determined experimentally for sheet specimens subjected to nonlinear loading paths [4.18]; in this case, stretch forming tests were carried out on sheets that were previously subjected to either uniaxial or equibiaxial tension. The tensile tests were performed at a speed of 5 mm/min using a servo-hydraulic Instron testing machine, and equibiaxial tests were conducted by stretch forming large blanks over a 210-mm diameter flat bottom punch.

Figure 4.6 shows good agreement between theoretical predictions and experimental data for this sheet steel in its as-received state. The level of FLC in the plane-strain region predicted by the mixed hardening rule is greater than that calculated with the isotropic hardening assumption, and is closer to the experimental data in this region. Since plane-strain deformation is the most critical deformation mode in sheet metal forming, it is important to accurately predict the FLC in this region. For other deformation modes, the difference in limit strains predicted with the two hardening models is not significant. However, the prediction with isotropic hardening is slightly closer to the experimental data on the left hand side of the FLC, whereas the mixed hardening rule yields a better prediction on the right side of the FLC.

FLCs were also calculated for specimens loaded along two types of non-linear strain paths: in one case, specimens were subjected to 8 percent prestrain in equibiaxial

tension, and in the other case, specimens were prestrained by 10 percent strain in uniaxial tension, and the corresponding FLCs are shown in Figures 4.7 and 4.8, respectively. After the equibiaxial prestrain (Figure 4.7), it can be seen once again that the two hardening rules lead to FLCs that are quite similar, except in the vicinity of plane-strain deformation (i.e. near the bottom of the cusp) where the difference is somewhat significant. However, the prediction of FLC with the mixed hardening rule is in better agreement with experimental data for lower levels of minor strain ($-0.1 \leq \varepsilon_2 \leq 0.05$), whereas the isotropic hardening assumption leads to a better prediction of the FLC on the far left hand side ($-0.3 \leq \varepsilon_2 \leq -0.15$).

Similar observations can be made for the prediction of FLC after a prestrain in uniaxial tension (Figure 4.8); the FLC predicted with the assumption of isotropic hardening is in better agreement with experimental forming limit data on the left hand side of the FLC ($\varepsilon_2 \leq -0.1$), but the prediction using the mixed hardening rule is more consistent with experimental data on the right side of the shifted FLC ($\varepsilon_2 \geq -0.05$).

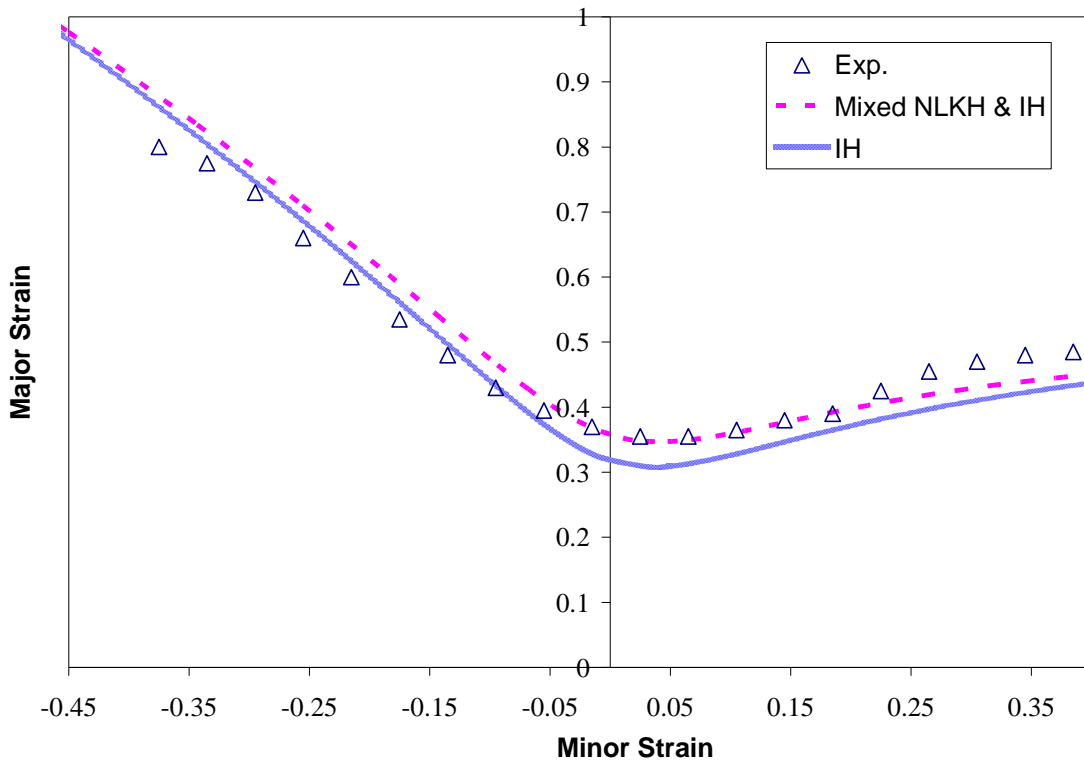


Figure 4.6. Comparison of predicted and experimental FLCs of as-received AISI-1012 steel sheets

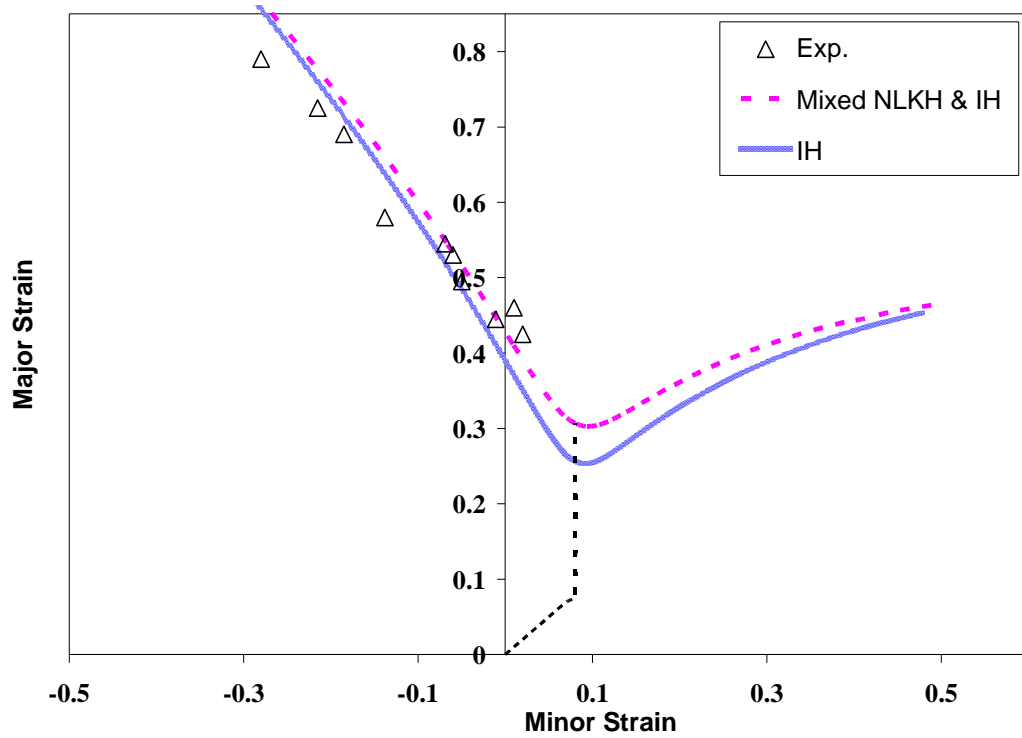


Figure 4.7. Comparison of predicted and experimental FLCs of AISI-1012 steel after 8% prestrain in equibiaxial tension

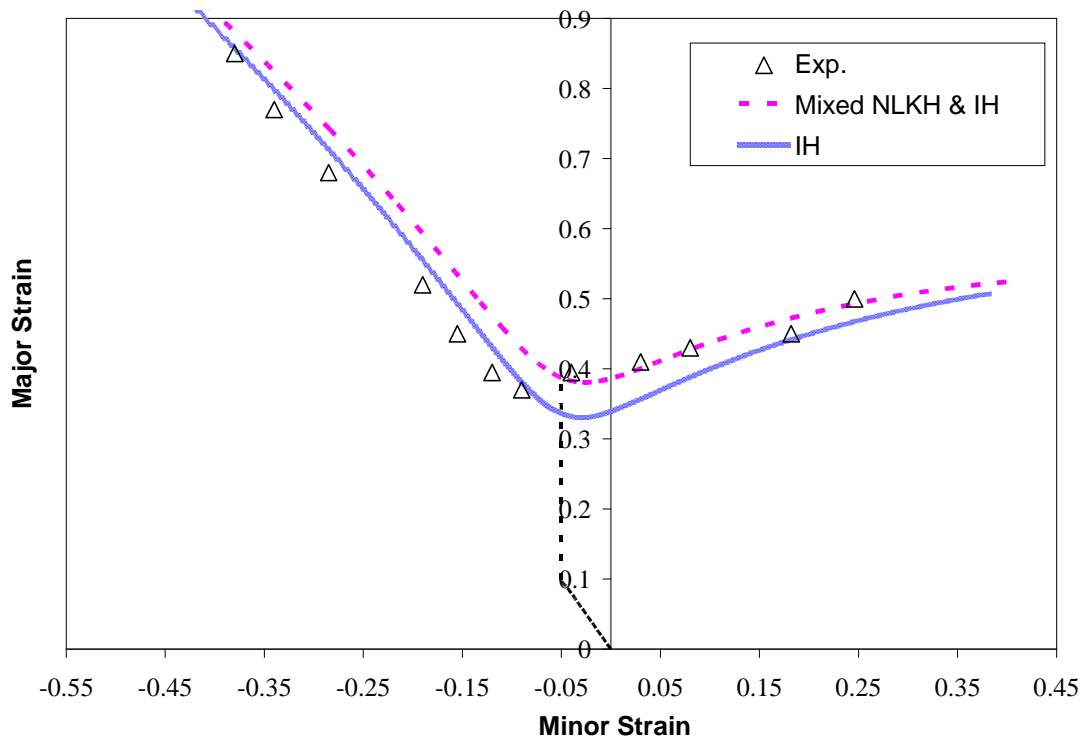


Figure 4.8. Comparison of predicted and experimental FLCs of AISI-1012 steel after 10% prestrain in uniaxial tension

The developed MK model was further validated by comparing predicted and experimental FLCs of 2008-T4 aluminum. FLCs were calculated using the two different strain hardening rules, and for both as-received sheets and sheets subjected to bilinear loading paths [4.19].

Graf and Hosford [4.19] determined the experimental FLCs of 2008-T4 aluminum by using an MTS formability tester with a 101.6 mm diameter hemispherical punch. Sheet specimens with different width and lubrication conditions were stretched over the punch as it moved at a speed of 25 mm/min. For most stretch-forming tests, neoprene rubber and/or oil were used for lubrication, but dry specimens (i.e. without lubrication) were used to determine intermediate data between plane-strain and equibiaxial tension. A pattern of non-interlaced 2.54 mm diameter circles was applied to each blank using a photo-resist technique and principal surface strains were measured from the distorted circles. Tests were interrupted as soon as a localized neck was observed. Graf and Hosford [4.19] reported that for this aluminum alloy, localized necks were sharp due to the negative strain rate sensitivity of the material, so it was easy to distinguish necked and safe locations. Further details regarding the experimental procedures for bi-linear loading are provided in [4.19]. Finally, Figures 4.9-4.11 show the comparison between predicted and experimental FLCs for this 2008-T4 aluminum.

Since some of the material constants (C , d_0 , R_{Z0}) used to calculate the initial imperfection factor (Eq. 2) of this 2008-T4 aluminum alloy were not provided by Graf and Hosford [4.19], they were adjusted so that the FLC predicted with the isotropic hardening assumption would be calibrated to the experimental as-received FLC. The FLC was also predicted for this alloy using the combined isotropic – nonlinear kinematic hardening model and Figure 4.9 shows that both hardening models lead to very similar curves.

Figure 4.10 shows the comparison of predicted and experimental FLCs after a prestrain of 0.04 and 0.12 in equibiaxial tension; once again, the two hardening models yield essentially the same FLC, except for a slight increase in limit strains in the vicinity of plane-strain deformation for the combined isotropic – nonlinear kinematic hardening model.

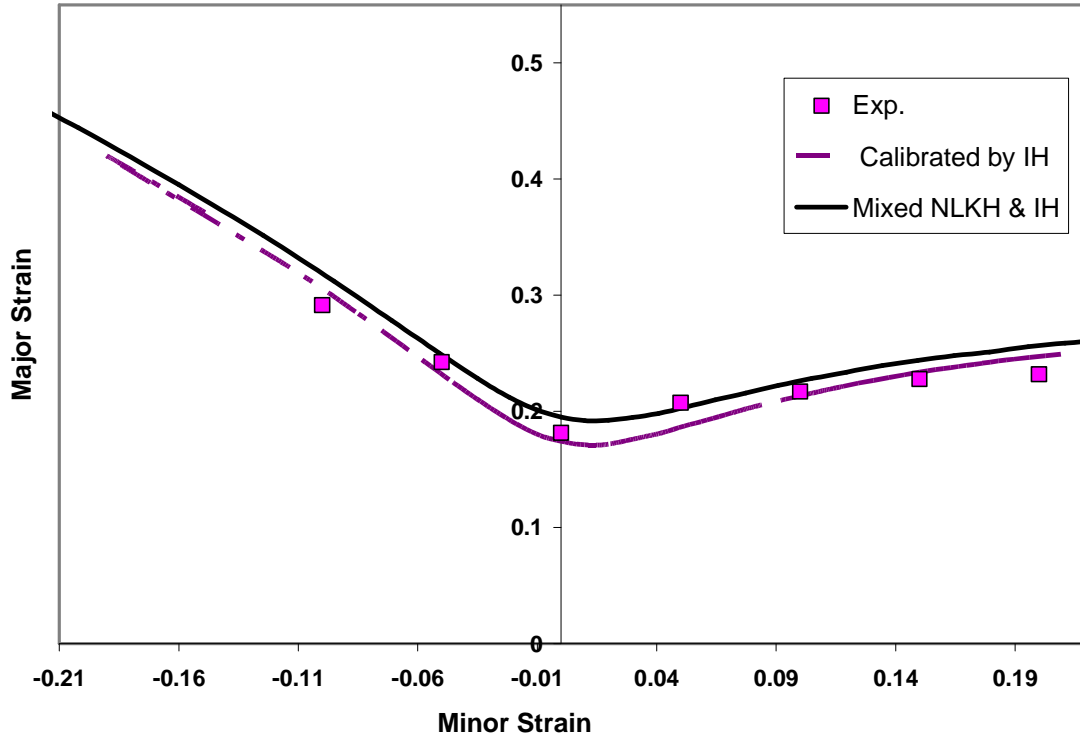


Figure 4.9. Comparison of predicted and experimental FLCs of as-received 2008-T4 aluminum sheets

Although the FLCs predicted with both hardening models are quite accurate, the mixed hardening model correlates somewhat better with the experimental data. The comparison between predicted and experimental FLC after preloading to 0.05 and 0.12 in uniaxial tension is shown in Figure 4.11; again, both hardening models lead to similar and accurate predictions of the experimental FLC data. Finally, it can be observed in Figures 4.10 and 4.11 that the shape of the FLC at the bottom of the cusp is less sharp, and therefore more realistic, with the mixed hardening model than it is with the isotropic hardening model; and this becomes more noticeable as the level of prestrain increases.

4.3.3. FLCs in bilinear strain paths

Having validated the present MK model with experimental FLCs obtained after a variety of bi-linear strain paths, this MK model was further used with the two different work hardening assumptions to predict the FLCs for the AISI-1012 steel sheet, but for additional preloading paths and prestrain levels. Although there is no available

experimental data with which to validate these predictions, the differences between the predicted FLCs can be observed and discussed.

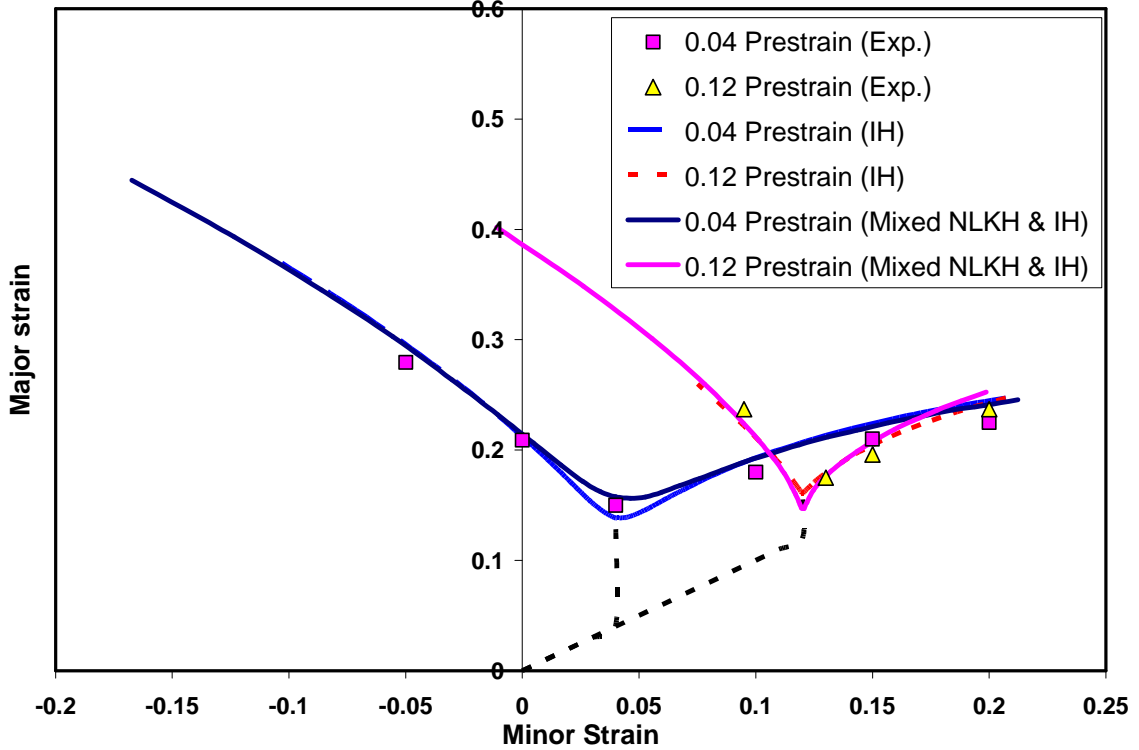


Figure 4.10. Comparison of predicted and experimental FLCs of 2008-T4 aluminum after different levels of prestrain in equibiaxial tension

FLCs were calculated for bilinear strain paths in which the first deformation stage was in either uniaxial tension, plane-strain tension, or equibiaxial tension. The second deformation stage consisted of different strain paths ranging from uniaxial tension ($\rho = -0.5$) to equibiaxial tension ($\rho = 1.0$) in small increments ($d\rho = 0.05$) to cover multiple strain paths in this range. For each secondary strain path, loading was continued until the onset of necking and the FLC was determined. As mentioned already, three bilinear loading histories were considered:

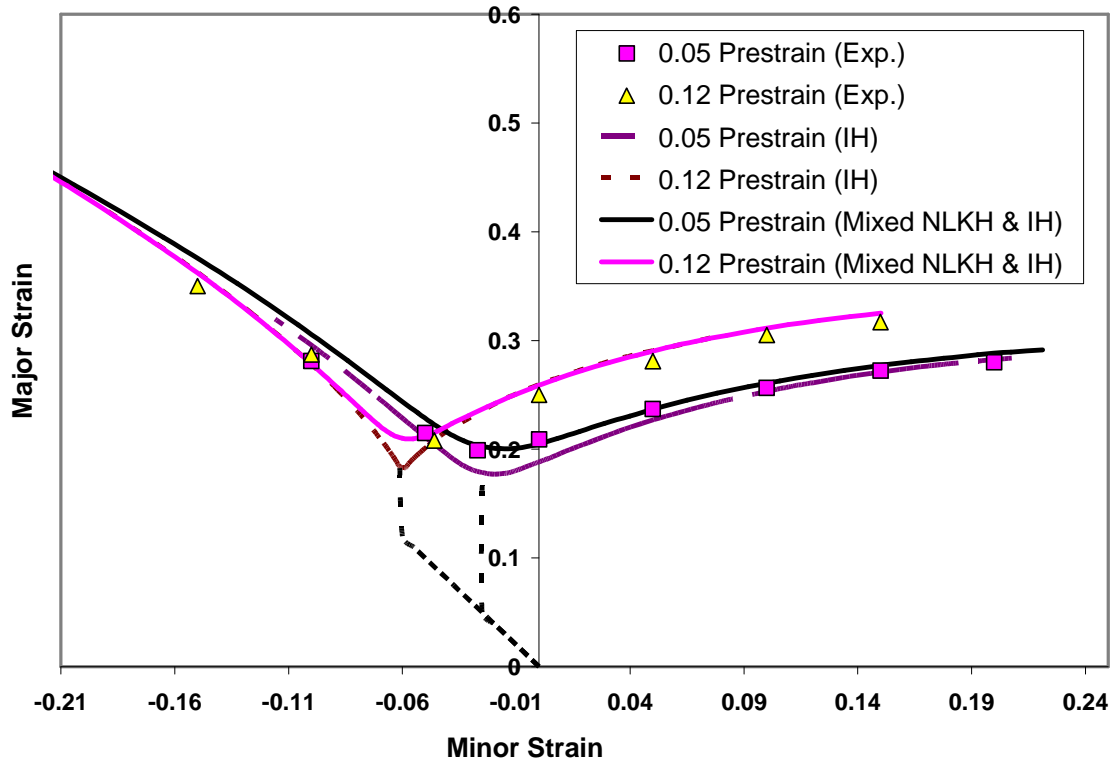


Figure 4.11. Comparison of predicted and experimental FLCs of 2008-T4 aluminum after different levels of prestrain in uniaxial tension

Case 1: The sheet metal was prestrained to 0.15 and 0.30 effective strain in uniaxial tension in the rolling direction, and further loaded in strain paths ranging from $-0.5 \leq \rho \leq 1.0$ up to the onset of necking. The FLCs calculated with the two different hardening rules are compared in Figure 4.12. This figure indicates that after a prestrain in uniaxial tension, formability decreases with increasing prestrain on the left hand side of the FLC, but improves on the right hand side of the FLC, which is consistent with prior published experimental data [4.18- 4.19]. Furthermore, the FLCs calculated with the mixed hardening rule are significantly higher in the region of plane-strain deformation than those predicted with the isotropic hardening rule.

Case 2: In order to observe the effects of a prestrain in plane-strain with different hardening rules, the material was preloaded to 0.15 and 0.30 effective strain in plane-strain with the greater principal strain being in the rolling direction, and followed by a second loading stage that covered a range of strain paths from uniaxial to equibiaxial tension. The effects of the plane-strain prestrain is shown in Figure 4.13 where it can be

seen that material formability improves somewhat with increasing magnitude of prestrain in all deformation modes apart from plane-strain deformation. It can be observed that the mixed hardening assumption predicts slightly higher formability in the plane-strain region compared to that predicted with the isotropic hardening rule, but for this grade of steel (AISI-1012) the difference between the FLCs predicted with these two hardening models is not significant for deformation modes other than plane-strain.

Case 3: In this case, 0.15 and 0.30 effective prestrains were applied in equibiaxial tension, followed by a second loading in the same range of strain paths as for previous cases. As it can be seen in Figure 4.14, there is a significant lateral translation of the FLC with equibiaxial prestrain. This leads to a remarkable increase in formability on the left side of the FLC but a slight decrease in formability in the region from plane-strain to equibiaxial tension. Again, the greatest difference between the FLC predicted with isotropic and mixed hardening models is in the plane-strain region. However the differences between the FLCs predicted with these two models seem to disappear with increasing equibiaxial prestrain.

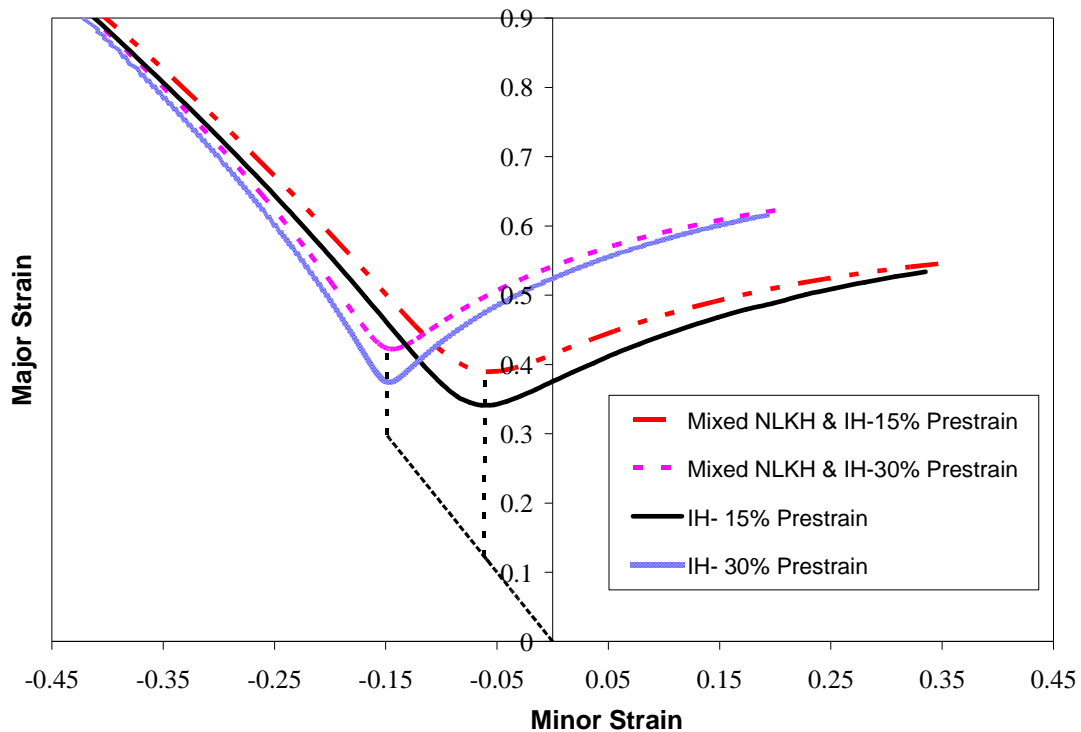


Figure 4.12. FLCs predicted after different amounts of prestrain in uniaxial tension using the MK model with isotropic and mixed hardening

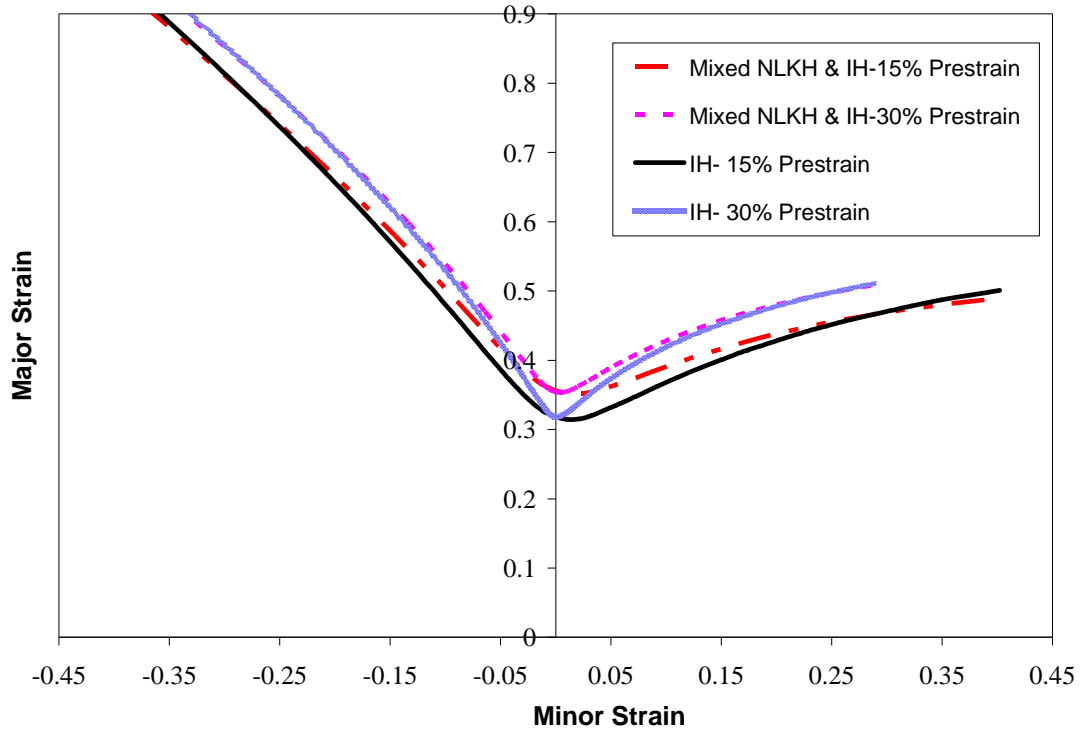


Figure 4.13. FLCs predicted after different amounts of prestrain in plane-strain tension using the MK model with isotropic and mixed hardening

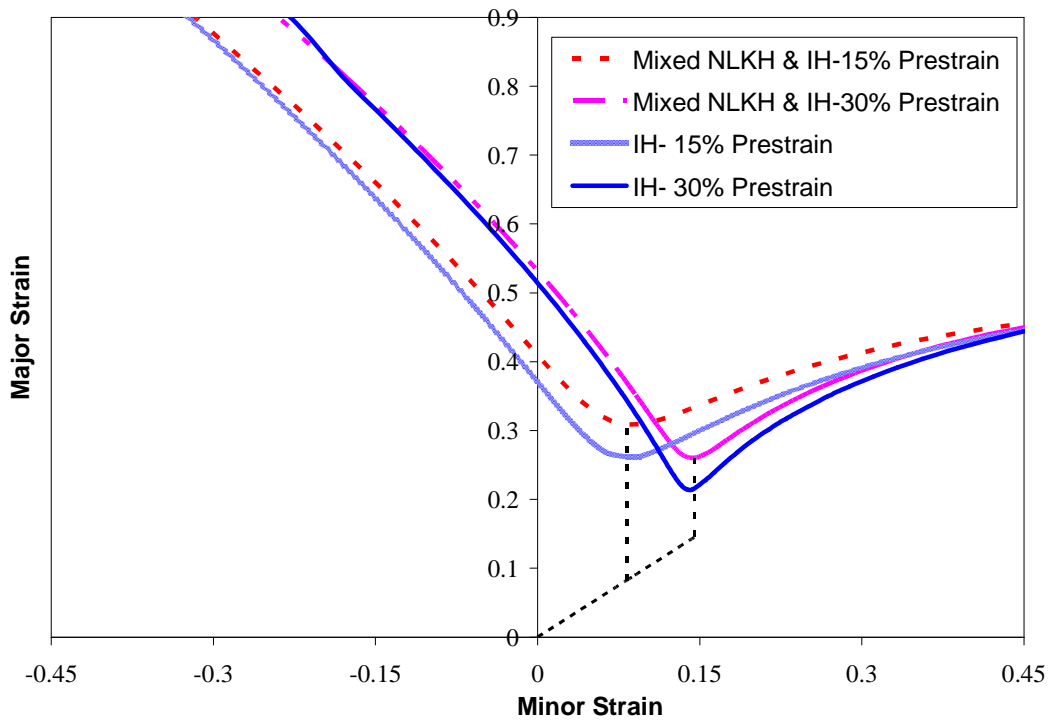


Figure 4.14. FLCs predicted after different amounts of prestrain in equibiaxial tension using the MK model with isotropic and mixed hardening

It is evident from Figures 4.12-4.14 that the greatest influence of the hardening rule on the prediction of FLC is in the mode of plane-strain deformation (i.e. at FLC_0 , the plane-strain intercept in the second stage of deformation). The combined isotropic – nonlinear kinematic hardening rule consistently predicts better formability in the vicinity of plane-strain than the isotropic hardening rule, regardless of the level and type of prestrain.

The differences in FLC_0 from isotropic to mixed hardening were determined for each prestrain path and for each level of effective prestrain and the results are shown in Figure 4.15. It can be seen that the smallest difference (about 11%) between the FLC_0 predicted with both hardening rules is in the mode of plane-strain and the largest difference (from 18-21%) is in the mode of equibiaxial tension. Figure 4.15 also shows that the differences between the predictions with these two hardening rules decreases with increasing prestrain for a prestrain in uniaxial tension (i.e. on the left hand side of the FLC), whereas the differences increase with increasing prestrain for a prestrain in equibiaxial tension (i.e. on right hand side of the FLC).

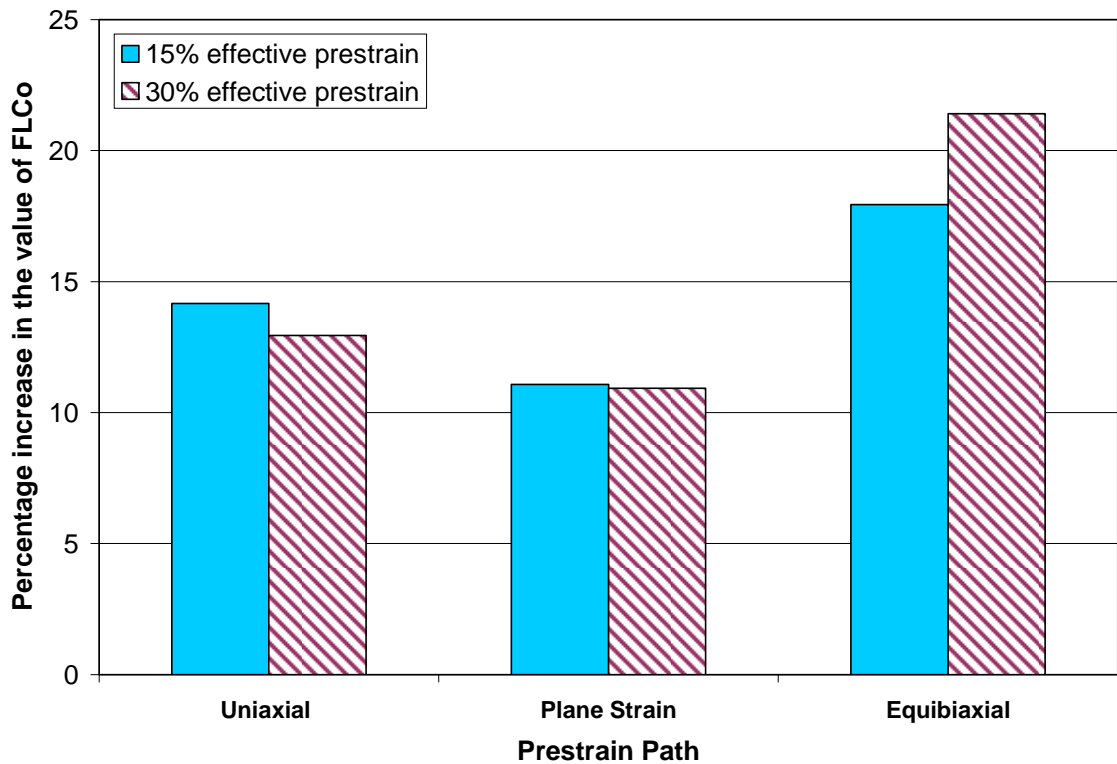


Figure 4.15. Percentage increase in FLC_0 from IH to mixed hardening after different amounts of prestrain in different loading paths

4.4. Conclusion

In this paper, isotropic and mixed (isotropic-nonlinear kinematic) hardening rules were employed in conjunction with the MK analysis to predict the FLCs of a low carbon steel sheet AISI-1012 and a 2008-T4 aluminum alloy. The current model incorporates the effects of material properties such as grain size, surface roughness, and rotation of the initial imperfection. The value of the thickness inhomogeneity was considered as a function of surface roughness, and grain size of the sheet material. In this analysis, the imperfection rotation, the surface roughness and the thickness ratio, f , were updated throughout the loading history. In this investigation, the FLC was predicted for non-linear strain paths in which the prestrain was either in uniaxial tension, plane-strain tension or equibiaxial tension.

The MK model was developed with both hardening rules and was validated with available experimental data for AISI-1012 steel and 2008-T4 aluminum sheets in their as-received state and also for non-proportional loading histories. Good agreement between theoretical predictions and experimental data was observed for both steel and aluminum. For as-received sheet materials, the differences observed between the FLCs predicted with isotropic hardening and mixed hardening rules were not significant, except for the plane-strain region. Under bi-linear loading paths, the FLCs predicted with the mixed hardening rule were consistently higher in the plane-strain region than those calculated with isotropic hardening. The FLC predicted with the mixed hardening model was in better agreement with experimental data when the prestrain was in the direction of positive minor strains, but the assumption of isotropic hardening led to acceptable agreement with experimental data when the prestrain was in the direction of negative minor strains in both the steel and the aluminum alloy.

For a given level of prestrain, there is an increase in formability on the right hand side of the FLC when the sheet is prestrained towards negative minor strains and a more significant increase in formability on the left hand side of the FLC when the sheet is prestrained towards positive minor strains. For prestrains in plane-strain, both hardening models yielded similar results except in the plane-strain region where the difference is somewhat significant.

It is likely that differences in the FLCs predicted with these two hardening models would be more significant for sheet materials that exhibit greater Bauschinger effect.

4.5. References

- [4.1] Keeler S.P., Backhofen W.A., Plastic instability and fracture in sheet stretched over rigid punches, *ASM Transactions Quarterly* 56 (1964) 25-48.
- [4.2] Goodwin G.M., Application of strain analysis to sheet metal forming in the press shop, SAE (1968) paper# 680093.
- [4.3] Kleemola H.J., Pelkkikangas M.T., Effect of pre-deformation and strain path on the forming limits of steel, copper and brass, *Sheet Metal Industries* 63 (1977) 559-591.
- [4.4] Hill R., On discontinuous plastic states, with special reference to localized necking in thin sheets, *Journal of Mechanics and Physics of Solids* 1 (1952) 19-30.
- [4.5] Stören S., Rice J.R., Localized necking in thin sheets, *Journal of the Mechanics and Physics of Solids* 23 (1975) 421-41.
- [4.6] Hutchinson J.W., Neale K.W., Sheet necking—II: time-independent behaviour. *Mechanics of Sheet Metal Forming*, eds. Koistinen, D.P., Wang, N.M., Plenum, New York (1978a) 127-153.
- [4.7] Hutchinson J.W., Neale K.W., Sheet necking—III: strain-rate effects. *Mechanics of Sheet Metal Forming*, eds. Koistinen, D.P., Wang, N.M., Plenum, New York (1978b) 269-285.
- [4.8]. Tjotta S., Formability and the growth of damage. *Numerical Methods in Industrial Forming Processes*, eds. Wood, R.D., Zienkiewicz, O.C. (1992) 187.
- [4.9] Huang H.M., Pan J., Tang S.C., Failure prediction in anisotropic sheet metals under forming operations with consideration of rotating principal stretch directions, *International Journal of Plasticity* 16 (2000) 611-633.
- [4.10] Marciniak Z., Kuczynski K., Limit strains in the processes of stretch-forming sheet metal, *International Journal of Mechanical Sciences* 9 (1967) 609-620.

- [4.11] Marciniak Z., Kuczynski K., Influence of the plastic properties of a material on the forming limit curve for sheet metal in tension, *International Journal of Mechanical Sciences* 15 (1973) 789-805.
- [4.12] McCarron T.J., Kain K.E., Hahn G.T., Flanagan W.F., Effect of geometrical defects in forming sheet steel by biaxial stretching, *Metallurgical and Materials Transactions* 19A (1988) 2067-2074.
- [4.13] Chow C.L., Yang X.J., Chu E., Viscoplastic constitutive modeling of anisotropic damage under non-proportional loading, *Journal of Engineering Materials and Technology* 123 (2001) 403-408.
- [4.14] Prager W., The theory of plasticity: a survey of recent achievements, *Proceedings of the Institution of Mechanical Engineers* 169 (1955) 41-57.
- [4.15] Ziegler H., A modification of Prager's hardening rule, *Quarterly of Applied Mathematics* 17 (1959) 55-65.
- [4.16] Armstrong P.J., Frederick C.O., A mathematical representation of the multi-axial Bauschinger effect, CEGB report # RD/B/N 731 (1966).
- [4.17] Chaboche J.L., Constitutive equations for cyclic plasticity and cyclic viscoplasticity, *International Journal of Plasticity* 5 (1989) 247-302.
- [4.18] Molaei B., Strain path effects on sheet metal formability, Amirkabir University of Technology, Iran (1999) PhD thesis.
- [4.19] Graf A., Hosford W., Effect of changing strain paths on forming limit diagrams of Al 2008-T4, *Metallurgical Transactions* 24A (1993) 2503-12.
- [4.20] Butuc M.C., Gracio J.J., Barata da Rocha A, An experimental and theoretical analysis on the application of stress-based forming limit criterion, *International Journal of Mechanical Sciences* 48 (2006) 414-429.
- [4.21] Yoshida K., Kuwabara T., Kuroda M., Path-dependence of the forming limit stresses in a sheet metal, *International Journal of Plasticity* 23 (2007) 361-384.
- [4.22] Barlat F., Crystallographic texture, anisotropic yield surfaces and forming limits of sheet metals, *Materials Science and Engineering* 91 (1987) 55-72.
- [4.23] Xu S., Weinmann K.J., Effect of deformation-dependent material parameters on forming limits of thin sheets, *International Journal of Mechanical Sciences* 40 (2000) 913-925.

- [4.24] Brunet M., Morestin F., Experimental and analytical necking studies of anisotropic sheet metal, *Journal of Materials Processing Technology* 112 (2001) 214-226.
- [4.25] Aretz H., Numerical analysis of diffuse and localized necking in orthotropic sheet metals, *International Journal of Plasticity* 23 (2007) 798-840.
- [4.26] Stachowicz F., Effect of annealing temperature on plastic flow properties and forming limits diagrams of Titanium and Titanium alloy sheets, *Transactions of the Japan Institute of Metals* 29 (1988) 484-493.
- [4.27] Nurcheshmeh M., Green D.E., Investigation on the strain-path dependency of stress-based forming limit curves, *International Journal of Material Forming* 5 (2011) 25-37.
- [4.28] Sing W.M., Rao K.P., Influence of material properties on sheet metal formability limits, *Journal of Material Processing Technology* 48 (1995) 35-41.
- [4.29] Dunne F., Petrinic N., *Introduction to computational plasticity*, Oxford University Press (2005).
- [4.30] Hill R., *The mathematical theory of plasticity*, University Press, Oxford (1950).
- [4.31] Wu H.C., Hong H.K., Shiao YP, Anisotropic plasticity with application to sheet metals, *International Journal of Mechanical Sciences* 41 (1999) 703-724.
- [4.32] Stoughton T.B., Stress-based forming limits in sheet metal forming, *Journal of Engineering Materials and Technology*, ASME 123 (2001) 417-422.

Chapter 5

Influence of out-of-plane compression stress on limit strains in sheet metals

5.1. Introduction

The poor correlation between the common “cupping” test and the actual performance of sheet metal in industrial forming operations led researchers to look at some more fundamental parameters. A significant breakthrough came in 1963, when Keeler and Backofen [5.2] reported that during sheet stretching, localized necking required a critical combination of major and minor strains (along two perpendicular directions in the plane of the sheet). Subsequently, this concept was extended by Goodwin [5.3] to sheet drawing and the resulting curve is known as the Keeler-Goodwin curve or the forming limit curve (FLC). In other words, Keeler developed the right side of the FLC (i.e., positive minor strain), and Goodwin extended the forming limit curve to include negative minor strains.

In order to predict the FLC, Marciniak and Kuczynski [5.1] proposed that the inhomogeneity of the sheet material could be modeled by a geometric defect in the sheet. In their study, an imperfection in the form of a shallow groove was applied to specimens stretched in equibiaxial tension. The severity of the imperfection was quantified by the ratio of the thickness in the groove to the nominal thickness of the sheet. In general, no reductions in the forming limit would be seen when the value of the imperfection factor is

between 0.99 and 1.00. In this model, the initial inhomogeneity of the material develops continuously with plastic deformation until a localized neck eventually appears.

In 1970, Azrin and Backofen [5.4] subjected a large number of materials to in-plane stretching. They discovered that an imperfection factor of about 0.97 or less was required to obtain agreement between the MK analysis and experimental FLC data. Accordingly, even though the MK method provided a simple predictive model, there was inconsistency between its predictions and experimental data. Similar trends were also observed by Sowerby and Duncan [5.5] as well as by Marciniak *et al.* [5.6]. In addition, Sowerby and Duncan [5.5] also reported that limit strains predicted with the MK method showed a considerable dependence on material anisotropy.

Ghosh [5.7] found that material strain rate sensitivity is important during post-uniform deformation. The additional hardening due to strain rate sensitivity plays a significant role in increasing the forming limits by delaying strain localization inside the neck.

The physical soundness and the simplicity of the MK analysis has no doubt been the reason this method has been the most popular theoretical approach for FLC calculation, and it has been used by many researchers, even in recent years: for instance Butuc *et al.* [5.8] in 2006, Yoshida *et al.* [5.9] in 2007 and Nurcheshmeh and Green [5.10] in 2011.

The prediction of the FLC of sheet metals traditionally assumes plane stress loading conditions and the effect of the normal stress is usually neglected. Therefore FLC predictions are only strictly valid for open die and free forming processes. However, many metal forming processes lead to the development of non-negligible normal stresses in the sheet when it is formed over a die radius. Through-thickness stresses become even more significant in hydroforming processes, where a pressurized fluid compresses a sheet or a tube against the surface of the die. In many hydroforming applications, the pressure of the forming fluid can generate such high contact pressures that the through-thickness stress exceeds the in-plane stresses. The existence of a significant through-thickness compressive stress creates a hydrostatic stress state that has the potential to increase the formability of the sheet and therefore requires consideration in the prediction of the FLC.

Very few sheet formability studies have taken into account the effect of the normal stress and further research is required in this area. Gotoh *et al.* [5.11] presented an analytical expression that predicts an increase in the plane-strain forming limit in strain space due to the presence of through-thickness compressive stresses. They demonstrated theoretically that an out-of-plane stress (even as small as one tenth of the yield stress) can raise the forming limit strain and thus can be effectively used to delay the onset of fracture in press forming. Smith *et al.* [5.12] developed a new sheet metal formability model that takes into account the through-thickness normal stress for materials that exhibit planar isotropy. Their model predicts a greater increase in formability due to compressive stresses than that predicted by Gotoh's model. They also examined the influence of the strain hardening coefficient (n value) on the sensitivity of the FLC to the normal stress.

Finally, Banabic and Soare [5.13] used the MK analysis to study the influence of fluid pressure normal to the sheet surface on the forming limits of thin, orthotropic sheets. Their model was used to predict the FLC of AA3104-H19 aluminum alloy subject to different fluid pressures ranging from 0 (plane stress condition) to 200 MPa. They showed that the formability of this aluminum alloy improves with the application of a fluid pressure, especially on the right side of the forming limit diagram. Experimental data was available in the plane stress condition which was predicted satisfactory and used to calibrate their model.

In the present paper, a three-dimensional stress state was implemented in a modified version of the MK model to predict FLC with different through-thickness stress values. The imperfection factor was related to the surface roughness and grain size of the sheet and was updated throughout the deformation of the sheet. The imperfection band was oriented perpendicular to the first principal stress, and its rotation was also considered as the sheet was plastically deformed. This modified MK model was validated in plane-stress conditions with experimental FLC data obtained for AISI-1012 steel [5.14] and it was also compared with other theoretical results obtained by the present authors [5.10]. The validation of the model for cases that involved through-thickness stresses was done with published experimental FLC data for AA6011 aluminum [5.15] and STKM-11A steel [5.16] sheets. The sensitivity of the predicted FLC to the applied

out-of-plane stress component was also analyzed as a function of variations in different material properties and the results of this sensitivity analysis will be discussed.

5.2. Theoretical approach

Marciniak and Kuczynski [5.1, 5.6] presented a theoretical framework for prediction of FLC that is commonly known as the MK method, which has been shown to predict FLCs with reasonable accuracy. This approach is based on the fact that inhomogeneities are unavoidable in actual sheet materials, and it is assumed that this inherent material inhomogeneity can be modeled as a geometric imperfection in the form of a narrow band (Figure 5.1) with a slightly different thickness than the rest of the sheet. Although this approach was originally proposed for plane stress conditions, the current work includes the third stress component in the MK model and is shown as σ_3 in Figure 5.1.

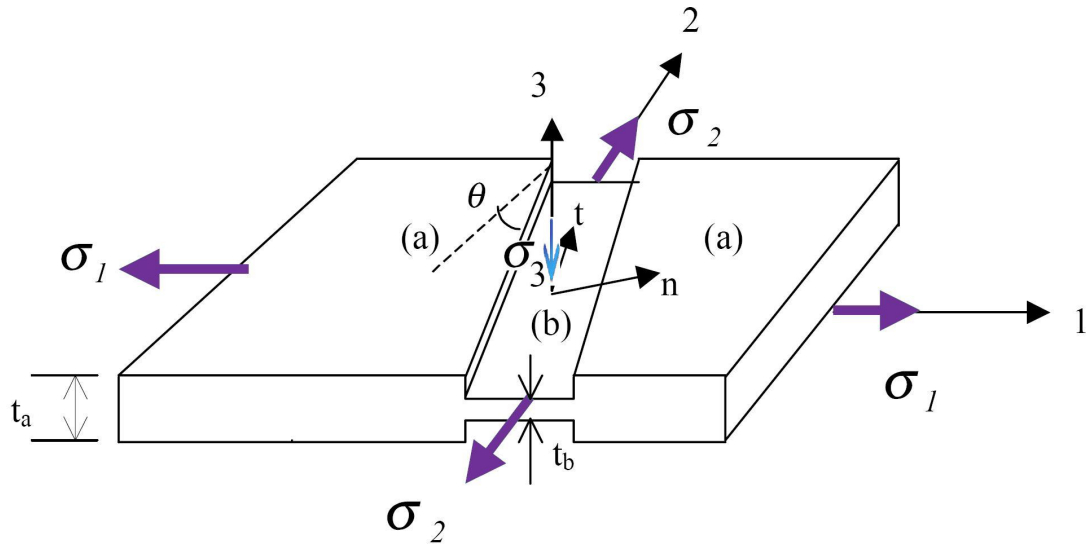


Figure 5.1. Thickness imperfection in the MK model

Figure 5.1 schematically represents a shallow groove on sheet surface, which effectively divides it into two separate regions: region (a) with nominal thickness, and region (b) with the reduced thickness in the groove. The initial imperfection factor of the groove, f_0 , is defined as the thickness ratio between the two regions as follows:

$$f_0 = \frac{t_0^b}{t_0^a} \quad (5.1)$$

where t denotes the sheet thickness and subscript ‘0’ denotes the initial state. The thickness difference between these two regions is critical element in the MK theory because the predicted limiting strains are very sensitive to the initial value of the imperfection factor. In most studies, this coefficient is simply assumed to have a fixed value close to 1.0 and that can be adjusted so that the predicted FLC will better fit the experimental data. However, it has been proposed [5.10] that a more realistic approach would be to relate the initial thickness difference between the two regions to the surface roughness of the sheet. Indeed, research carried out by Stachowicz [5.17] shows that surface roughness changes with deformation and these changes depend upon initial surface roughness, grain size, and effective plastic strain. By relating the thickness difference between regions (a) and (b) to the surface roughness of the sheet metal, the imperfection factor not only takes on a value that has physical meaning but also the option of adjusting this value so that the predicted FLC can better fit experimental data is eliminated. Stachowicz’s assumption was adopted in this work and the imperfection factor was assumed to change with the deformation of the sheet according to the following relationship:

$$f_0 = \frac{t_0^a - 2[R_{z0} + Cd_0^{0.5}\varepsilon_e^b]}{t_0^a} \quad (5.2a)$$

$$f = \frac{t_0^a - 2[R_{z0} + Cd_0^{0.5}\varepsilon_e^b]}{t_0^a} \exp(\varepsilon_3^b - \varepsilon_3^a) \quad (5.2b)$$

where R_{z0} is the surface roughness before deformation, C is a material constant, ε_e^b is the effective strain in region (b), and d_0 is the material’s initial grain size. Additional details on the calculation of the imperfection factor are provided in the authors’ previous work [5.10].

In general, the imperfection band is randomly oriented and its orientation can be determined by the angle θ between the groove axis and the direction of the second

principal stress (Figure 5.1). When plastic deformation begins, this angle will slowly start to change as the groove rotates with respect to the loading axes, and its orientation can affect the limiting strains. In order to obtain FLC predictions with good accuracy, the variations in the groove orientation should therefore be considered in the calculation of the forming limit strains by updating its value at each increment throughout the plastic deformation. This rotation of the imperfection band during deformation was well researched by Sing and Rao [5.18] and they proposed an empirical formula in which the orientation varies as a function of the true plastic strain increments in region (*a*) of the sheet as follows:

$$\tan(\theta + d\theta) = \tan(\theta) \frac{1 + d\varepsilon_1^a}{1 + d\varepsilon_2^a} \quad (5.3)$$

where $d\varepsilon_1^a$ and $d\varepsilon_2^a$ are the major and minor principal strains in the nominal area of the sheet, respectively.

A constitutive equation was derived in which the yield function can be expressed in the following general form for isotropic hardening:

$$f = \left(\frac{3}{2} S_{ij} : N : S_{ij} \right)^{1/2} - \sigma_e \quad (5.4)$$

where, S is the deviatoric stress tensor and N is a tensor that describes the anisotropy of the sheet material in terms of the anisotropic constants in Hill's 1948 yield function [5.19].

With consideration of the third principal stress component, the three-dimensional plastic potential function was implemented in the MK analysis:

$$2h = \sigma_x^2 + (F + H)\sigma_y^2 + (F + G)\sigma_z^2 - 2H\sigma_x\sigma_y - 2F\sigma_z\sigma_y - 2G\sigma_z\sigma_x = f^2 \quad (5.5)$$

where the anisotropic coefficients F , G and H can be calculated from the yield stresses in the principal directions.

Strain hardening is described with the power hardening including strain rate sensitivity effect as follows:

$$\sigma_e = k \left(\dot{\varepsilon}_e \right)^m (\varepsilon_e + \varepsilon_0)^n \quad (5.6)$$

where ε_0 is a uniform prestrain applied to the sheet, m is the strain-rate sensitivity coefficient, n is the strain-hardening coefficient, σ_e and ε_e are the effective stress and strain, respectively.

The associated flow rule was employed to calculate plastic strain increments as follows:

$$d\varepsilon_{ij} = d\lambda \times \text{grad}(h) = d\lambda \times \frac{\partial h}{\partial \sigma_{ij}} \quad (5.7)$$

where $d\lambda$ is the plastic multiplier and h is the plastic potential function.

There are two main assumptions in the MK analysis. The first one is the geometric compatibility equation expressed as the equality of the tangential plastic strain components inside and outside the imperfection band,

$$d\varepsilon_{tt}^a = d\varepsilon_{tt}^b \quad (5.8)$$

and the second assumption is the equilibrium of the normal and shear forces across the imperfection, i.e.:

$$F_{nn}^a = F_{nn}^b \quad (5.9a)$$

$$F_{nt}^a = F_{nt}^b \quad (5.9b)$$

where subscripts n and t denote the normal and tangential directions of the groove, respectively, and F is the force per unit width, i.e.:

$$F_{nm}^a = \sigma_{nm}^a t^a \quad (5.10a)$$

$$F_{nm}^b = \sigma_{nm}^b t^b \quad (5.10b)$$

$$F_{nt}^a = \sigma_{nt}^a t^a \quad (5.10c)$$

$$F_{nt}^b = \sigma_{nt}^b t^b \quad (5.10d)$$

By combining Eq. (5.1), (5.6) and (5.10a,b) the following relation is obtained:

$$\left[\frac{\sigma_{nm}^a}{\sigma_e^a} \right] / \left[\frac{\sigma_{nm}^b}{\sigma_e^b} \right] = f \left(\left[\varepsilon_0 + \varepsilon_e^b \right]^n \dot{\varepsilon}_e^b \right) / \left(\left[\varepsilon_0 + \varepsilon_e^a \right]^n \dot{\varepsilon}_e^a \right) \quad (5.11a)$$

Since the strain rate is defined as $\dot{\varepsilon}_e = d\varepsilon_e/dt$, it follows that:

$$\left[\frac{\sigma_{nm}^a}{\sigma_e^a} \right] / \left[\frac{\sigma_{nm}^b}{\sigma_e^b} \right] = f \left(\left[\varepsilon_0 + \varepsilon_e^b \right] / \left[\varepsilon_0 + \varepsilon_e^a \right] \right)^n \left[d\varepsilon_e^b / d\varepsilon_e^a \right]^m \quad (5.11b)$$

Finally, the stress transformation rule leads to the expressions:

$$\sigma_{nm}^a = \sigma_x^a \cos^2(\theta) + \sigma_y^a \sin^2(\theta) \quad (5.12a)$$

$$\sigma_{nt}^a = -(\sigma_x^a - \sigma_y^a) \sin(\theta) \cos(\theta) = \sigma_x^a [(\alpha - 1) \sin(\theta) \cos(\theta)] \quad (5.12b)$$

where α is the ratio of the second true principal stress component (σ_2) to the first true principal stress component (σ_1) in the nominal area which indicates the stress path. Expressions similar to Eq. (5.12a) and (5.12b) can be written for region (b), and using Eq. (5.9), (5.10), and (5.12) we obtain:

$$\frac{\sigma_{nt}^b}{\sigma_{nn}^b} = \frac{\sigma_{nt}^a}{\sigma_{nn}^a} = \frac{(\alpha - 1) \sin(\theta) \cos(\theta)}{\cos^2(\theta) + \alpha \sin^2(\theta)} \quad (5.13)$$

With consideration of the consistency condition, the plastic potential function and the strain transformation rule:

$$\begin{aligned} \frac{d\varepsilon_e^a}{\sigma_e^a} \left\{ [(F + H) \times \alpha^a - F\beta^a - H] \sigma_x^a \cos^2 \theta + (1 - G\beta^a - H\alpha^a) \sigma_x^a \sin^2 \theta \right\} = \\ \sigma_x^b \frac{d\varepsilon_e^b}{\sigma_e^b} \left\{ [(F + H) \times \alpha^b - F\beta^b - H] \cos^2 \theta + (1 - G\beta^b - H\alpha^b) \sin^2 \theta \right\} \end{aligned} \quad (5.14)$$

where β is the ratio of the third true stress component to the first true stress component, such that:

$$\beta = \sigma_3 / \sigma_1 = \sigma_z / \sigma_x \quad (5.15)$$

By combining Eq. (5.11), (5.13), and (5.14), the final governing equation was analytically determined as a function of the ratio of the effective plastic strain inside and outside the imperfection band $\eta = \varepsilon_e^b / \varepsilon_e^a$. This final differential equation indicates the evolution of the effective plastic strain ratio η as the sheet is deformed under a three-dimensional loading condition.

The plastic deformation of the sheet begins as strain increments are imposed along a linear strain path (i.e. for a constant value of $\rho = \varepsilon_2 / \varepsilon_1$) in the nominal region, and the stress components are calculated from the strain state in the nominal area. Then the strains and stresses in the imperfection region are calculated from the strains and stresses in the nominal area by using the governing equations described above. During the analysis, it is assumed that the normal stress applied on the surface of the sheet or tube is identical for both region (a) and region (b) of the MK model. But since the thickness in region (b) is less than that in the rest of the sheet, the strain rate increases

faster in region (*b*) than in region (*a*). Moreover, the difference in strain rate between the two regions will intensify as the deformation progresses, and eventually the strains will localize in the imperfection region. It is generally assumed that plastic instability occurs when the effective plastic strain in the imperfection region reaches 10 times that in nominal area ($\varepsilon_e^b = 10\varepsilon_e^a$). Once the onset of necking takes place, the in-plane plastic strain components in the nominal area (ε_1^a and ε_2^a) identify a point on the FLC for the specified strain path ρ . In order to generate the entire FLC, the value of the strain ratio ρ is modified and the procedure is repeated for each new strain path. The FLC is thus determined from the limiting strain data obtained for strain paths that vary in increments $\Delta\rho = 0.05$ from uniaxial tension ($\rho = -0.5$) to equibiaxial tension ($\rho = 1.0$).

5.3. Experimental validation of the modified MK model

The theoretical MK analysis model presented in the previous section was implemented into a numerical code. This proposed model was then used to predict the FLC of actual sheet and tube materials, both with and without applied normal stresses, in order to validate the numerical code.

5.3.1. Description of materials

The materials that were considered for the validation of the proposed MK model are a low carbon steel (AISI-1012) [5.14], AA6011 aluminum alloy [5.15], and STKM-11A steel [5.16] (the designation of this last steel grade follows the Japanese standard and it is equivalent to an MT1010 steel in the ASTM standard). The mechanical properties of these materials are listed in Table 5.1. It is also worth noting that in these publications, AISI-1012 refers to a flat stock sheet metal, whereas AA6011 and STKM-11A refer to thin walled tubes.

Table 5.1. Mechanical properties of materials

Material	K (MPa)	n	m	R (Normal)	t₀ (mm)
AISI-1012 [5.14]	238	0.35	0.015	1.21	2.5
AA6011 [5.15]	254.9	0.265	-----	0.574	1.86
STKM-11A [5.16]	1450	0.14	-----	2.14	1.4

Eq. (5.2a) was used to calculate the initial imperfection factor value in the MK analysis. It was found that $f_0 = 0.995$ for AISI-1012 steel, $f_0 = 0.997$ for AA6011 aluminum, and $f_0 = 0.991$ for STKM-11A steel.

5.3.2. Validation of the proposed MK model

In order to validate the three-dimensional FLC model described in the previous section, theoretical FLCs were calculated in both plane stress and three-dimensional stress conditions and the predicted FLCs were compared with published experimental data [5.14-5.16].

The new model was verified first under plane stress conditions, in the absence of through-thickness stresses ($\beta = 0$). Theoretical FLC were compared with the experimental FLC of as-received AISI-1012 sheet steel [5.14] which were obtained by carrying out stretch forming tests using rectangular and notched blanks of various widths with different conditions of lubrication to achieve a range of strain states $-0.5 \leq \rho = \varepsilon_2/\varepsilon_1 \leq 1.0$. Each blank was electro-etched with a 3.0 mm diameter circle grid and formed over a hemispherical punch until the onset of local necking. The major and minor strains were measured directly from the deformed grids using a profile projector. The FLC predicted with the proposed MK model was also compared with the FLC predicted by a different MK analysis code developed previously by the same authors for purely plane stress conditions [5.10]. The predicted and experimental FLCs for this grade of steel are shown in Figure 5.2.

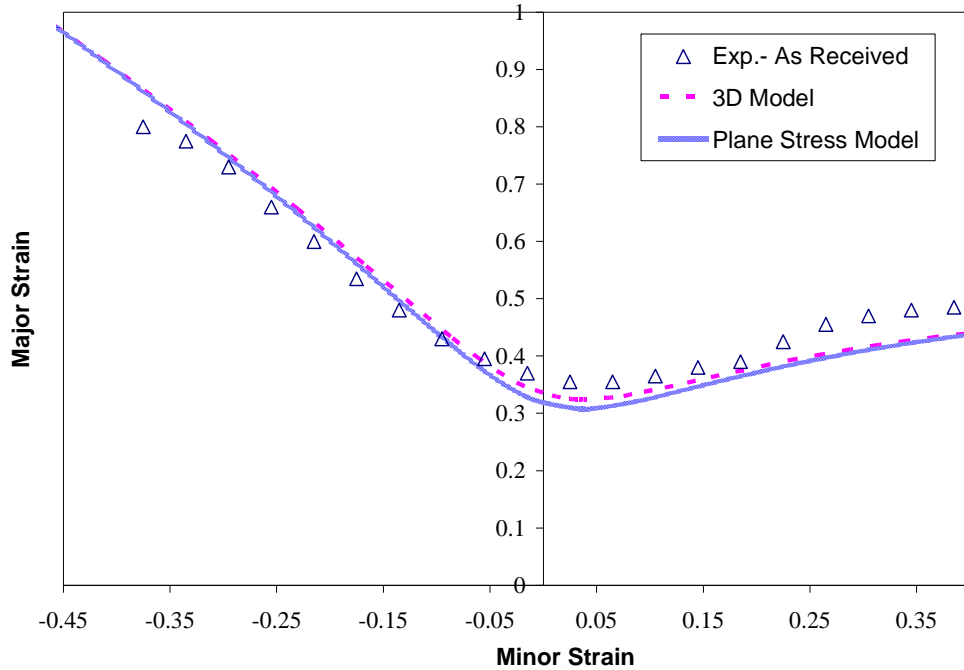


Figure 5.2. Comparison of predicted and experimental FLCs of AISI-1012 steel sheet in-plane stress condition [5.14]

Figure 5.2 shows good agreement between the theoretical and experimental FLCs obtained under plane stress conditions, and the developed model predicts the FLC for this steel with acceptable accuracy. Furthermore, it can be seen that the FLC predicted under plane stress conditions with the new three-dimensional model is essentially identical to the FLC predicted with the previous two-dimensional analysis code [5.10].

The proposed MK analysis model was also verified for more general loading conditions where the out-of-plane stress component is non-negligible ($\beta \neq 0$). This further validation of the three-dimensional MK model was carried out by predicting the FLC of AA6011 aluminum tubes that were hydroformed with up to 15-MPa internal pressure (which corresponds to $\sigma_3 \approx 7.5$ MPa). Hwang *et al.* [5.15] prepared 200-mm long tube specimens with a 1.86-mm wall thickness, and a 51.9-mm outer diameter. The tube specimens were annealed at 410°C for 2 hours and then a grid of 5-mm-diameter circles with a spacing of 1-mm was electrochemically etched onto the surface of undeformed tubes for the purpose of strain measurement. Tubes were pressurized in a bulge test apparatus without axial feeding to generate positive minor strains. Other tubes were also pressurized in a hydroforming test machine with axial feeding to generate strain paths

with negative minor strains. After the tubes were deformed, the circle grids in the vicinity of the burst were measured by a three-dimensional digital image processing system and the major and minor strains were determined. The limiting strain data from these tests was used to construct the left side of the FLC of these aluminum tubes. The comparison of the predicted and experimental FLCs is shown in Figure 5.3.

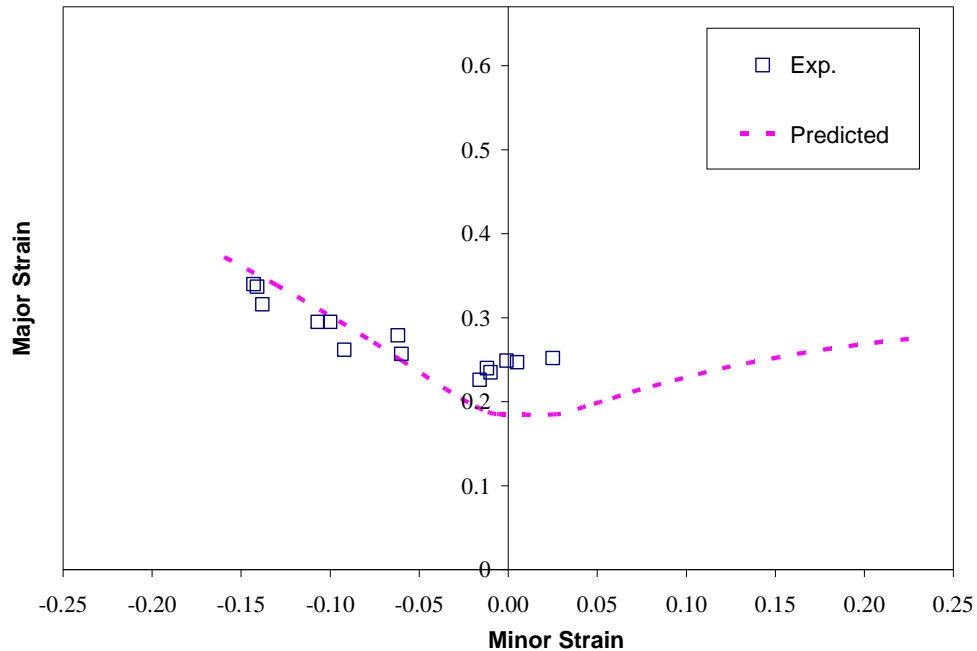


Figure 5.3. Comparison of predicted and experimental FLCs of AA6011 aluminum sheets under 15 MPa internal pressure [5.15]

It can be seen from Figure 5.3 that there is good agreement between the experimental data and the predicted FLC on the left side of the diagram. This may seem surprising considering that the analysis was carried out using Hill's 1948 yield criterion. Indeed, it is well known that Hill's quadratic yield function is not suitable for predicting the biaxial behaviour of aluminum alloys and more recent, non-quadratic yield functions have been shown to be much more appropriate [5.20]. However, it can be seen that the experimental FLC data in Figure 5.3 corresponds with deformation modes between plane strain and uniaxial tension, and for such deformation modes the quadratic yield function is capable of predicting reasonably accurate results. Non-quadratic yield functions typically lead to improved predictions of the forming behaviour of aluminum alloys for deformations in

biaxial tension, because they are better able to represent the shape of the yield locus between plane strain and balanced biaxial tension: this corresponds with the right side of the FLC for which no experimental data is available. No doubt the predictions of FLC in the region of plane strain would be improved with the use of a non-quadratic yield function.

The proposed model was also validated with another set of experimental limiting strain data for STKM-11A steel presented by Kim *et al.* [5.16]. These authors determined the experimental FLC by hydroforming straight tubes with both an axial end-feed force and 56-MPa internal pressure (leading to $\sigma_3 \approx 28$ MPa). A constant ratio of high internal pressure and relatively low axial force was applied with an end displacement rate of 2.33-mm/s using a PC-based controller. During these experiments, tubes were pressurized until they burst, and the average burst pressure was 56 MPa, with the split occurring parallel with the tube axis and positioned toward the middle of the tube. Strain measurements were taken as near to the fractured edge as possible in order to determine limit strains. Figure 5.4 shows a comparison of predicted and experimental FLC for negative minor strains.

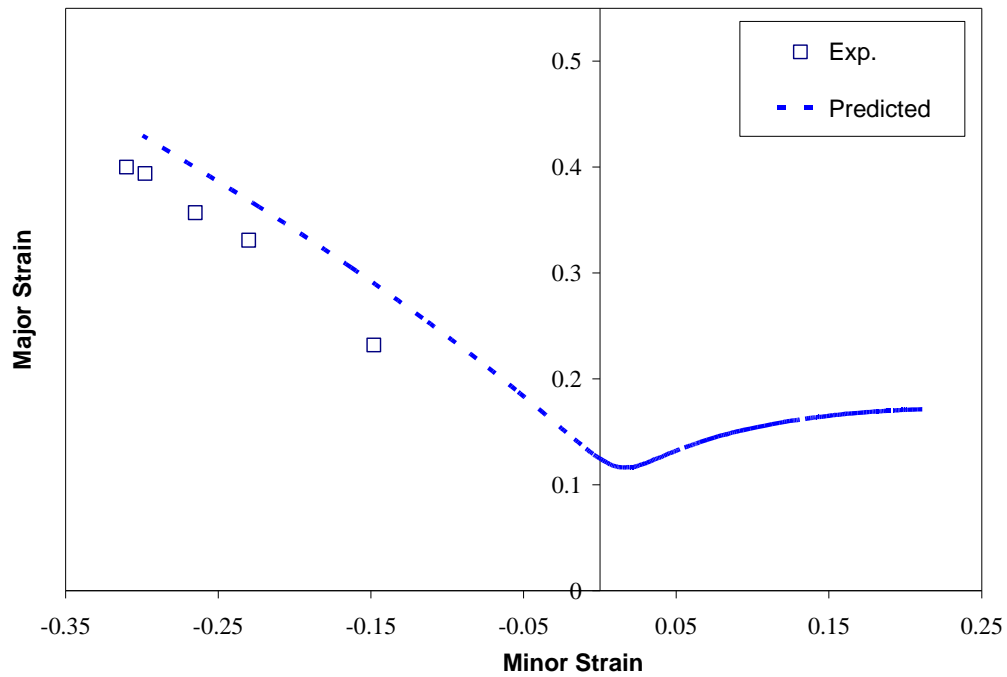


Figure 5.4. Comparison of predicted and experimental FLCs of STKM-11A steel sheet under 56MPa internal pressure [5.16]

It can be seen in Figure 5.4 that the FLC predicted by the proposed MK analysis lies slightly above the experimental FLC for this grade of steel. This discrepancy between the theoretical and the experimental FLC data is likely due to the fact that experimental strains were not actually measured in local necks since these tubes were allowed to burst, but they were measured in the uniformly deformed material right next to the fractured edge of burst tubes. Therefore these experimental strain data represent a conservative estimation of the actual FLC. Limiting strain data was not available for the right hand side of the diagram because Kim *et al.* [5.16] were only able to apply a compressive axial force to the ends of the tubes, whereas a tensile axial force is required to obtain positive minor strains [5.21].

It is also worth pointing out that the experimental FLC data [5.14-5.16] used to validate the current MK model were obtained using the well-known circle grid analysis technique. This technique relies on the measurement of deformed grids on the surface of the specimens as well as the somewhat subjective interpretation about whether necking has begun or not in a specific grid location. This technique is therefore dependent on the experimentalist's experience and the accuracy of the strain measurements, and therefore it inevitably leads to some variability in the results. According to the author's experience, the experimental error that can be expected in FLC strain data obtained with the circle grid technique is estimated to be within $\pm 2.5\%$ strain. More advanced techniques are now being used to determine the forming limits of sheet materials with greater repeatability and reproducibility. For instance, digital image correlation is used to measure the strain field across the entire specimen gauge area and numerical interpolation methods are then used to determine the strains at the onset of necking [5.22-5.26]. These techniques are very powerful as they can determine limiting strains even for very high strength materials that tend to fracture without necking.

However, although there is some experimental error in the published experimental FLC data [5.14-5.16], the comparisons between the predicted and experimental FLC (Figures 5.2-5.4) nevertheless show that the proposed three-dimensional MK model provides a good prediction of the FLC, whether the through-thickness stress component is significant or not.

5.4. Influence of the through-thickness stress on the FLC

The primary purpose of this work is to study the effect of the through-thickness stress component on the forming limit curve. In this section, the sensitivity of the FLC to the out-of-plane stress component will be studied by applying different levels of through-thickness stress to the surface of AISI-1012 steel sheets. The FLC was predicted for a normal stress ranging from $\sigma_3 = 0$ (plane stress condition) to $\sigma_3 = 35$ MPa. The theoretical results are presented in Figure 5.5.

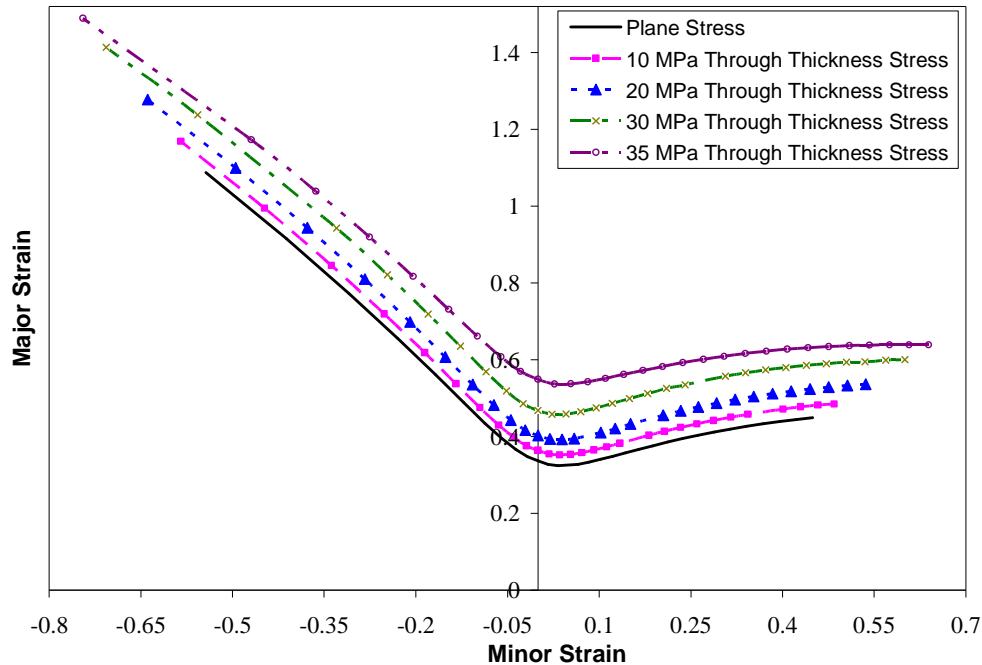


Figure 5.5. FLC of AISI-1012 sheet steel predicted as a function of the applied normal stress

It can be seen from Figure 5.5 that the FLC is quite sensitive to the normal stress: indeed, the entire FLC is observed to shift up the vertical axis when the applied normal stress increases. The formability of this sheet steel is seen to improve with a normal stress as low as 10 MPa. Furthermore, it is apparent from Figure 5.5 that the increase in formability is not proportional to the increase in normal stress: indeed, the rate of increase in formability also increases with the normal stress.

5.5. Influence of mechanical properties on the sensitivity of FLC to out-of-plane stresses

In the previous section it was shown (Figure 5.5) that the FLC of AISI-1012 sheet steel is dependent on the magnitude of the applied normal stress. Therefore it is also of further interest to determine if this dependence varies from one material to another, and if so, how individual material properties may affect the sensitivity of the FLC to the normal, or through-thickness, stress. The constitutive equations in this three-dimensional version of the MK model are capable of fully describing the elasto-plastic behaviour of sheet materials; therefore it is possible to investigate the effect of individual material parameters on the sensitivity of the FLC to the out-of-plane stress. In this study, the influence of some of the more significant properties of sheet materials – the strain hardening coefficient (n), the strain rate sensitivity (m), the plastic anisotropy coefficients (R), grain size (d_0) and initial sheet thickness (t_0) were investigated. Each parameter was therefore modified one by one to observe its effect on the sensitivity of the FLC to increases in the out-of-plane stress, and the results of this study are presented in this section.

Since the work hardening ability of a sheet material is such a significant material property in sheet metal forming, the effect of a change in the strain hardening coefficient is presented first. All the mechanical properties of the AISI-1012 sheet steel (Table 5.1) were kept unchanged except for the value of the strain hardening coefficient which was doubled from $n = 0.35$ to $n = 0.70$. While this change leads to a fictitious material for which the experimental FLC is not readily available, the present three-dimensional version of the MK analysis nevertheless enables us to predict the dependence of the FLC on the applied normal stress. Figure 5.6 shows the FLC of a very formable sheet material ($n = 0.7$) for various levels of applied normal stress ranging from $\sigma_3 = 0$ (plane stress) to $\sigma_3 = 35$ MPa.

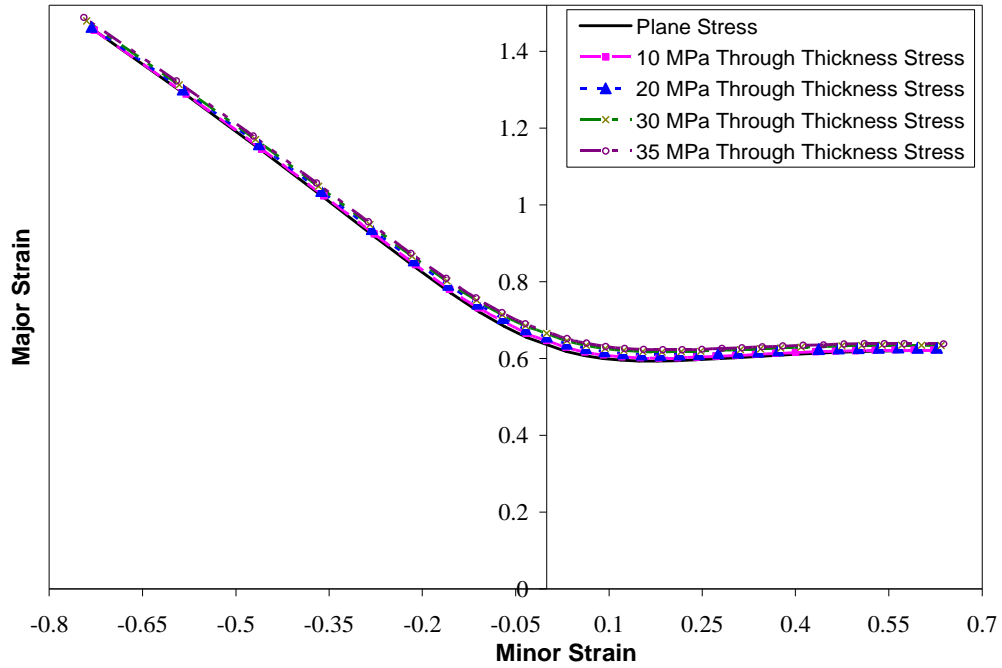


Figure 5.6. FLC of a sheet material that differs from AISI-1012 only by its strain hardening coefficient ($n=0.70$), predicted as a function of the applied normal stress

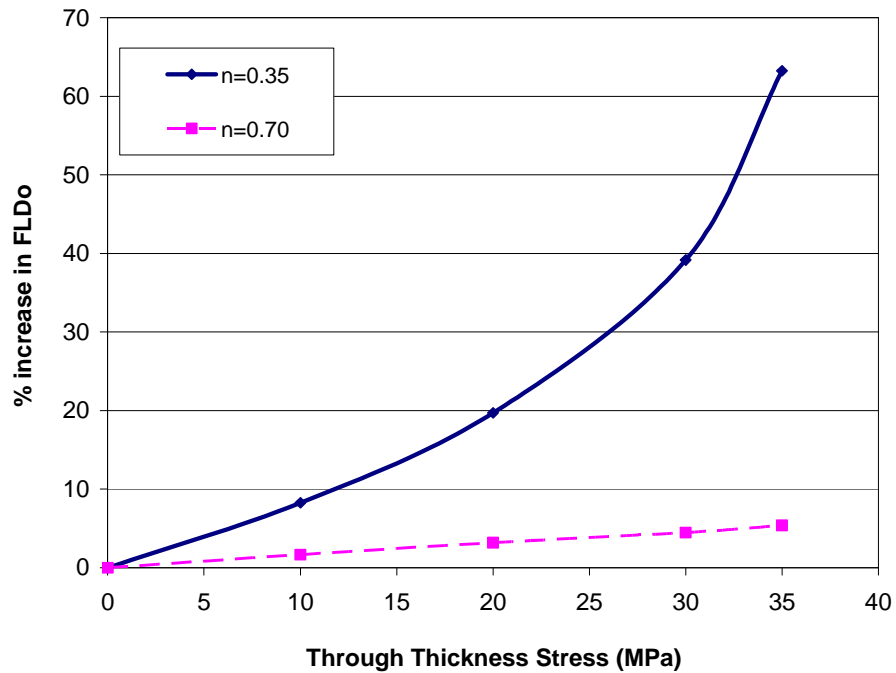


Figure 5.7. Increase in FLC_0 as a function of the applied normal stress for two sheet steels that differ only by their strain hardening coefficient ($n=0.35$ and $n=0.70$)

Figure 5.6 shows that the predicted FLC is almost independent of the applied normal stress for a sheet material with a very high strain hardening coefficient. In order to better visualize the effect of the strain hardening coefficient on the FLC, the vertical shift of the FLC relative to the plane stress condition was plotted as a function of the applied normal stress. More specifically, the percent increase in the limiting major strain in plane strain (FLC_0) due to increases in the out-of-plane stress component was plotted for both materials considered ($n = 0.35$ and $n = 0.70$) and shown in Figure 5.7. This figure indicates that through-thickness stresses always improve the formability of sheet materials, but the positive effect of the out-of-plane stress is far more significant for lower-formability sheet materials than it is for higher-formability materials.

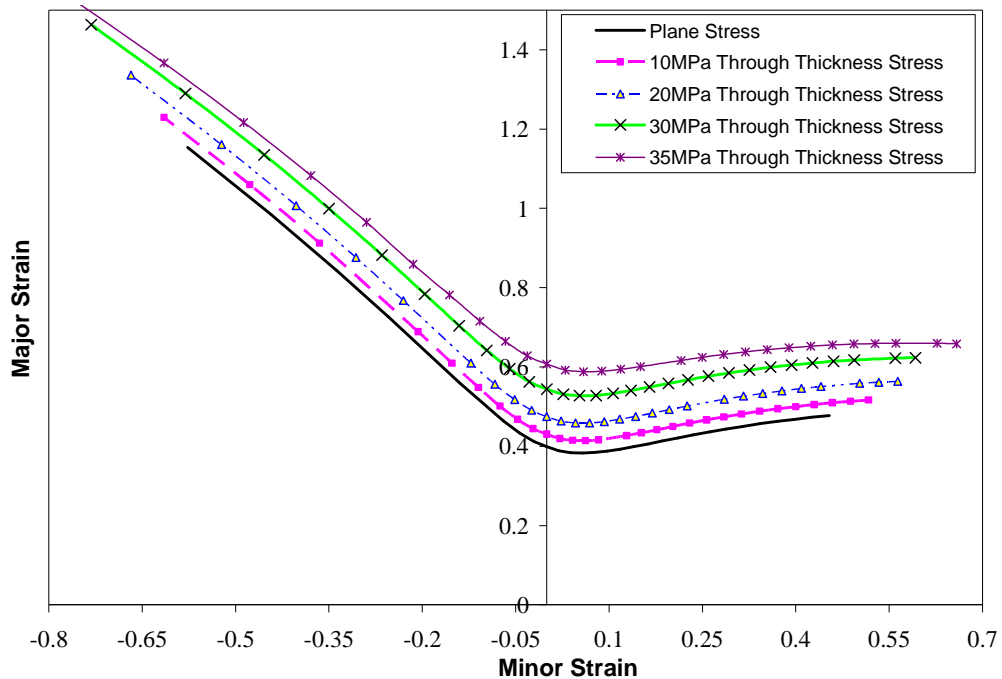


Figure 5.8. FLC of a sheet material that differs from AISI-1012 only by its strain rate sensitivity ($m=0.030$) predicted as a function of the applied normal stress

The next mechanical property considered in this study on the forming limits of sheet metal formed under three-dimensional stress states is the strain rate sensitivity (m). It is well known that positive strain rate sensitivity helps to improve formability by delaying the onset of necking and by strengthening the material as the strain rate increases in the area where strains are localizing. In this investigation, all the mechanical

properties of the AISI-1012 sheet steel (Table 5.1) were kept unchanged except for the strain rate sensitivity which was doubled from $m = 0.015$ to $m = 0.030$. The three-dimensional MK model was then used to calculate the FLC for each level of applied normal stress, and the predicted FLCs are plotted in Figure 5.8. It is evident from Figure 5.8 that the predicted FLC remains very dependent on the through-thickness stress after the strain rate sensitivity was increased by a factor of two. However, comparing Figure 5.8 to Figure 5.5, the sensitivity of the FLC to the through-thickness stress does not appear to have changed significantly.

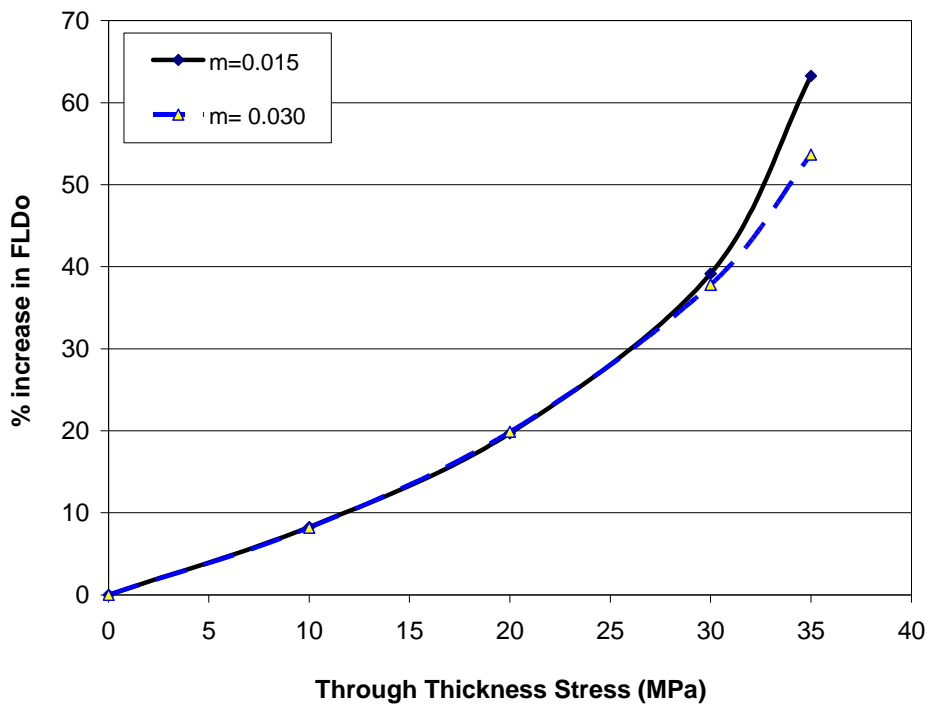


Figure 5.9. Increase in FLC_0 as a function of the applied normal stress for two sheet steels that differ only by their strain rate sensitivity ($m=0.015$ and $m=0.030$)

In order to quantify the effect of the strain rate sensitivity (m value) on the dependence of FLC to the normal stress the percentage increase in FLC_0 was plotted as a function of the applied normal stress for both sheet steels ($m = 0.015$ and $m = 0.030$), and the results are shown in Figure 5.9. It is immediately apparent from this figure that, while formability significantly increases with normal stress for both materials, changes in strain rate sensitivity practically have no effect on the dependence of FLC to the through-thickness stress.

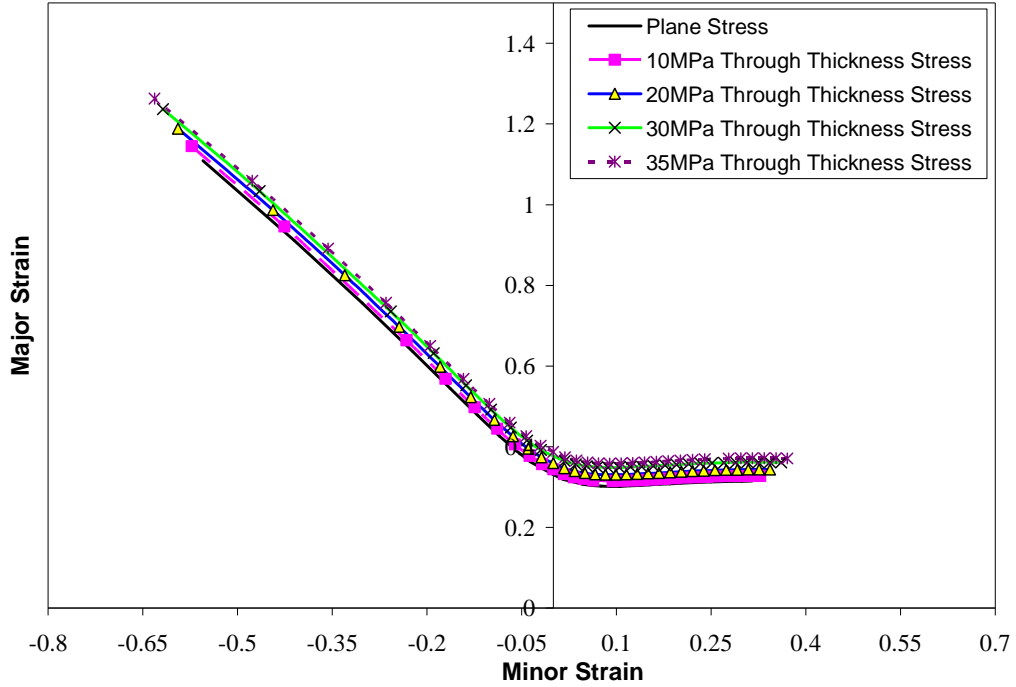


Figure 5.10. FLC of a sheet material that differs from AISI-1012 only by its plastic anisotropy coefficients ($R_0=2.8$ and $R_{90}=2.7$), predicted as a function of the applied normal stress

Another mechanical parameter that was considered in this investigation is the anisotropy of the sheet material. It is well known that, according to the MK analysis, variations in anisotropy are seen to have a significant effect on the formability of a sheet material, and this effect is primarily evident on the right hand side of the FLC (i.e. for positive minor strains). Although experimental FLC data do not generally show such an influence of anisotropy on the forming limits [5.27], the sensitivity of FLC to the applied through-thickness stress was nevertheless calculated for a fictitious material whose mechanical properties are identical to those of AISI-1012 steel except for the anisotropy coefficients; the plastic anisotropy coefficients were doubled from $R_0 = 1.4$ and $R_{90} = 1.35$ to $R_0 = 2.8$ and $R_{90} = 2.7$. It can be pointed out that, while the anisotropy of this fictitious material is expressed in terms of planar anisotropy coefficients (R_0 and R_{90}) the level of planar anisotropy is actually low ($\Delta R = (R_0 + R_{90} - 2R_{45})/2 = 0.85$), but the normal anisotropy, that is, the through-thickness anisotropy, is quite significant ($\bar{R} = (R_0 + R_{90} + 2R_{45})/4 \approx 2.42$). The FLC of this material was then calculated for increasing levels of applied normal stress and the results are shown in Figure 5.10.

Figure 5.10 shows that the formability of a sheet material with significant normal anisotropy also increases with increasing normal stresses. Nevertheless, a comparison of Figures 5.5 and 5.10 seems to indicate that the FLC becomes somewhat less sensitive to the through-thickness stress as normal anisotropy increases. To better evaluate the sensitivity of the FLC to the normal stress for different degrees of normal anisotropy, the percent increase in FLC_0 from the plane stress condition was calculated for both sets of anisotropy coefficients and plotted in Figure 5.11.

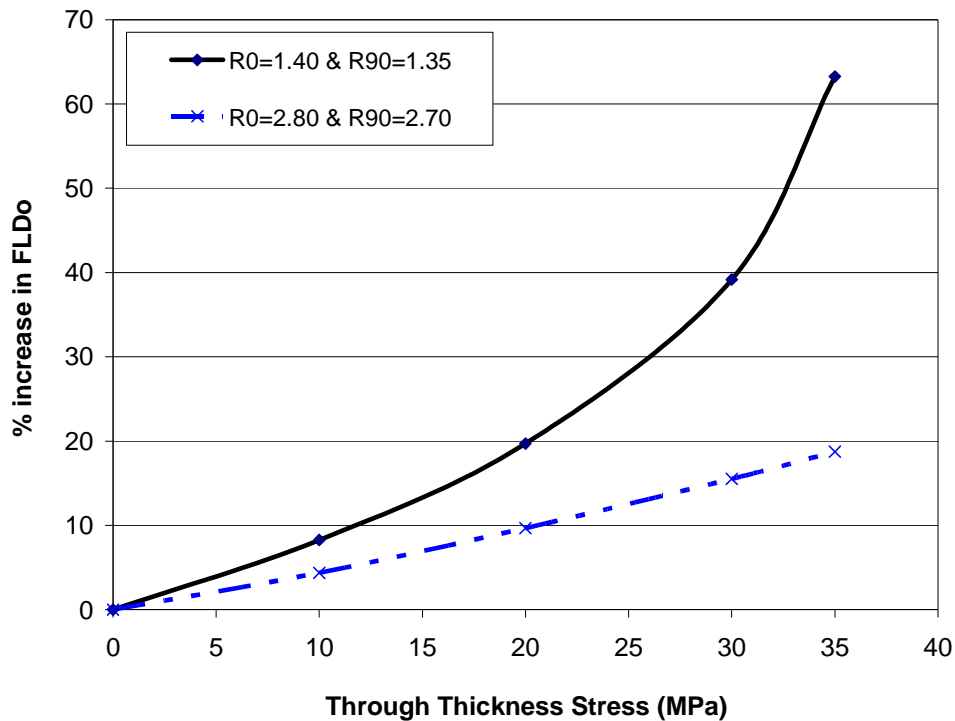


Figure 5.11. Increase in FLC_0 as a function of the applied normal stress for two sheet steels that differ only by their plastic anisotropy coefficients ($R_0=1.4$ and $R_{90}=1.35$ versus $R_0=2.8$ and $R_{90}=2.7$)

Figure 5.11 indeed supports the observation made from Figure 5.10 that, while FLC_0 continues to increase with the normal stress, the rate of increase of FLC_0 is lower for sheet materials with more pronounced normal anisotropy. It can also be observed that the increase in formability is practically proportional to the increase in normal stress for the sheet material with the greater anisotropy.

In this investigation the imperfection factor in the MK analysis was defined, amongst other parameters, as a function of the grain size (d_0) of the sheet material. It is

therefore of interest to determine if the sensitivity of the FLC to the normal stress varies as a function of the grain size. In order to assess the effect of the grain size, the FLC of a fictitious sheet material, identical to the AISI-1012 steel except for its initial grain size that was doubled from 25 μm to 50 μm , were calculated for different values of the applied normal stress. The predicted FLC are plotted in Figure 5.12, and once again, it is evident that sheet formability continues to be dependent on the applied normal stress.

Similar to the previous cases, the percentage increase in the predicted FLC_0 was plotted as a function of the through-thickness stress for both the AISI-1012 steel and the fictitious material with the increased grain size, and these data are presented in Figure 5.13. It appears that when the grain size of the material increases the dependence of FLC on the applied out-of-plane stress decreases somewhat, but the rate of increase in formability still increases with the normal pressure. The initial grain size of the sheet does not appear to have a significant effect on the dependence of the FLC to the through-thickness stress.

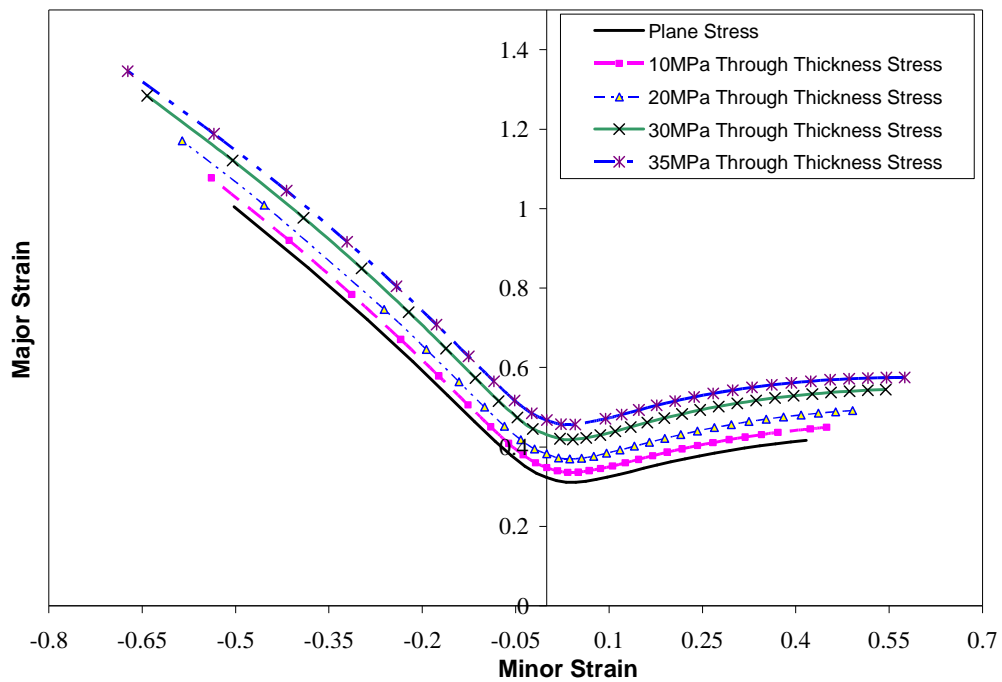


Figure 5.12. FLC of a sheet material that differs from AISI-1012 only by its grain size ($d_0=50 \mu\text{m}$), predicted as a function of the applied normal stress

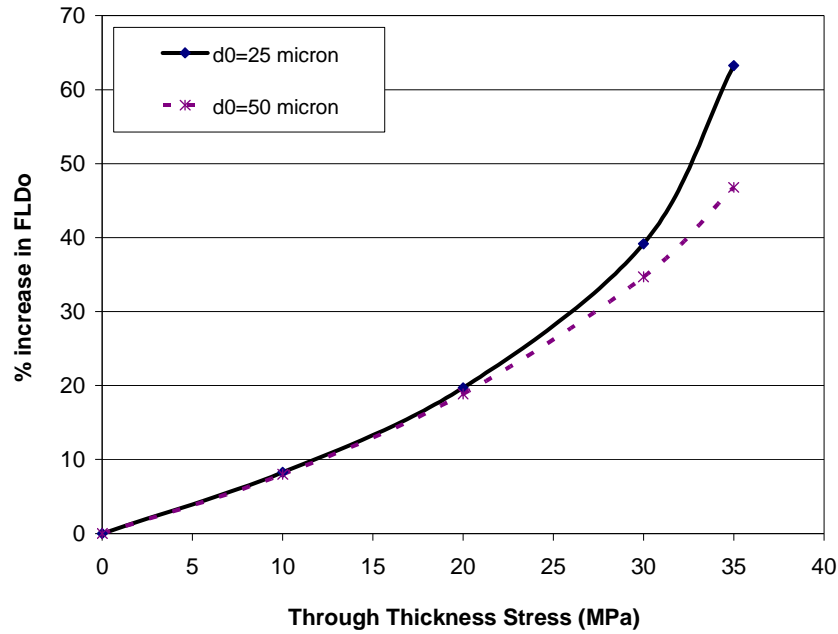


Figure 5.13. Increase in FLC_0 as a function of the applied normal stress for two sheet steels that differ only by their initial grain size ($d_0=25 \mu\text{m}$ and $d_0=50 \mu\text{m}$)

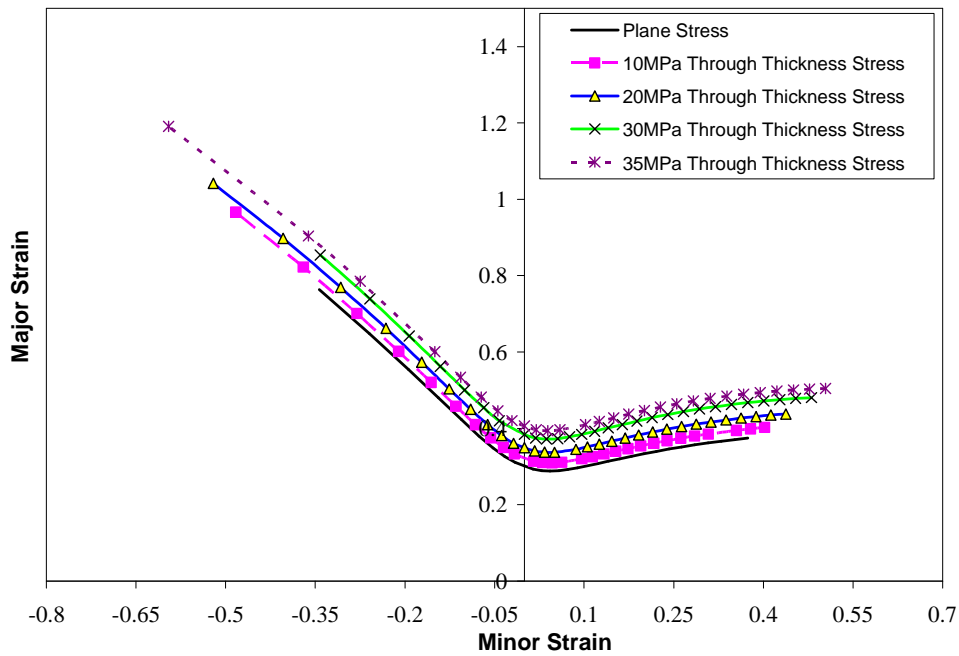


Figure 5.14. FLC of a sheet material that differs from AISI-1012 only by its initial thickness ($t_0=1.25\text{mm}$), predicted as a function of the applied normal stress

The sheet material's initial thickness was the last parameter that was considered in this investigation. Once again, the FLC of a sheet material with identical mechanical

properties to those of AISI-1012 steel except for the initial thickness that was reduced by a half from 2.5 mm to 1.25 mm (it did not appear reasonable to predict the FLC for a sheet thickness that was doubled to 5.0 mm), was calculated for different levels of applied normal stress, and the predicted FLC are shown in Figure 5.14.

Figure 5.14 shows that the sheet material with a thinner gauge is still sensitive to the applied normal stress, but that the dependence of the FLC on the through-thickness stress seems to decrease somewhat as the initial sheet thickness drops. Figure 5.15 confirms that this sensitivity to the through-thickness stress decreases when the sheet thickness decreases, although the actual rate of increase in formability continues to increase slightly with normal stress for this particular material with a 1.25 mm gauge.

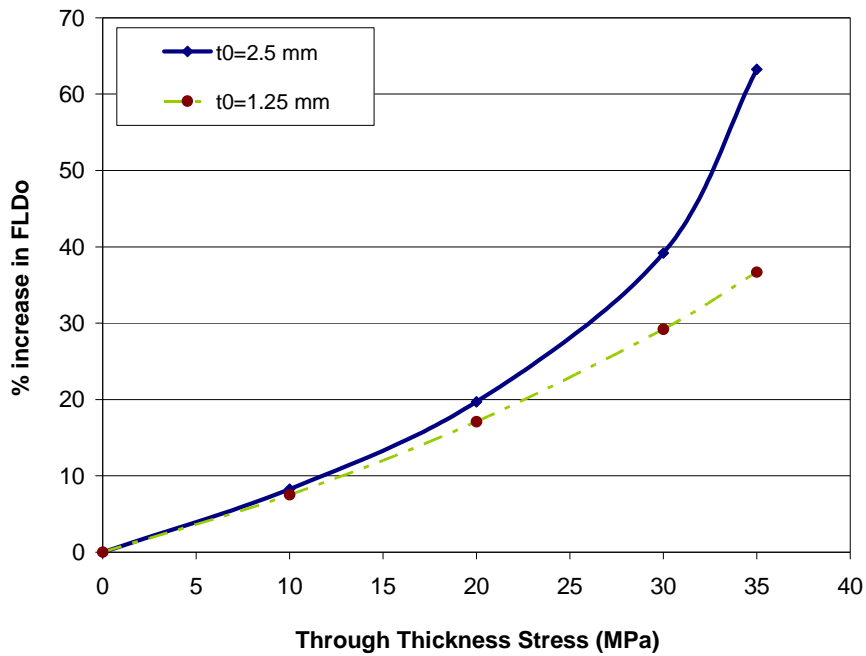


Figure 5.15. Increase in FLC₀ as a function of the applied normal stress for two sheet steels that differ only by their initial thickness (t₀=1.25mm and t₀=2.5mm)

It should be mentioned, however, that the current model does not address the influence of sheet thickness on limit strains in the presence of significant bending. Indeed, when a sheet is drawn over a punch radius the combination of stretching and bending lead to inhomogeneous through-thickness deformation. Furthermore, the through-thickness strain gradient increases with initial sheet thickness and with the severity of the bend. Ghosh and Hecker [5.28] showed that an increase in out-of-plane

(i.e. bending) deformation tends to delay the onset of necking and shifts the forming limits toward higher strains. Therefore a different approach is required to predict limit strains in cases where there is significant bending [5.29].

In order to compare the effect of each of these material parameters on the sensitivity of FLC to the through-thickness stress, the percent increase in FLC_0 (compared to the plane stress condition) was plotted in Figure 5.16 for each of the factors discussed. It can be seen that variations in the strain hardening coefficient clearly have the most significant effect on the sensitivity of the FLC to the normal stress: the sensitivity to the normal stress increases sharply when the work hardening ability of the material decreases. Similarly, the pressure sensitivity of the FLC increases when the normal anisotropy decreases. Another factor that has a significant effect on the sensitivity of FLC to the normal stress is the initial sheet thickness however its effect is the reverse of that of the other properties: the sensitivity of the FLC to the normal stress increases with the sheet thickness. Finally, any variation in grain size or in strain rate sensitivity does not appear to significantly affect the dependence of FLC on the normal stress unless the normal stress becomes very large ($\sigma_3 > 30$ MPa in this case).

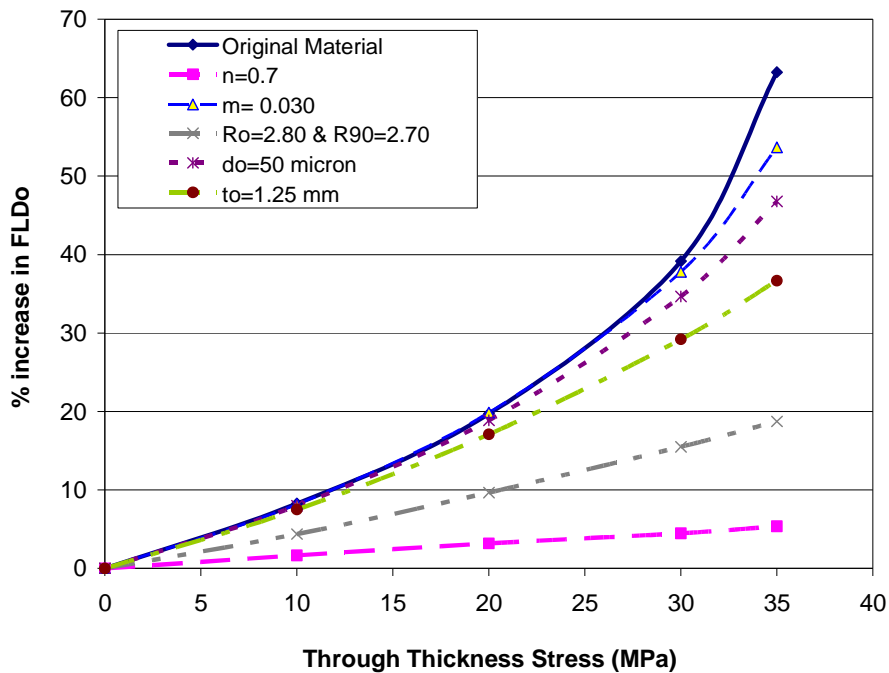


Figure 5.16. Increase in FLC_0 as a function of the applied normal stress for sheet steels that differ from AISI-1012 by only one mechanical property (see Table 5.1)

5.6. Conclusion

In this research, the through-thickness stress component was included in the traditional MK analysis to predict FLC in conditions where an out-of-plane stress is applied to the sheet surface. The current model was validated by comparing its predictions to experimental FLC data with different levels of applied normal stress. The FLC of an AISI-1012 steel sheet obtained under plane stress conditions, and the FLC of AA6011 aluminum and STKM-11A steel tubes subjected to various levels of internal pressure were all used to verify the proposed model. A good correlation between the theoretical and experimental FLCs was observed in all three cases.

The current MK model takes into account the effects of material properties such as grain size, surface roughness, and rotation of the initial imperfection. The value of the thickness inhomogeneity was defined as a function of surface roughness and grain size of the sheet material. In addition, the rotation of the imperfection band, the surface roughness and the thickness ratio (f) were updated throughout the loading history. This MK analysis was implemented into a numerical code, and the FLC of AISI-1012 sheet steel was predicted for different values of the applied compressive normal stress. The results obtained from this series of analyses showed that the FLC of a typical sheet steel is very sensitive to the applied normal stress, and the formability of the sheet always improves as the through-thickness stress increases. Therefore whenever it is applicable the addition of, or increase in, through-thickness stress would undoubtedly help to improve the formability of sheet materials in industrial sheet and tube forming processes. In many instances, the rate of increase in formability also increases with the normal stress, providing additional benefit to even small increases in applied normal stress.

Finally, the influence of certain sheet mechanical properties on the sensitivity of FLC to the through-thickness stress was also investigated using this predictive MK analysis code. It was found that the work hardening ability of the material has the greatest influence on the pressure dependence of FLC. Indeed, the dependence of FLC on the applied out-of-plane stress increases significantly as the strain hardening exponent decreases. Similarly, the sensitivity to the normal stress increases as the normal anisotropy (\bar{R}) decreases. The grain size and the strain rate sensitivity were found to

have only a minor influence on the pressure dependence of the FLC. Finally, the dependence of FLC on the normal stress was seen to increase quite significantly with the thickness of the sheet metal.

All in all, this investigation has shown that, while the dependence of the FLC on the through-thickness stress can vary from one material to another, the stress applied normal to the sheet surface invariably enhances sheet formability. Therefore the pressure dependence of the forming limits of metal sheets and thin-walled tubes cannot be ignored if the forming severity of formed components is to be accurately evaluated and the robustness of forming processes is to be optimized.

5.7. References

- [5.1] Marciniak Z., Kuczynski K., Limit strains in processes of stretch-forming sheet metal, *International Journal of Mechanical Sciences* 9 (1967) 609-620.
- [5.2] Keeler S.P., Backofen W.A., Plastic instability and fracture in sheets stretched over rigid punches, *ASM Transactions* 56 (1963) 25-48.
- [5.3] Goodwin G.M., Application of strain analysis to sheet metal forming in the press shop, SAE technical paper 680093 (1968).
- [5.4] Azrin M., Backofen W.A., The deformation and failure of a biaxially stretched sheet, *Metallurgical Transactions A (Physical Metallurgy and Materials Science)* 1 (1970) 2857-2865.
- [5.5] Sowerby R., Duncan J.L., Failure in sheet metal in biaxial tension, *International Journal of Mechanical Sciences* 13 (1971) 217-229.
- [5.6] Marciniak Z., Kuczynski K., Pokora T., Influence of the plastic properties of a material on the forming limit diagram for sheet metal in tension, *International Journal of Mechanical Sciences* 15 (1973) 789-805.
- [5.7] Ghosh A.K., A numerical analysis of the tensile test for sheet metals, *Metallurgical Transactions A (Physical Metallurgy and Materials Science)* 8A (1977) 1221-1232.
- [5.8] Butuc M.C., Gracio J.J., Da Rocha A.B., An experimental and theoretical analysis on the application of stress-based forming limit criterion, *International Journal of*

- Mechanical Sciences 48 (2006) 414-429.
- [5.9] Yoshida K., Kuwabara T., Kuroda M., Path-dependence of the forming limit stresses in a sheet metal, *International Journal of Plasticity* 23 (2007) 361-384.
- [5.10] Nurcheshmeh M., Green D.E., Investigation on the strain-path dependency of stress-based forming limit curves, *International Journal of Material Forming* 4 (2011) 25-37.
- [5.11] Gotoh M., Chung T., Iwata N., Effect of out-of-plane stress on the forming limit strain of sheet metals, *JSME International Journal Series A* 38 (1995) 123-132.
- [5.12] Smith L.M., Averill R.C., Lucas J.P., Stoughton T.B., Matin P.H., Influence of transverse normal stress on sheet metal formability, *International Journal of Plasticity* 19 (2003) 1567-1583.
- [5.13] Banabic D., Soare S., On the effect of the normal pressure upon the forming limit strains, *Proceedings of NUMISHEET* (2008) 199-204.
- [5.14] Molaei B., Strain path effects on sheet metal formability, Amirkabir University of Technology, Iran (1999) PhD thesis.
- [5.15] Hwang Y.M., Lin Y.K., Chuang H.C., Forming limit diagrams of tubular materials by bulge tests, *Journal of Materials Processing Technology* 209 (2009) 5024-5034.
- [5.16] Kim J., Kim S.W., Song W.J., Kang B.S., Analytical and numerical approach to prediction of forming limit in tube hydroforming, *International Journal of Mechanical Sciences* 47 (2005) 1023-1037.
- [5.17] Stachowicz F., Effect of annealing temperature on plastic flow properties and forming limit diagrams of titanium and titanium alloy sheets, *Transactions of the Japan Institute of Metals* 29 (1988) 484-493.
- [5.18] Sing W.M., Rao K.P., Influence of material properties on sheet metal formability limits, *Journal of Materials Processing Technologies* 48 (1995) 35-41.
- [5.19] Hill R., *The mathematical theory of plasticity*, Oxford University Press (1950).
- [5.20] Banabic D., Bunge H.J., Pöhlandt K., Tekkaya A.E., *Formability of metallic materials*, Springer-Verlag Berlin Heidelberg (2000).
- [5.21] Green D.E., Experimental determination of tube forming limits, *Proceedings of the International Conference on Hydroforming*, Oct. 28-29 (2003), Fellbach,

Germany, ed. K. Siebert, University of Stuttgart, 299-312.

- [5.22] Patterson E., Brailly P., Burguete R., Hack E., Siebert T., Whelan M., A challenge for high-performance full field strain measurement systems, *Strain* 43 (2007) 167–180.
- [5.23] Patterson E., Hack E., Brailly P., Burguete R.L., Saleem Q., Siebert T., Tomlinson R.A., Whelan M.P., Calibration and evaluation of optical systems for full-field strain measurement, *Optics and Lasers in Engineering* 45 (2007) 550–564.
- [5.24] Hung Y.Y., Ho H.P., Shearography: An optical measurement technique and applications, *Shearography: An optical measurement technique and applications, Materials Science and Engineering* 49 (2005) 61–87.
- [5.25] Francis D., James S.W., Tatam R.P., Surface strain measurement using multi-component shearography with coherent fiber-optic imaging bundles, *Measurement Science and Technology* 18 (2007) 3583–3591.
- [5.26] Pan B., Qian K., Xie H., Asundi A., Two-dimensional digital image correlation for in-plane displacement and strain measurement: a review, *Measurement Science and Technology* 20 (2009) 1-17.
- [5.27] Hosford W.F., Caddell R.M., *Metal Forming: Mechanics and Metallurgy*, 3rd edition, Cambridge University Press (2007) Section 15.4.
- [5.28] Ghosh A.K., Hecker S.S., Stretching limits in sheet metals: in-plane versus out-of-plane deformation, *Metallurgical Transactions* 5 (1974) 2161-2164.
- [5.29] Kitting D., Ofenheimer A., Pauli H., Till E.T., A phenomenological concept to predict formability in stretch-bending forming operations, *International Journal of Material Forming* 3-1 (2010) 1163-1166.

Chapter 6

Prediction of FLC using Hosford's 1979 yield function

6.1. Introduction

According to the well-established mathematical theory of continuum plasticity [6.1], three essential elements are required to describe the plastic behaviour of metallic materials [6.2]:

- a yield criterion that determines the boundary of elastic deformation and the onset of yielding in stress space
- a flow rule that establishes a relationship between the stress state and the plastic strain increments
- a strain hardening rule that describes the work hardening behaviour of the material and the manner in which the yield locus evolves with plastic deformation

The yield stress on a uniaxial stress-strain curve is the point at which deformation ceases to be elastic and fully recoverable, and when irreversible, plastic deformation takes place. Since the transition from elastic to plastic behaviour is generally quite gradual, common engineering practice is to define the yield stress in uniaxial tension at 0.2 percent plastic strain. For multiaxial loading, however, the determination of yielding is not as straightforward and a yield criterion is required. In order to determine the onset of yielding in a multiaxial stress state, a relation must be established between the (principal) stress components and the experimental yield stress. This relationship is called a yield function and usually has an implicit form:

$$f(\sigma_1, \sigma_2, \sigma_3, Y) = 0 \quad (6.1)$$

where $\sigma_1, \sigma_2, \sigma_3$ are the principal stress components and Y is the yield stress which can be obtained experimentally from a tension, compression or shearing test. The function described by Equation 6.1 actually represents a closed, smooth and convex surface in three-dimensional principal stress space and is therefore called a yield surface.

For incompressible materials such as metals, the yield surface has a cylindrical shape with a cross section which varies depending on the anisotropy of the material. For isotropic materials, the yield surface can be defined by von Mises' yield criterion, and in this case the cross-section will be circular as shown in Figure 6.1.

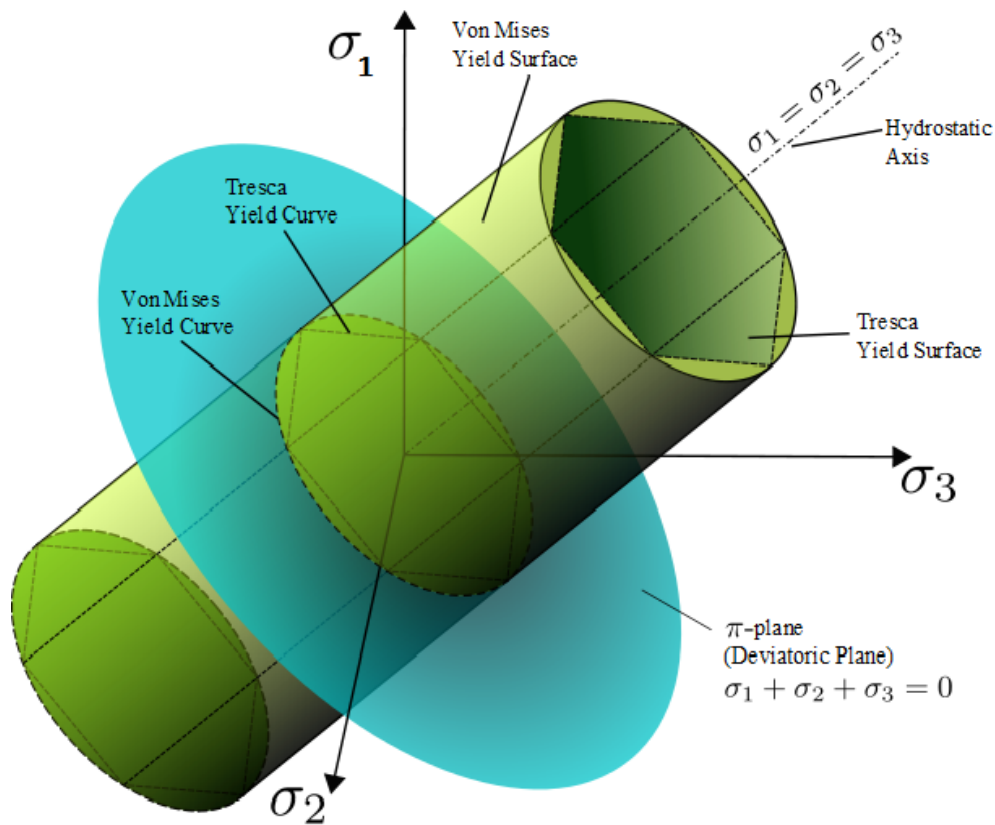


Figure 6.1. Von Mises and Tresca yield surfaces [6.3]

All the points inside the yield surface denote elastic stress states and points on the yield surface represent a condition in which plastic flow is occurring. As plastic

deformation progresses, the yield surface may expand, translate or rotate in stress space or perhaps distort by a combination of these. Therefore, points in stress space that lie outside the yield surface do not have any physical meaning.

In case of plane-stress loading (e. g. $\sigma_3=0$), the yield surface can be represented by a closed curve on the plane defined by the first and second principal stress components (e. g. σ_1, σ_2) and is referred to as the yield locus.

In this research, two different yield functions were employed in the MK analysis to predict forming limit curves following both linear and nonlinear (i.e. bilinear or multi-linear) loading paths. These two yield criteria are Hill's 1948 quadratic yield function and Hosford's 1979 non-quadratic yield function. These yield criteria will now be explained in detail in the following paragraphs.

6.2. Hill's 1948 yield criterion

6.2.1. Description of Hill's 1948 yield criterion

In 1948 Hill [6.1] introduced a yield function that became one of the most widely used yield criteria for anisotropic sheet materials. This quadratic yield function was an extension of the Huber-Mises-Hencky criterion which was proposed independently by Huber in 1904 [6.4] and by von Mises in 1913 [6.5] and later improved by Hencky [6.6]. Hill's 1948 yield criterion can be written in terms of the stress components as follows:

$$2f(\sigma_{ij}) = F(\sigma_y - \sigma_z)^2 + G(\sigma_z - \sigma_x)^2 + H(\sigma_x - \sigma_y)^2 + 2L\tau_{yz}^2 + 2M\tau_{zx}^2 + 2N\tau_{xy}^2 = 1 \quad (6.2)$$

where f denotes the yield function, F, G, H, L, M, N are anisotropic constants and subscripts x, y, z represent the principal orthotropic axes, where 'x' is taken as the rolling direction, 'y' is the transverse direction and 'z' is the normal direction to the sheet surface.

Considering the yield stress in uniaxial tension in the three principal anisotropy directions as $\sigma_x^y, \sigma_y^y, \sigma_z^y$, respectively, the anisotropic coefficients can be defined as:

$$\frac{1}{\sigma_x^{y2}} = G + H; \quad \frac{1}{\sigma_y^{y2}} = H + F; \quad \frac{1}{\sigma_z^{y2}} = F + G \quad (6.3)$$

Coefficients F , G and H can also be determined as a function of yield stress data in different directions $(\sigma_x^y, \sigma_y^y, \sigma_z^y)$, as follows:

$$2F = \frac{1}{\sigma_y^{y2}} + \frac{1}{\sigma_z^{y2}} - \frac{1}{\sigma_x^{y2}} \quad (6.4a)$$

$$2G = \frac{1}{\sigma_z^{y2}} + \frac{1}{\sigma_x^{y2}} - \frac{1}{\sigma_y^{y2}} \quad (6.4b)$$

$$2H = \frac{1}{\sigma_x^{y2}} + \frac{1}{\sigma_y^{y2}} - \frac{1}{\sigma_z^{y2}} \quad (6.4c)$$

If the yield stress in simple shear in the x , y , and z directions are τ_x^y , τ_y^y , and τ_z^y , respectively, then:

$$2L = \frac{1}{\tau_x^{y2}}; \quad 2M = \frac{1}{\tau_y^{y2}}; \quad 2N = \frac{1}{\tau_z^{y2}} \quad (6.5)$$

Coefficients F , G , and H are generally positive and only one of them would be negative in the unusual situation where there is a significant difference between stress data in different directions. However, coefficients L , M and N are always positive.

Therefore six independent axial and shear yield stresses $(\sigma_x^y, \sigma_y^y, \sigma_z^y, \tau_x^y, \tau_y^y, \text{ and } \tau_z^y)$ should be determined in the principal axes of anisotropy for a complete description of yielding behaviour, and the yield function would be considered as a surface in six-dimensional stress space. In plane-stress state $(\sigma_z = \tau_{xz} = \tau_{yz} = 0; \sigma_x \neq 0; \sigma_y \neq 0; \tau_{xy} \neq 0)$, the yield function reduces to:

$$2f(\sigma_{ij}) = (G + H)\sigma_x^2 - 2H\sigma_x\sigma_y + (H + F)\sigma_y^2 + 2N\tau_{xy}^2 = 1 \quad (6.6)$$

Using the definitions of F , G , H , and N as a function of yield stresses (σ_x^y , σ_y^y , σ_z^y , τ_x^y , τ_z^y), Equation 6.6 can be written in the following form:

$$\frac{1}{\sigma_x^{y2}}\sigma_x^2 - \left(\frac{1}{\sigma_x^{y2}} + \frac{1}{\sigma_y^{y2}} - \frac{1}{\sigma_z^{y2}}\right)\sigma_x\sigma_y + \frac{1}{\sigma_y^{y2}}\sigma_y^2 + \frac{1}{\tau_z^{y2}}\tau_{xy}^2 = 1 \quad (6.7)$$

In the event that the principal directions of stress coincide with the principal anisotropic axes, the shear stress term disappears and Hill's 1948 yield function can be rewritten as:

$$\frac{1}{\sigma_x^{y2}}\sigma_1^2 - \left(\frac{1}{\sigma_x^{y2}} + \frac{1}{\sigma_y^{y2}} - \frac{1}{\sigma_z^{y2}}\right)\sigma_1\sigma_2 + \frac{1}{\sigma_y^{y2}}\sigma_2^2 = 1 \quad (6.8)$$

where σ_1 , σ_2 are non-zero principal stresses.

In sheet metal forming simulations, anisotropy coefficients are normally determined from Lankford's coefficients (R_0 , R_{45} , and R_{90}) and the yield stresses in the principal anisotropic axes are designated as $\sigma_x^y = \sigma_0$ and $\sigma_y^y = \sigma_{90}$. Therefore the relation between the anisotropic coefficients (F , G , H) and Lankford's coefficients is as follows:

$$R_0 = \frac{H}{F}; \quad R_{90} = \frac{H}{F}; \quad R_{45} = \frac{H}{F + G} - \frac{1}{2} \quad (6.9)$$

There is another relation between the yield stresses and Lankford's coefficients as:

$$\frac{\sigma_0}{\sigma_{90}} = \sqrt{\frac{R_0(1 + R_{90})}{R_{90}(1 + R_0)}} \quad (6.10)$$

From Equation 6.9 it can be deduced that:

$$H = (F + G) \left(R_{45} + \frac{1}{2} \right) \quad (6.11)$$

or, from Equations 6.4a,b,c:

$$2H = \frac{1}{\sigma_z^2} \frac{2R_{45} + 1}{2} = \frac{1}{\sigma_0^2} \frac{R_0 + R_{90}}{R_{90}(1 + R_0)} (2R_{45} + 1) \quad (6.12)$$

Finally the following equation can be written [6.2]:

$$\begin{aligned} & \frac{1}{\sigma_0^2} \sigma_x^2 - \left(\frac{1}{\sigma_0^2} + \frac{1}{\sigma_{90}^2} - \frac{1}{\sigma_0^2} \frac{R_0 + R_{90}}{R_{90}(1 + R_0)} \right) \sigma_x \sigma_y + \\ & + \frac{1}{R_{90}^2} \sigma_y^2 + \frac{1}{\sigma_0^2} \frac{R_0 + R_{90}}{R_{90}(1 + R_0)} (2R_{45} + 1) \tau_{xy}^2 = 1 \end{aligned} \quad (6.13)$$

If the directions of principal stress are coincident with the principal anisotropic axes ($\sigma_x = \sigma_1$, $\sigma_y = \sigma_2$, $\tau_{xy} = 0$), Hill's 1948 yield function can be rewritten as:

$$\sigma_1^2 - \frac{2R_0}{1 + R_0} \sigma_1 \sigma_2 + \frac{R_0(1 + R_{90})}{R_{90}(1 + R_0)} \sigma_2^2 = \sigma_0^2 \quad (6.14)$$

or equivalently, by taking into account the Equation 6.10:

$$\sigma_1^2 - \frac{2R_0}{1 + R_0} \sigma_1 \sigma_2 + \frac{R_0(1 + R_{90})}{R_{90}(1 + R_0)} \sigma_2^2 = \frac{R_0(1 + R_{90})}{R_{90}(1 + R_0)} \sigma_{90}^2 \quad (6.15)$$

Equations 6.14 and 6.15 show that only three mechanical properties are required to define the yield condition of sheet metals in plane-stress state. These three mechanical properties are R_0 , R_{90} , and one of the uniaxial yield stresses (either σ_0 or σ_{90}), because parameters R_0 , R_{90} , σ_0 and σ_{90} are related by Equation 6.10. In practice, the values of the

anisotropy coefficients and an average of the uniaxial yield stress ($\sigma_{ave} = (\sigma_0 + \sigma_{90})/2$) are used.

6.2.2. Advantages and disadvantages of Hill's 1948 yield criterion

The main advantage of Hill's 1948 yield function is the simplicity with which the anisotropy coefficients can be determined from basic sheet mechanical properties. Moreover, only a limited number of material data are needed to fully define yielding behaviour. As already pointed out, only three independent material properties are sufficient to define the coefficients in Hill's 1948 yield function in plane-stress applications. Furthermore, many other yield criteria are only applicable to plane-stress sheet metal forming analyses but Hill's 1948 yield function is not limited in this way and is applicable to a variety of three-dimensional metal forming processes. Therefore this yield function continues to be widely used in numerical simulations.

Hill's 1948 yield criterion does however have some drawbacks. Many non-ferrous alloys including aluminum alloys have an average anisotropic coefficient that is $\bar{R} = (R_0 + 2R_{45} + R_{90})/4 < 1.0$ and, for such sheet materials, Hill's 1948 yield function does not adequately represent the shape of the yield surface. This observation was reported by Pearce [6.7] in 1968 and by Woodthorpe and Pearce [6.8] in 1970. Also second order "anomalous" behaviour ($R_0/R_{90} > 1$ and $\sigma_0/\sigma_{90} < 1$) was observed in some materials and Hill's 1948 is also not able to represent the anisotropy of such materials. Another limitation of this yield criterion is that this yield function can only predict two or four ears in axi-symmetric cup-drawing, whereas it is possible to observe six and occasionally eight ears in cups drawn with sheet materials which possess a high degree of anisotropy. For these reasons, many researchers have developed yield criteria that are able to more accurately represent the anisotropic behaviour of metal sheets.

6.3. Non-Quadratic yield criteria

The research to develop more accurate and versatile yield criteria started in the 1970s and the outcome of this work was to propose non-quadratic yield functions for the analysis of anisotropic plasticity of sheet materials. In this section, some of the better known non-quadratic yield criteria will be reviewed. Since Hosford's 1979 yield criterion overcomes the limitations of Hill's function, it was implemented into the current MK analysis code, and therefore this particular yield criterion will be reviewed in greater detail.

6.3.1. Hosford's 1979 yield criterion

In 1979 Hosford [6.9] introduced a non-quadratic yield criterion as follows:

$$F|\sigma_y - \sigma_z|^a + G|\sigma_z - \sigma_x|^a + H|\sigma_x - \sigma_y|^a = \sigma^a \quad (6.16)$$

This yield function is the generalized form of another yield function Hosford proposed in 1972 [6.10] for isotropic materials as:

$$\frac{1}{2}|\sigma_y - \sigma_z|^a + \frac{1}{2}|\sigma_z - \sigma_x|^a + \frac{1}{2}|\sigma_x - \sigma_y|^a = \sigma^a \quad (6.17)$$

where a is a positive integer much greater than two. Hosford and coworkers related the value of this exponent to the crystallographic structure of the material [6.11-6.14] and proposed $a=8$ for face centered cubic (FCC) materials and $a=6$ for body centered cubic (BCC) materials as the most appropriate values to describe the shape of the yield surface [6.13].

For plane-stress deformation, Hosford's 1979 anisotropic yield criterion can be written as:

$$R_{90}|\sigma_x|^a + R_0|\sigma_y|^a + R_0R_{90}|\sigma_x - \sigma_y|^a = R_{90}(R_0 + 1)\sigma_0^a \quad (6.18a)$$

or equivalently:

$$H|\sigma_x - \sigma_y|^a + F|\sigma_y|^a + G|\sigma_x|^a = \sigma_0^a \quad (6.18b)$$

The ratio between the effective strain and the major principal strain ($\lambda = \varepsilon_e / \varepsilon_1$) is:

$$\lambda = \frac{1}{\xi}(1 + \alpha\rho) \quad (6.19)$$

where ξ is the ratio between the effective stress and the major principal stress ($\xi = \sigma_e / \sigma_1$) and can be defined as follows in the case of normal anisotropy:

$$\xi = \left(\frac{1}{1 + \bar{R}} (1 + |\alpha|^a + \bar{R}|1 - \alpha|^a) \right)^{1/a} \quad (6.20)$$

and the relation between the strain and stress path indicators (i.e. the relation between $\rho = \varepsilon_2 / \varepsilon_1$ and $\alpha = \sigma_2 / \sigma_1$) is:

$$\rho = \frac{\alpha^{a-1} - r(1 - \alpha)^{a-1}}{1 + r(1 - \alpha)^{a-1}} \quad (6.21a)$$

or also:

$$\rho = \frac{F\alpha^{a-1} - H(1 - \alpha)^{a-1}}{H(1 - \alpha)^{a-1} + G} \quad (6.21b)$$

The inverse relation, $\alpha = \alpha(\rho)$ cannot be given explicitly but must be numerically solved for each value of ρ using the equation $\rho = \rho(\alpha)$. There are seven solutions to this equation when $a=8$ and five solutions when $a=6$. However, only one of the solutions is real.

Using the associated flow rule, the plastic strain increments can be written as:

$$d\varepsilon_x = d\lambda [H(1-\alpha)^{a-1} + G] \sigma_x^{a-1} \quad (6.22a)$$

$$d\varepsilon_y = d\lambda [F\alpha^{a-1} - H(1-\alpha)^{a-1}] \sigma_x^{a-1} \quad (6.22b)$$

$$d\varepsilon_z = -(d\varepsilon_x + d\varepsilon_y) = -d\lambda [G + F\alpha^{a-1}] \sigma_x^{a-1} \quad (6.22c)$$

Hosford's non-quadratic yield criterion was implemented into the author's MK numerical code, and the limit strain was calculated in the same way as was presented in chapters 3, 4 and 5.

6.3.2. Hill's 1979 yield criterion

A very similar non-quadratic yield function was proposed by Hill [6.15] in the same year:

$$\begin{aligned} & F|\sigma_2 - \sigma_3|^m + G|\sigma_3 - \sigma_1|^m + H|\sigma_1 - \sigma_2|^m + \\ & L|2\sigma_1 - \sigma_2 - \sigma_3|^m + M|2\sigma_2 - \sigma_3 - \sigma_1|^m + N|2\sigma_3 - \sigma_1 - \sigma_2|^m - 1 = 0 \end{aligned} \quad (6.23)$$

The main difference between Hosford's and Hill's non-quadratic yield criteria is related to the method employed to determine the exponent 'm' (m can be an integer or a real non-integer number greater than one) which is determined by matching the effective stress-strain curves for uniaxial and biaxial tests.

6.3.3. Hill's 1990 yield criterion

Hill (1990) [6.16] proposed another, more versatile, non-quadratic yield criterion for thin orthotropic sheets:

$$|\sigma_1 + \sigma_2|^m + \left(\frac{\sigma_{EB}}{\tau}\right)^m |\sigma_1 - \sigma_2|^m + |\sigma_1^2 + \sigma_2^2|^{(m/2)-1} \times \quad (6.24)$$

$$\left\{-2a(\sigma_1^2 - \sigma_2^2) + b(\sigma_1 - \sigma_2) + b(\sigma_1 - \sigma_2)^2 \cos 2\alpha\right\} \cos 2\sigma - (2\sigma_{EB})^m = 0$$

where τ is the yield stress in simple shear, σ_{EB} is the yield stress in equibiaxial tension and α is the angle between the first principal stress and the orthotropic axes. Parameters a and b are defined as:

$$a = \frac{F - G}{F + G}, \quad b = \frac{F + G + 4H - 2N}{F + G}$$

This yield function has proven to be more accurate than the original 1948 quadratic criterion, since it is defined by a greater number of parameters. The exponent m has often been used to fit the yield locus to the experimental yield data. However, besides the mechanical properties in uniaxial tension, it also requires the experimental yield stress in equibiaxial tension and in simple shear; both of these properties require specialized testing equipment and therefore the tendency, at least in the industry, has generally been to use a simpler yield function.

6.3.4. Hill's 1993 yield criterion

In 1993, Hill developed a new, supposedly user-friendly, non-quadratic yield criterion [6.17]. In this yield criterion the tensile yield behaviour in both the rolling and transverse directions is assumed to be essentially identical, which is a somewhat of a restriction, but the associated strain ratios are accounted differently

$$\sigma_1^2 - \left(2 - \frac{\sigma_u^2}{\sigma_{EB}^2}\right) \sigma_1 \sigma_2 + \sigma_2^2 + \left[(p+q) - \frac{p\sigma_1 + q\sigma_2}{\sigma_{EB}} \right] \sigma_1 \sigma_2 - \sigma_u^2 = 0 \quad (6.25)$$

where p and q are dimensionless anisotropic coefficients. This function is not homogeneous and is not actually as user-friendly as it was claimed to be. Finally, Hill's 1993 yield criterion is recommended for use with thin anisotropic sheets but is limited only to the first tension quadrant of the plane-stress space.

6.3.5. Barlat and Lian's 1989 yield criterion

In 1989, Barlat and Lian [6.18] introduced a non-quadratic yield criterion which is frequently called *Yld89*. This yield function was developed for textured polycrystalline sheets with planar anisotropy and is written as follows:

$$a|K_1 + K_2|^m + a|K_1 - K_2|^m + (2-a)|2K_2|^m - 2\bar{\sigma}^m = 0 \quad (6.26)$$

where K_1 and K_2 are defined by:

$$K_1 = \frac{\sigma_{xx} + h\sigma_{yy}}{2}, \quad K_2 = \sqrt{\left(\frac{\sigma_{xx} - h\sigma_{yy}}{2}\right)^2 + (p\sigma_{xy})^2}$$

and a , c , h , p are anisotropy coefficients calculated from the mechanical properties, and exponent m can be derived from the other anisotropy parameters. Although this yield criterion is limited to plane-stress applications, it has been shown to predict the shape of the yield locus of aluminum sheets much better than Hill's yield criteria.

6.3.6. Barlat's Yld2000-2d yield criterion

There were some issues in *Yld96* such as it is not always possible to prove the convexity of the yield surface defined by this function and therefore it is not always possible to ensure the uniqueness of the plastic strain increment. Moreover, it is difficult to determine the first and second derivatives of yield function in the form of an analytic expression which creates a challenge for the implementation of this yield criterion into numerical codes.

In order to overcome the limitations of the previous yield function (*Yld96*), Barlat *et al.* 2003 [6.19] proposed a yield criterion capable of modelling the behaviour of metals in a full three-dimensional stress state. This yield criterion guarantees yield locus convexity and is easier to implement in a finite element code. In plane-stress conditions it is written as follows:

$$2\bar{\sigma}^a = |X'_1 - X'_2|^a + |2X''_2 + X''_1|^a + |2X''_1 + X''_2|^a \quad (6.27)$$

with

$$X' = L'\sigma \quad \text{and} \quad X'' = L''\sigma \quad (6.28)$$

where L' and L'' are linear transformation tensors which can be fully defined with eight independent anisotropy coefficients (α_1 to α_8) and which can be determined from eight uniaxial and biaxial mechanical properties. This yield function is generally referred to as the *Yld2000-2D* criterion and it has become widely accepted as one of the most suitable criteria for describing the plastic behaviour of aluminum sheets.

6.3.7. Other Yield Criteria

Many other non-quadratic yield criteria have been proposed such as that of Barlat *et al.* 1991 [6.20], Karafillis and Boyce 1993 [6.21], Barlat *et al.* 1997 [6.22], Banabic *et al.* [6.23] and Barlat *et al.* 2005 [6.24]. These more recent yield functions are generally from the same family of functions as Hosford's yield criterion.

As mentioned already, Hosford's 1979 non-quadratic yield criterion was implemented in the author's MK analysis code. The main reasons for selecting it are as follows:

- a) In the MK analysis used in this dissertation there are no shear stress components and in these cases, the plastic strains calculated from Hosford's yield criterion are very similar to those predicted with more recent non-quadratic yield functions such as *Yld2000-2D*.
- b) In plasticity calculations using Hosford's yield function there is a real benefit to working with fewer material constants. Indeed, one of the challenges with more recent yield criteria is the fact that a large number of parameters need to be defined from the various sheet mechanical properties and therefore a large number of material

- characterization tests are required. One recent yield criterion requires 18 different mechanical properties obtained in 7 different orientations relative to the rolling direction of the sheet. This is really too onerous for use in industrial simulations of sheet metal forming operations.
- c) A survey of the literature reveals that Hosford's 1979 yield function has been a successful non-quadratic yield criterion for FLC prediction of sheet materials that have an average plastic anisotropy ratio less than one [6.25-6.32].

6.4. Results

Following the implementation of Hosford's 1979 yield criterion into our MK analysis code, the predicted FLCs were compared with corresponding experimental FLCs for both as-received and bilinear loading paths. Two alloys were considered for the comparison: a low carbon sheet steel AISI-1012 [6.33] and the AA-2008-T4 aluminum sheets reported by Graf and Hosford [6.34]. The material properties of these two alloys were presented in chapter 3 (Tables 3.1 and 3.2). Moreover, in order to compare the accuracy of FLCs obtained from quadratic and non-quadratic yield criteria, the same FLCs were predicted using Hill's 1948 yield function and are included in the comparisons.

Figure 6.2 shows good agreement between both theoretical predictions and experimental data for AISI-1012 sheet steel in its as-received state. In this figure, the FLC predicted with Hosford's yield function fits very well with the corresponding experimental curve in all regions of the diagram. Both yield criteria lead to the same prediction of the FLC in the region of plane-strain deformation which is a critical deformation mode in sheet metal forming. As anticipated, the FLC predicted with the non-quadratic yield function is in better agreement with the experimental data than that predicted with the quadratic yield function on the right side of the diagram (i.e. for positive minor strains) but the two criteria predict the left side of the FLC (i.e. for negative minor strains) with a similar level of accuracy.

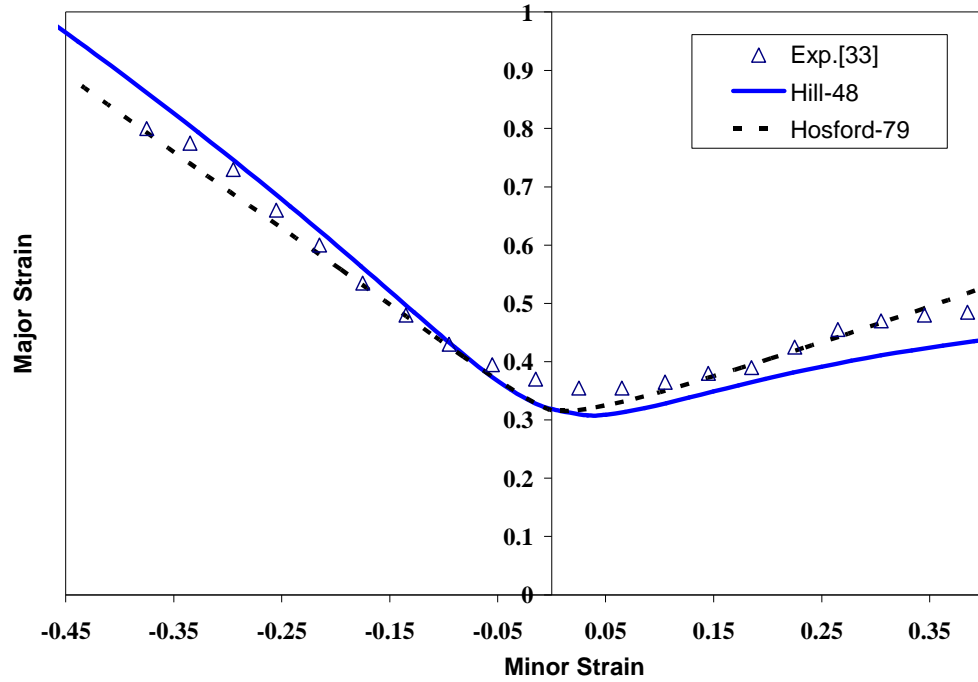


Figure 6.2. Comparison of predicted and experimental FLCs of as-received AISI-1012 steel sheets

The FLCs of AISI-1012 steel were also calculated for two nonlinear loading paths. In the first case sheet specimens were preloaded to 8% strain in equibiaxial tension and the FLC was determined following this prestrain by simulating a whole series of linear load paths in the range between $\rho=-0.5$ and $\rho=1$ (i.e. between uniaxial tension and equibiaxial tension). In the second case the sheet material was subject to a 10% prestrain in uniaxial tension followed by a range of linear loading paths between uniaxial tension and equibiaxial tension. The FLCs predicted for these two types of bilinear strain paths with either Hill's or Hosford's yield criterion are shown in Figures 6.3 and 6.4, respectively, along with the corresponding experimental data.

In Figure 6.3, the published experimental data was only available for the left side of the FLC, however both plasticity models show good agreement with the experimental data after a prestrain in equibiaxial tension. Once again it can be observed that both yield criteria lead to the same prediction of limiting strains in the plane-strain region for both loading histories. But we also observe that Hosford's non-quadratic yield criterion gives a better prediction in the regions to the left and right of plane-strain for steel specimens prestrained in uniaxial tension, as shown in Figure 6.4.

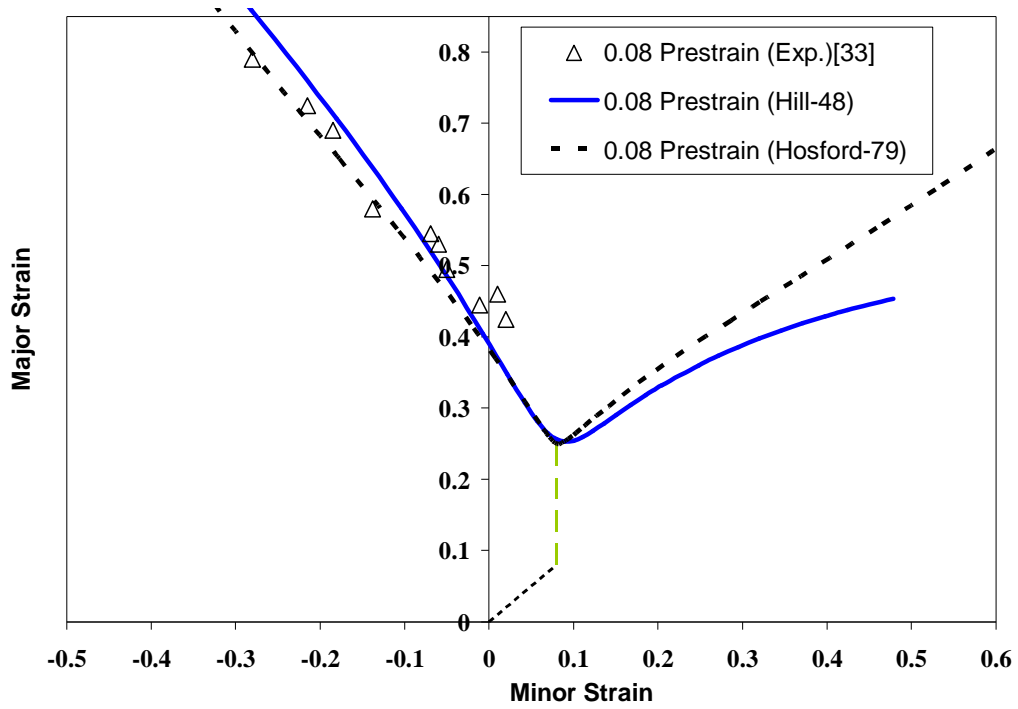


Figure 6.3. Comparison of predicted and experimental FLCs of AISI-1012 steel after 8% prestrain in equibiaxial tension

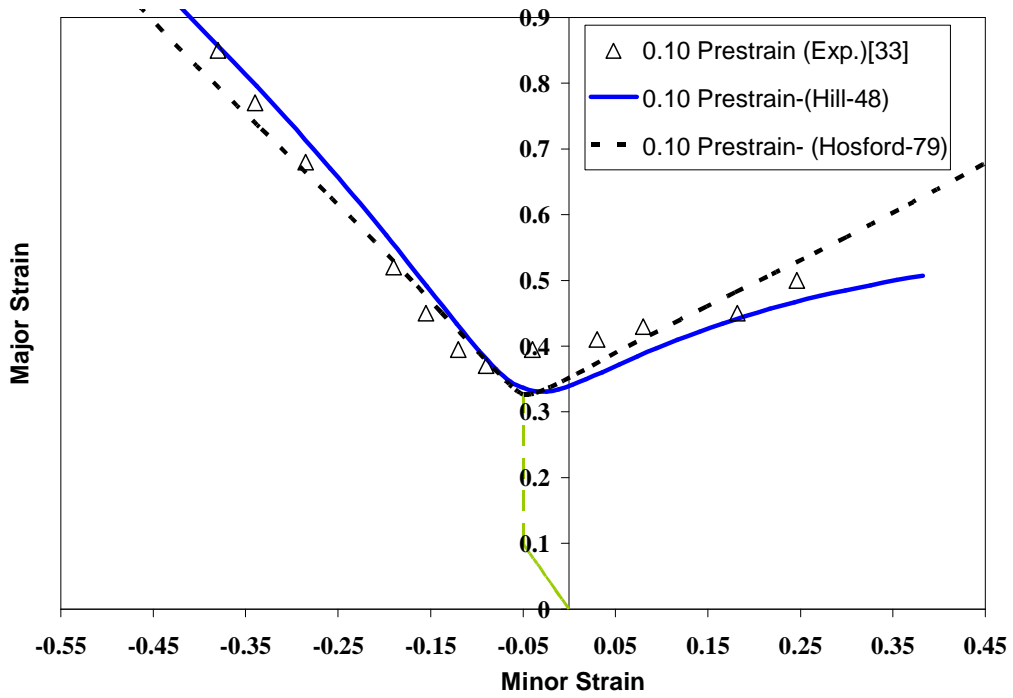


Figure 6.4. Comparison of predicted and experimental FLCs of AISI-1012 steel after 10% prestrain in uniaxial tension

Overall, it can be seen that the differences between the predictions using these two yield criteria is not significant for this particular grade of steel.

The FLC of the AA-2008-T4 aluminum alloy sheet predicted with both Hosford's and Hill's yield criteria and the corresponding experimental data for the as-received condition are shown in Figure 6.5. As mentioned in chapters 3 and 4, some material constants (C , d_0 , R_{Z0}) were not provided in Graf and Hosford's publication [6.34], therefore these values were determined by calibrating the FLC of the AA-2008-T4 alloy predicted using Hill's 1948 yield criterion to the experimental as-received FLC: the values determined by the calibration were $C = 0.70$, $d_0 = 8.00\mu\text{m}$ and $R_{Z0} = 2.5 \mu\text{m}$ and the prediction of the FLC using Hosford's yield function was also performed with the same material constants. It can be observed in Figure 6.5 that the predicted curves correlate very well with the experimental data, but the FLC predicted with the non-quadratic yield criterion appears to provide a better fit than the one predicted with the quadratic function.

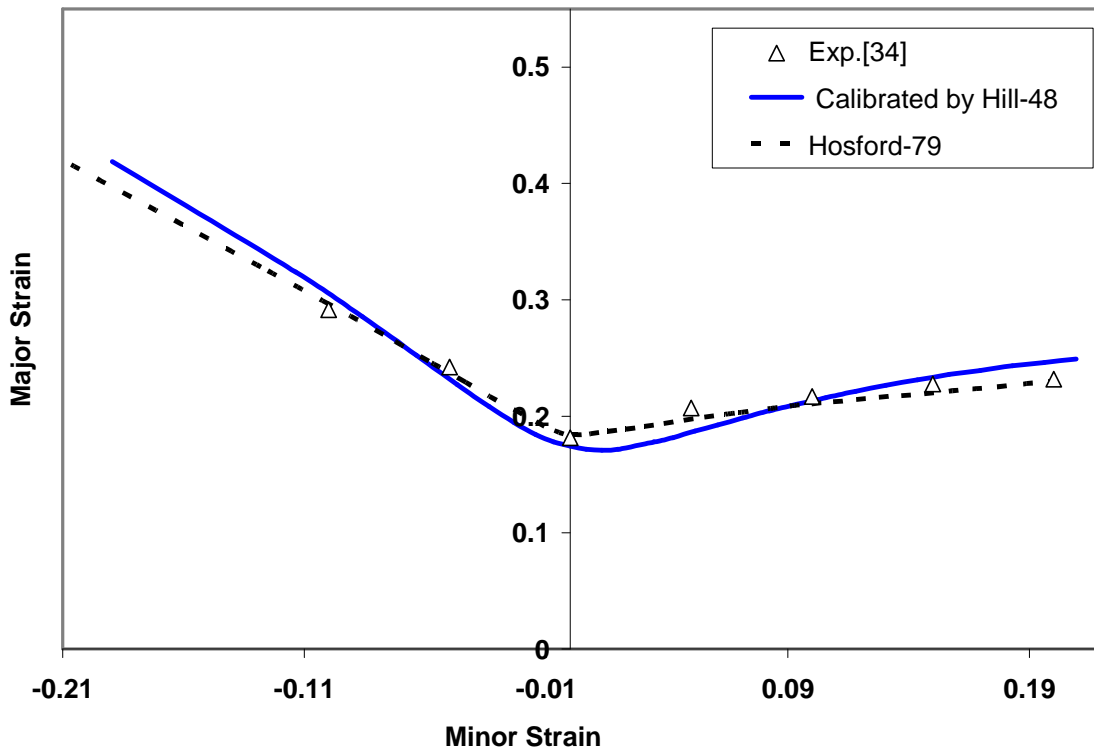


Figure 6.5. Comparison of calibrated/predicted and experimental FLCs of as-received 2008-T4 aluminum sheets

The FLC of AA-2008-T4 sheet was also predicted for bilinear loading paths in which the prestrain was obtained in different modes of deformation. In the first case, the FLC was predicted for sheets prestrained to either 4% or 12% in equibiaxial tension. The curves calculated using both quadratic and non-quadratic yield functions are shown along with the corresponding experimental data in Figures 6.6 and 6.7, respectively.

In Figure 6.6, it appears that Hosford's yield criterion leads to a better prediction of the FLC for the samples with a 4% prestrain in equibiaxial tension. However, when a greater magnitude of prestrain is applied along the same strain path ($\rho=1$), Hill's quadratic yield criterion seems to provide a slightly better correlation with experimental data. Nevertheless, both yield functions give very similar predictions and both criteria lead to an acceptable level of accuracy for this aluminum alloy.

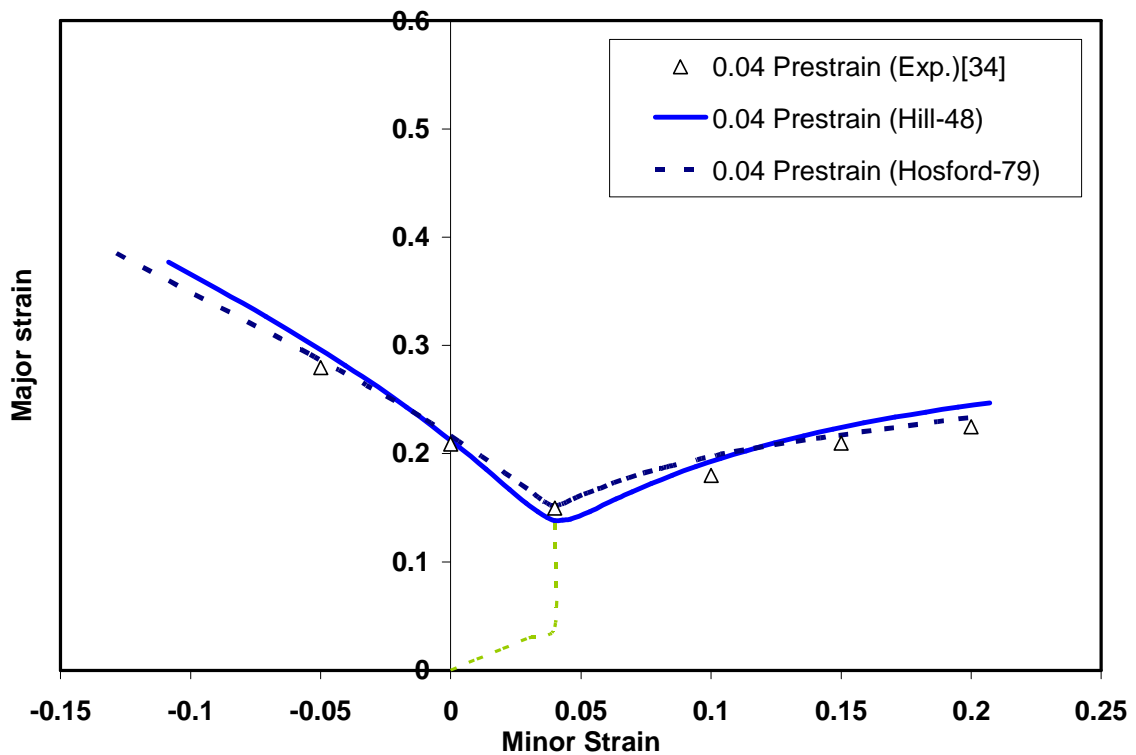


Figure 6.6. Comparison of predicted and experimental FLCs of 2008-T4 aluminum after 4% prestrain in equibiaxial tension

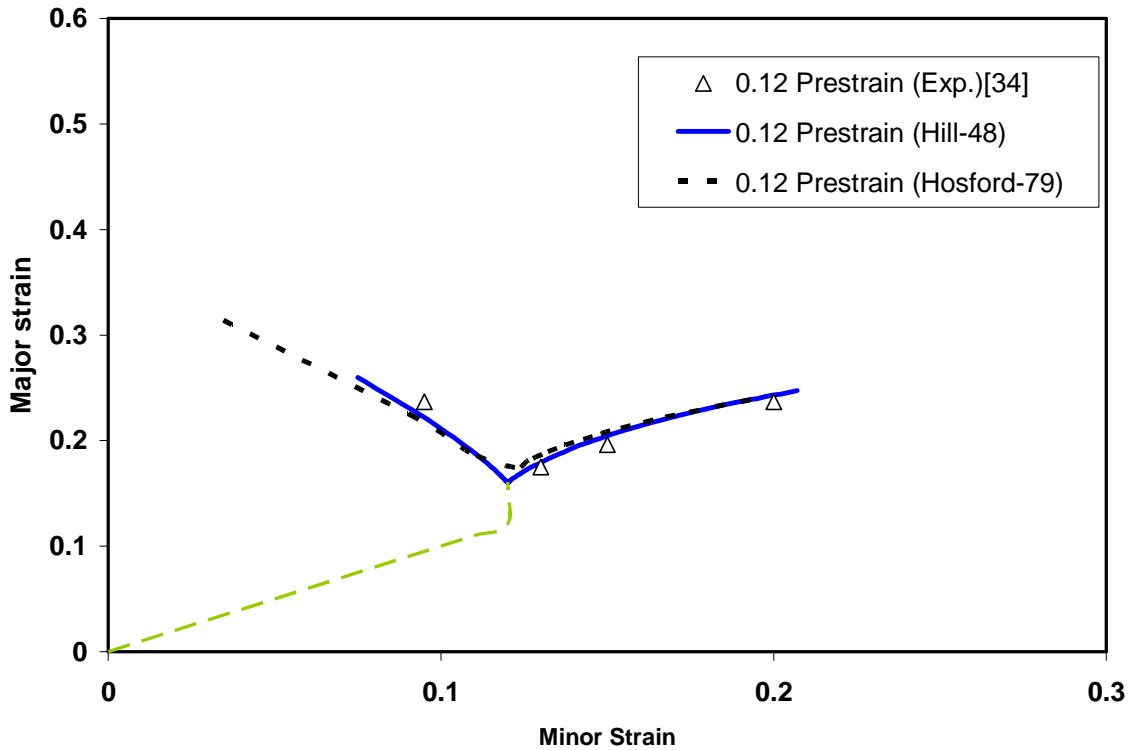


Figure 6.7. Comparison of predicted and experimental FLCs of 2008-T4 aluminum after 12% prestrain in equibiaxial tension

Graf and Hosford also published experimental FLC data for this aluminum alloy for a prestrain of either 5% or 12% in uniaxial tension. In order to further validate the FLC predictions using these two different plasticity models, the FLC was predicted for both strain histories with the present MK model. The predicted FLCs and the corresponding experimental data are shown in Figures 6.8 and 6.9. In Figure 6.8, after a 5% prestrain in uniaxial tension, it can be seen that Hill's yield criterion gives a better prediction of the right side of the FLC than Hosford's criterion; but this is the only case amongst those investigated where the quadratic function gives a better prediction than the non-quadratic function. It can also be pointed out that, in this case, Hosford's criterion still gives a better prediction in the region of plane-strain deformation and shows a more accurate trend on the left side of the FLC. For the AA-2008-T4 sheet samples deformed to a 12% prestrain in uniaxial tension, although the two plasticity models yield similar results, the non-quadratic criterion clearly provides a more accurate prediction than the quadratic yield function for both sides of the FLC.

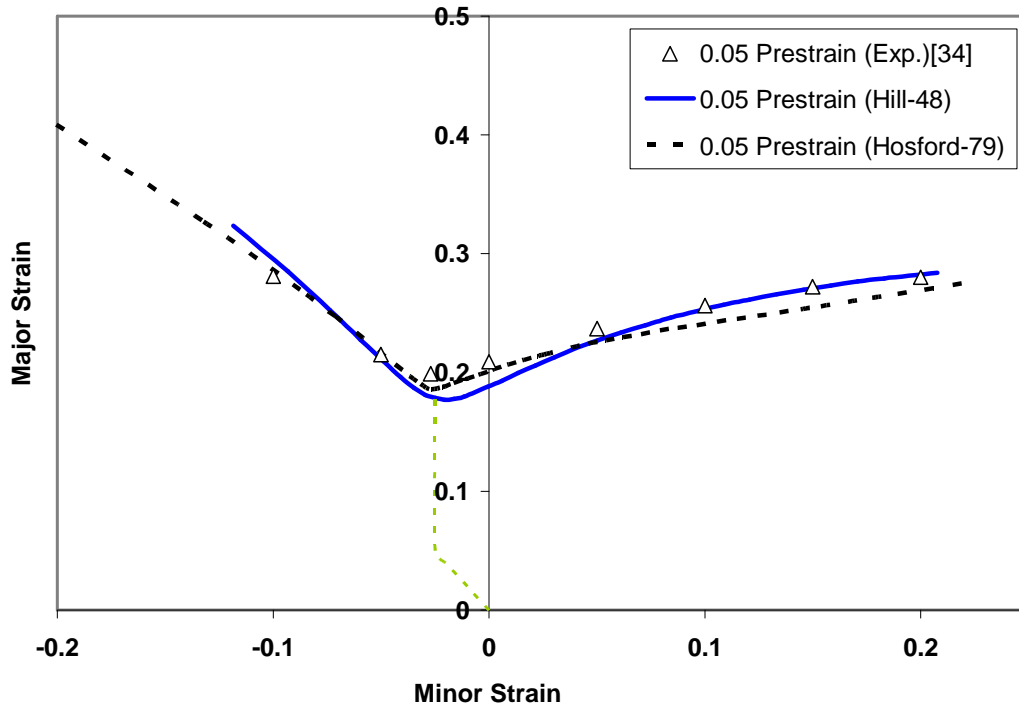


Figure 6.8. Comparison of predicted and experimental FLCs of 2008-T4 aluminum after 5% prestrain in uniaxial tension

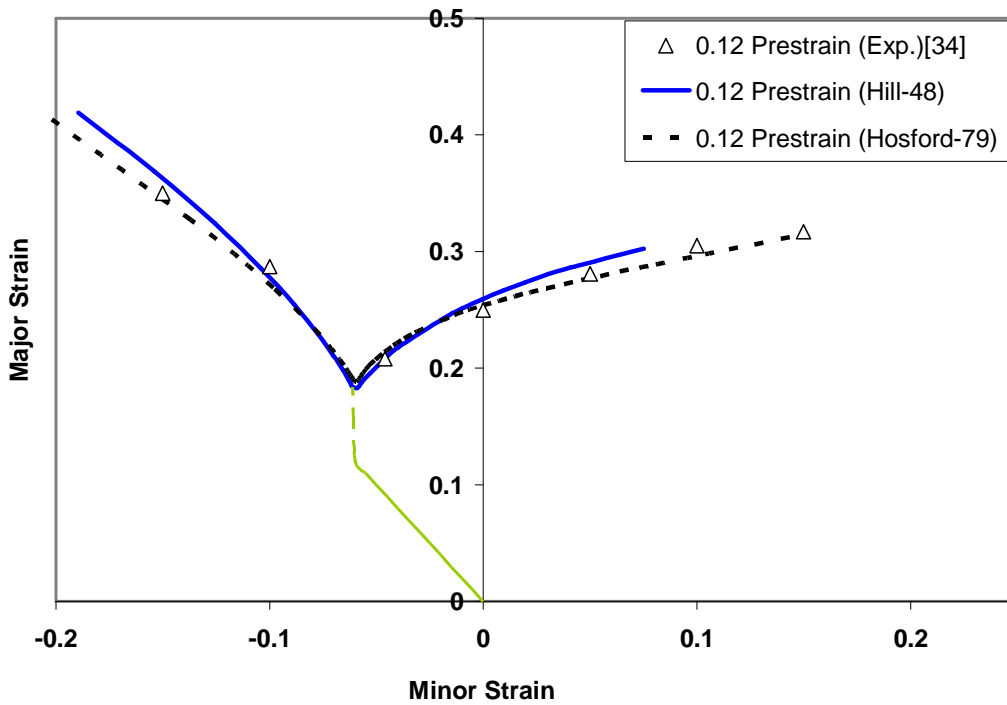


Figure 6.9. Comparison of predicted and experimental FLCs of 2008-T4 aluminum after 12% prestrain in uniaxial tension

6.5. Conclusion

In this chapter a numerical MK analysis code was developed to predict the FLC of sheet metal using Hosford's 1979 non-quadratic yield criterion. Forming limits were predicted for both linear and bilinear loading paths for AISI-1012 steel and AA-2008-T4 aluminum sheets. The theoretical results that were obtained were compared with the corresponding experimental data and also with the FLCs predicted with Hill's 1948 yield function at the same condition.

Both anisotropic plasticity theories are able to predict the FLC of these two sheet materials very well, for both the as-received condition and also for samples prestrained in uniaxial or equibiaxial tension. Not only do the predicted FLCs follow the general shape of the experimental FLC, but their accuracy is also very good considering there is an estimated error of $\pm 2.5\%$ strain on the vertical position of an experimental FLC [6.35]. However, on the whole, the prediction of FLC using Hosford's yield function is somewhat better than when Hill's criterion is employed, especially on the right side of the FLC. In most cases, the predictions made with these two yield criteria were very similar, with only minor variations on the left side of the FLC. There was only one case where the prediction using Hill's criterion was more consistent with experimental data than Hosford's criterion, and this was on the right side of the FLC of the 2008-T4 aluminum alloy after a 5% percent prestrain in uniaxial tension.

Based on the observations made in this chapter, it may be concluded that Hosford's non-quadratic yield function generally leads to more accurate predictions of limiting strains than Hill's quadratic function, for as-received as well as prestrained material, whether it is prestrained in either uniaxial tension or equibiaxial tension, and for both steel and aluminum sheets.

6.6. References

- [6.1] Hill R., The mathematical theory of plasticity, University Press, Oxford (1950).
- [6.2] Banabic D., Bunge H.J., Pöhlandt K., Tekkaya A.E., Formability of metallic

materials, Springer-Verlag Berlin Heidelberg (2000).

- [6.3] Wikipedia online link, http://en.wikipedia.org/wiki/Von_Mises_yield_criterion, accessed on March 15, 2011.
- [6.4] Huber M. T.: C T 22 (1904) 34-81.
- [6.5] Von Mises R., Mechanics of solids in plastic state 592, Göttinger Nachrichten Math. Phys. Klasse 1 (1913) 582.
- [6.6] Hencky H., On the theory of plastic deformations 592, Z. Ang. Math. Mech. 4 (1924) 323-334.
- [6.7] Pearce R., Some aspects of anisotropic plasticity in sheet metals, International journal of Mechanical Sciences 10 (1968) 995-1001.
- [6.8] Woodthorpe J., Pearce R., The anomalous behaviour of aluminium sheet under balanced biaxial tension, International journal of Mechanical Sciences 12 (1970) 341-347.
- [6.9] Hosford W.F., On yield loci of anisotropic cubic metals. In: Proceedings of the 7th North American Metalworking Conference (NMRC), SME, Dearborn, MI (1979) 191-197.
- [6.10] Hosford W.F., A generalised isotropic yield criterion, Journal of Applied Mechanics 39 (1972) 607-609.
- [6.11] Hosford W.F., The Mechanics of Crystals and Textured Polycrystals, New York, Oxford University Press (1993).
- [6.12] Logan R., Hosford W.F., Upper-bound anisotropic yield locus calculations assuming (111) - pencil glide, International journal of Mechanical Sciences 22 (1980) 419-430.
- [6.13] Hosford W.F., On the crystallographic basis of yield criteria, Texture and Microstructures 26-27 (1996) 479-493.
- [6.14] Hosford W.F., Comments on anisotropic yield criteria, International journal of Mechanical Sciences 27 (1985) 423-427.
- [6.15] Hill R., Theoretical plasticity of textured aggregates, Mathematical Proceedings of the Cambridge Philosophical Society 85 (1979) 179-191.
- [6.16] Hill R., Constitutive modeling of orthotropic plasticity in sheet metal, Journal of Mechanics and Physics of Solids 38 (1990) 405.

- [6.17] Hill R., A user-friendly theory of orthotropic plasticity in sheet metals, *International Journal of Mechanical Sciences* 35 (1993) 19.
- [6.18] Barlat F., Lian J., Plastic behaviour and stretchability of sheet metals, Part I, A yield function for orthotropic sheet under plane stress conditions, *International Journal of Plasticity* 5 (1989) 51-66.
- [6.19] Barlat F., Brem J.C., Yoon J.W., Chung K., Dick R.E., Lege D.J., Pourboghrat F., Choi S.H., Chu E., Plane stress yield function for aluminum alloy sheet - Part I: theory, *International Journal of Plasticity* 19 (2003) 1297-1319.
- [6.20] Barlat F., Lege D.J., Brem J.C., A six-component yield function for anisotropic materials, *International Journal of Plasticity* 7 (1991) 693.
- [6.21] Karafillis A.P., Boyce M.C., A general anisotropic yield criterion using bounds and a transformation weighting tensor, *Journal of Mechanics and Physics of Solids* 41 (1993) 1859.
- [6.22] Barlat F., Becker R.C., Hayashida Y., Maeda Y., Yanagawa M., Chung K., Brem J.C., Lege D.J., Matsui K., Murtha S.J., Hattori S., Yielding description for solution strengthened aluminum alloys, *International Journal of Plasticity* 13 (1997) 385.
- [6.23] Banabic D., Comsa D.S., Balan T., A new yield criterion for orthotropic sheet metals under plane stress conditions, in D. Banabic ed. *Proceedings of the 7th TPR 2000 Conference on Cold Metal Forming*, Cluj Napoca, 2000, Printek Publishing House, Cluj Napoca, Romania (2000) 217-224.
- [6.24] Barlat F., Aretz H., Yoon J.W., Karabin M.E., Brem J.C., Dick R.E., Linear transformation-based anisotropic yield functions, *International Journal of Plasticity* 21 (2005) 1009-1039.
- [6.25] Graf A.F., Hosford W.F., Calculations of Forming limit diagrams, *Metallurgical Transactions A* 21a (1990) 87-94.
- [6.26] Graf A.F., Hosford W.F., Calculations of forming limit diagrams for changing strain paths, *Metallurgical Transactions A*, 24a (1993) 2497-2501.
- [6.27] Padwal S.B., Chaturvedi R.C., Prediction of forming limits using Hosford's modified yield criterion, *International Journal of Mechanical Sciences* 34(1992) 541-547.

- [6.28] Friedman P.A., Pan J., Effects of plastic anisotropy and yield criteria on prediction of forming limit curves, *International Journal of Mechanical Sciences* 42 (2000) 29-48.
- [6.29] Kim Y.S., Won S.Y., Na K.H., Effect of material damage on forming limits of voided anisotropic sheet metals, *Metallurgical and Materials Transactions A: Physical Metallurgy and Materials Science* 34 A (2003) 1283-1290.
- [6.30] Kim Y., Kim C., Lee S., Won S., Hwang S., Forming limits for anisotropic sheet metals, *JSME International Journal, Series A (Solid Mechanics and Material Engineering)* 46 (2003) 627-34.
- [6.31] Chow C.L., Jie M., Hu S.J., Forming limit analysis of sheet metals based on a generalized deformation theory, *Transactions of the ASME Journal of Engineering Materials and Technology* 125(2003) 260-5.
- [6.32] Aghaie-Khafri M., Mahmudi R., Predicting of plastic instability and forming limit diagrams, *International Journal of Mechanical Sciences* 46 (2004) 1289-1306.
- [6.33] Molaei B., Strain path effects on sheet metal formability, Amirkabir University of Technology, Iran (1999) PhD thesis.
- [6.34] Graf A, Hosford W, Effect of changing Strain paths on Forming Limit Diagrams of Al 2008-T4, *Metallurgical Transactions* 24A (1993) 2503- 2512.
- [6.35] Nurcheshmeh M., Green D.E., Influence of out-of-plane compression stress on limit strains in sheet metals, *International Journal of Material Forming*, Accepted on March 18, 2011, Manuscript Number: IJFO-D-10-00144.

Chapter 7

Summary and conclusions

7.1. Summary

This dissertation presents a number of advanced mechanical models that help to calculate the forming limits of sheet materials more accurately and for a wider range of loading conditions than was previously possible. The well-known Marciniak-Kuczynski (MK) model was used as the basic method to predict forming limit curves both in strain space (FLC) and in stress space (SFLC). In order to predict the onset of plastic instability for sheets deformed in complex, multi-stage forming operations, the MK model was adapted to compute forming limits for sheets subject to nonlinear strain paths. Theoretical predictions of FLCs for linear and bilinear loading paths were compared with the corresponding experimental data for AISI-1012 steel and AA-2008-T4 aluminum alloys. The path dependency of SFLCs predicted for different non-proportional loading histories was also investigated.

The MK approach was also used to compute the FLC in conjunction with two different work-hardening models: an isotropic hardening model and a mixed isotropic-nonlinear kinematic hardening model which is capable of describing the Bauschinger effect. Once again, published experimental FLCs of AISI-1012 low carbon steel and AA-

2008-T4 aluminum sheets that were subjected to various non-linear loading paths were compared to predictions using both hardening models.

The conventional MK model was also extended to predict FLC for general, three-dimensional stress states. Indeed, the influence of the through-thickness principal stress on the formability of different grades of sheet metal was investigated in terms of the ratio of the third to the first principal stress components ($\beta = \sigma_3/\sigma_1$). An analysis was also carried out to determine how the sensitivity of the FLC prediction to the through-thickness stress changes with variations in mechanical properties and sheet thickness. The validation of the model for cases involving three-dimensional stresses was done with published experimental FLC data for AA-6011 aluminum and STKM-11A steel tubes.

Finally the effect of the yield function on FLC prediction was investigated by implementing both a quadratic and a non-quadratic yield criterion into the MK analysis. FLCs were calculated with Hill's 1948 quadratic yield function and Hosford's 1979 non-quadratic yield function using a numerical code that accounts for linear and nonlinear loading paths. Predictions of FLC were again compared with experimental data for AISI-1012 steel and AA-2008-T4 alloys.

7.2. Conclusions

The following conclusions can be drawn from the research presented in this dissertation:

1. This research emphasizes that the FLC is significantly strain-path dependent. Although the industrial practice of using a 10 percent safety margin beneath the FLC can, in many cases, be an effective way to ensure a robust sheet metal forming process, there are also many instances where FLC variation due to nonlinear loading can be significantly greater than this safety margin. Therefore the as-received FLC ought not to be used for formability evaluation unless it can be shown that the loading history is quasi-linear throughout the formed part.

2. The MK analysis was shown to predict both the FLC and the SFLC of sheet metals with acceptable accuracy provided critical material parameters, such as the imperfection factor, are defined appropriately.
3. It is strongly recommended to include the rotation of the imperfection band, material anisotropy, and strain rate sensitivity in the MK analysis. The FLC can be very sensitive to the strain rate sensitivity of the sheet material.
4. The SFLC remains practically strain-path independent for a significant range of prestrains. However, some path dependency is observed if the magnitude of the prestrain exceeds a certain level of equivalent strain ($\bar{\epsilon} \geq 0.35$ for AISI-1012 steel) or when there are abrupt changes in strain path.
5. In spite of some path dependency, the SFLC remains a good failure criterion for virtual forming simulations because the path dependency of SFLCs is much less significant than that of strain-based FLCs.
6. Predictions of the FLC using the MK analysis have been shown to be dependent on the shape of the initial yield locus and on its evolution during work hardening; therefore the hardening model has a considerable influence on the predicted FLC. This work showed that the isotropic hardening rule leads to acceptable accuracy on the left side of the FLC (i.e. for negative minor strains), but that the mixed hardening rule provides a more accurate prediction of FLC in plane-strain and on the right side of the FLC (i.e. for positive minor strains) for the sheet materials considered.
7. The formability of sheet metal was shown to be very sensitive to the applied normal stress, and the FLC always shifts upwards in strain space as the compressive through-thickness stress is increased. Therefore the assumption of plane-stress conditions is really only an approximation which can be made in a few cases such as open die stamping. Since many industrial sheet and tube forming processes lead to significant compressive through-thickness stresses, the effects of this normal stress on the formability of sheet metals should not be ignored.
8. The analysis showed that among the material parameters considered in this research, the strain hardening coefficient has the most significant effect on the

dependency of FLC to the through-thickness stress, while the strain rate sensitivity coefficient has the least influence on this sensitivity.

9. The anisotropy factor also has a significant effect on the dependency of FLC to the through-thickness stress. Sheet materials with a lower normal anisotropy, such as aluminum alloys, show greater formability improvement in the presence of a compressive stress than materials with a more pronounced normal anisotropy.
10. Both Hill's 1948 and Hosford's 1979 yield criteria predict the left side of the FLC of AISI-1012 steel and AA-2008-T4 aluminum sheets with acceptable accuracy for both linear and nonlinear strain paths. However the prediction of the right side of the FLC using Hosford's 1979 non-quadratic yield function was somewhat better than that with Hill's 1948 quadratic function.
11. Calculation of the FLC using a non-quadratic yield function gives a more accurate prediction of the FLC in biaxial tension than with a quadratic yield function because a non-quadratic function is able to represent the shape of the yield surface more accurately in the region of biaxial tension.

7.3. Future work

The implementation of various mechanical models into the MK analysis has been shown to improve the accuracy of the FLC, particularly in cases of multi-stage loading and in the presence of through-thickness stresses. The implementation of more relevant yield criteria and hardening models was also shown to enhance the prediction of FLC. However, further work should be carried out in this area so that the most advanced and up-to-date plasticity models may be incorporated into numerical predictive codes. Indeed, while Hosford's 1979 yield function and the mixed isotropic – nonlinear kinematic hardening model were helpful to improve the prediction of the FLC, there are no doubt other yield criteria and hardening models which would provide even more accurate forming limit data, especially in view of the increased use of advanced high strength steels, aluminum and magnesium alloys in the automotive metal forming industry.

Moreover, these various enhancements were implemented one at a time into the MK analysis, so that one code was initially developed with basic features such as the capability of following bilinear strain paths, Hill's quadratic yield function and isotropic hardening. This basic code was then modified to replace Hill's 1948 yield function with Hosford's non-quadratic yield criterion, thus making a second predictive code. The original MK code was modified again, as a separate code, to replace isotropic hardening with the mixed hardening model. And again a fourth code was developed with the capability of including the through-thickness stress in the analysis. Therefore it is suggested that these individual modelling features all be included in a single code that has the flexibility of being able to independently modify the yield criterion, the hardening model and the magnitude of the through-thickness stress.

In the MK approach, material inhomogeneity has generally been modelled as a geometric imperfection, and in this work, the geometric imperfection factor was related to the surface roughness of the sheet material. It is suggested, however, that the microstructural inhomogeneities in modern automotive sheet materials may be more significant than the surface roughness of the sheet. For instance, the segregation between softer and harder phases in advanced high strength steels such as martensite banding in dual phase steels may create a more severe inhomogeneity than the roughness at the surface of the sheet. It would be most interesting to investigate whether the imperfection factor in the MK analysis can be correlated to martensite banding, or with other sources of inhomogeneity that exist in other families of alloys.

Finally, the MK analysis is not currently capable of predicting the onset of plastic instability when bending is superimposed on the in-plane deformation. The addition of bending strains creates a through-thickness strain gradient, which is known to delay the onset of necking, particularly as the bending radius decreases and as the sheet thickness increases. Therefore, it would be extremely useful to develop an analytical model that does take the bending deformation into consideration.

Clearly, much more research is required to predict the forming limits of sheet materials with accuracy and reliability.

Appendix A

Determination of $\eta = d\varepsilon_e^b / d\varepsilon_e^a$ ratio in MK analysis

In chapters 3, 4, and 5 it was mentioned that localized necking in sheet metal occurs once the effective strain rate in the groove area reaches 10 times that in the nominal area, that is when $\eta = d\varepsilon_e^b / d\varepsilon_e^a > 10$. In the current research, the variation of η was monitored at every increment during the numerical prediction of the deformation. Figure A.1 shows a sample of the variation of η for a given loading path ($\rho = 0.95$).

The values of η shown in Figure A.1 indicate that the magnitude of η suddenly increases from 1.45 to 146.1 at the end of the deformation when necking occurs. This signifies that in this case, $\eta > 2.0$ would give the correct solution to the FLC calculation. Table A.1 presents the final η values for all the strain paths between uniaxial tension and equibiaxial tension for the AISI-1012 steel.

It can be seen from this table that the final value of η at the onset of necking varies between 1.44 and 3.55. From a theoretical point of view, any η value greater than 3.5 will result in a correct and repeatable prediction of the FLC for all strain paths. In this table there is only one strain path for which the limiting value of η lies outside the mentioned range ($\eta = 6.61$ when $\rho = -0.10$). For this particular loading path, the onset of necking will be virtually identical whether $\eta = 3.5$ or $\eta = 6.61$ because the difference in effective strain during this one additional increment is merely $\varepsilon_e = 0.001$. Although $\eta > 4$ will give a consistent prediction of FLC in different sheet metals, a broad survey of the literature shows that $\eta = 10$ is commonly used in MK-based FLC calculation codes.

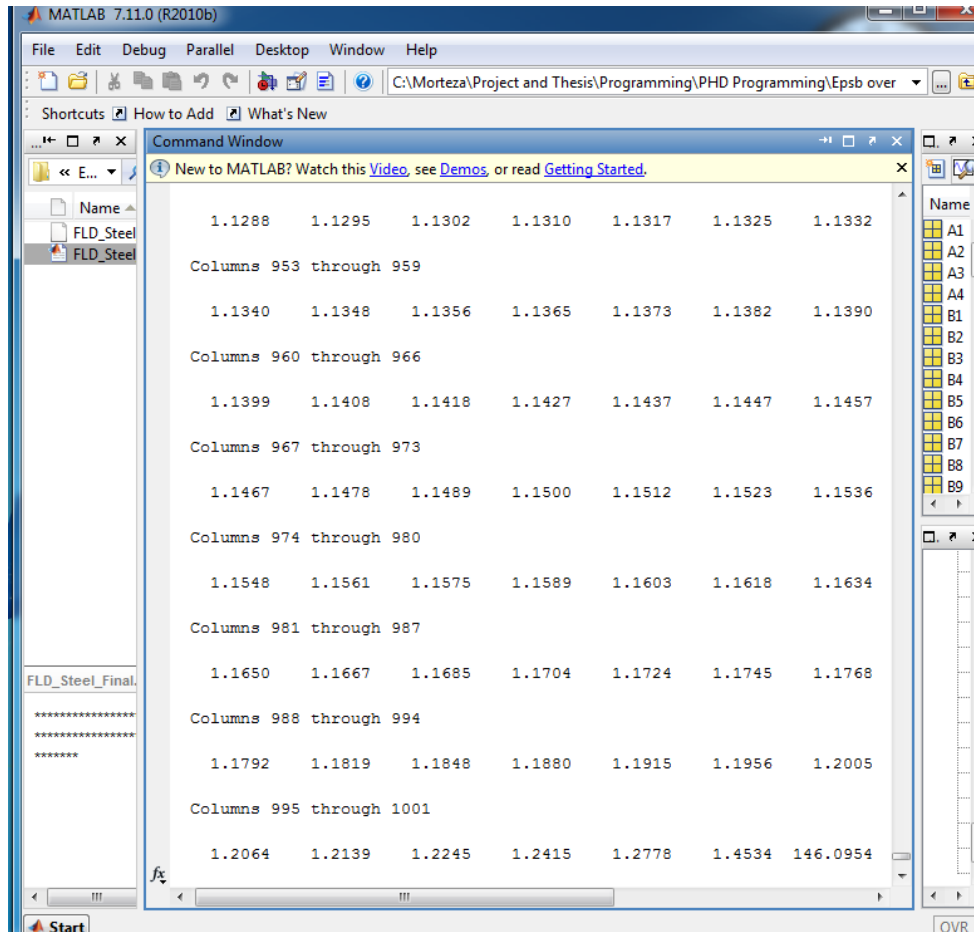


Figure A.1. Variation of $\eta = d\epsilon_e^b / d\epsilon_e^a$ during the computation of a FLC

It should also be mentioned that, during the current research some uniaxial tension tests were conducted on DP600 steel specimens. The effective strain values were recorded using a commercial optical strain measurement device that uses digital image correlation to calculate strains. In these tests the average experimental value for the η coefficient was found to be $\eta=4.1$.

Table A.1. Final values of η at the onset of instability for AISI-1012 steel

ρ	η	ρ	η	ρ	η
1.00	1.55	0.50	1.76	-0.05	2.34
0.95	1.45	0.45	2.93	-0.10	6.61
0.90	1.76	0.40	2.60	-0.15	2.90
0.85	1.47	0.30	1.87	-0.20	3.07
0.80	1.48	0.25	3.55	-0.25	1.78
0.75	1.60	0.20	3.25	-0.30	1.66
0.70	1.93	0.15	2.34	-0.35	2.78
0.65	2.34	0.10	2.22	-0.40	1.45
0.60	1.89	0.00	2.03	-0.45	1.44

Appendix B

Error between predicted and experimental FLCs

In order to quantify how well the predicted FLCs correlate with experimental curves, the area between the theoretical FLC and the experimental FLC was used to define a percentage of error for the theoretical results:

$$\text{Error \%} = \frac{\text{Area between the theoretical and the experimental FLC}}{\text{Area under the experimental FLC}} \times 100 \quad (\text{B1})$$

The area under predicted and experimental FLC was calculated numerically for the range of minor strains for which experimental data was available, and the error data that was obtained is listed in Table B.1.

Table B.1. Percent error of predicted FLCs

Predicted FLC	Error %
FLC of AISI-1012 steel alloy in the as-received state using isotropic hardening rule and Hill's 48 yield criterion (Figure 4.6)	8.26
FLC of AISI-1012 steel alloy in the as-received state using mixed hardening rule and Hill's 48 yield criterion (Figure 4.6)	5.43
FLC of AISI-1012 steel alloy in the as-received state using isotropic hardening rule and Hosford's 79 yield criterion (Figure 6.2)	2.84

Table B.1. Percent error of predicted FLCs (continued)

Predicted FLC	Error %
FLC of AISI-1012 steel alloy after 8% prestrain in equibiaxial tension using isotropic hardening rule and Hill's 48 yield criterion (Figure 4.7)	6.30
FLC of AISI-1012 steel alloy after 8% prestrain in equibiaxial tension using mixed hardening rule and Hill's 48 yield criterion (Figure 4.7)	7.13
FLC of AISI-1012 steel alloy after 8% prestrain in equibiaxial tension using isotropic hardening rule and Hosford's 79 yield criterion (Figure 6.3)	3.05
FLC of AISI-1012 steel alloy after 10% prestrain in uniaxial tension using isotropic hardening rule and Hill's 48 yield criterion (Figure 4.8)	5.88
FLC of AISI-1012 steel alloy after 10% prestrain in uniaxial tension using mixed hardening rule and Hill's 48 yield criterion (Figure 4.8)	5.00
FLC of AISI-1012 steel alloy after 10% prestrain in uniaxial tension using isotropic hardening rule and Hosford's 79 yield criterion (Figure 6.4)	2.29
FLC of 2008-T4 aluminum alloy after 4% prestrain in equibiaxial tension using isotropic hardening rule and Hill's 48 yield criterion (Figure 4.10)	4.68
FLC of 2008-T4 aluminum alloy after 4% prestrain in equibiaxial tension using mixed hardening rule and Hill's 48 yield criterion (Figure 4.10)	4.69
FLC of 2008-T4 aluminum alloy after 4% prestrain in equibiaxial tension using isotropic hardening rule and Hosford's 79 yield criterion (Figure 6.6)	2.31
FLC of 2008-T4 aluminum alloy after 12% prestrain in equibiaxial tension using isotropic hardening rule and Hill's 48 yield criterion (Figure 4.10)	4.18
FLC of 2008-T4 aluminum alloy after 12% prestrain in equibiaxial tension using mixed hardening rule and Hill's 48 yield criterion (Figure 4.10)	0.54
FLC of 2008-T4 aluminum alloy after 12% prestrain in equibiaxial tension using isotropic hardening rule and Hosford's 79 yield criterion (Figure 6.7)	4.23
FLC of 2008-T4 aluminum alloy after 5% prestrain in uniaxial tension using isotropic hardening rule and Hill's 48 yield criterion (Figure 4.11)	1.35
FLC of 2008-T4 aluminum alloy after 5% prestrain in uniaxial tension using mixed hardening rule and Hill's 48 yield criterion (Figure 4.11)	1.30
FLC of 2008-T4 aluminum alloy after 5% prestrain in uniaxial tension using isotropic hardening rule and Hosford's 79 yield criterion (Figure 6.8)	3.3
FLC of 2008-T4 aluminum alloy after 12% prestrain in uniaxial tension using isotropic hardening rule and Hill's 48 yield criterion (Figure 4.11)	2.45
FLC of 2008-T4 aluminum alloy after 12% prestrain in uniaxial tension using mixed hardening rule and Hill's 48 yield criterion (Figure 4.11)	0.93
FLC of 2008-T4 aluminum alloy after 12% prestrain in uniaxial tension using isotropic hardening rule and Hosford's 79 yield criterion (Figure 6.9)	0.45

Table B.1. Percent error of predicted FLCs (continued)

Predicted FLC	Error %
FLC of AA6011 aluminum alloy under 15 MPa internal pressure using isotropic hardening rule and Hill's 48 yield criterion (Figure 5.3)	10.23
FLC of STKM-11A steel alloy under 56 MPa internal pressure using isotropic hardening rule and Hill's 48 yield criterion (Figure 5.4)	13.54

VITA AUCTORIS

NAME	Morteza Nurcheshmeh
DATE AND PLACE OF BIRTH	1977, Miyana, East Azerbaijan, Iran
EDUCATION	
High School,	Miyana, East Azerbaijan, Iran, 1992-1996
B.Sc.	Mechanical Engineering University of Tabriz, Tabriz, Iran, 1996-2000
M.Sc.	Mechanical Engineering Sharif University of Technology, Tehran, Iran, 2000-2003
Ph.D.	Mechanical Engineering University of Windsor, Windsor, ON, Canada, 2007-2011